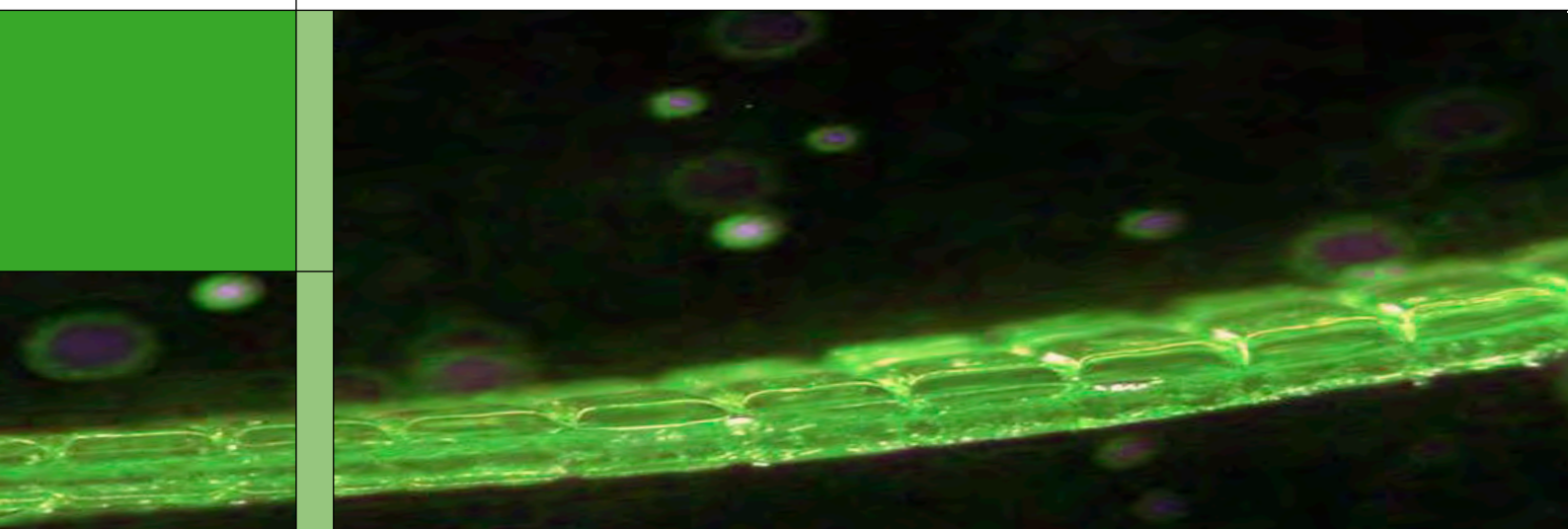


PAUL SCHERRER INSTITUT



# Annual Report 2006

Electrochemistry Laboratory

<http://ecl.web.psi.ch>

**COVER PHOTO:**

Cross-section of a microstructured  
proton-conducting membrane.

© Paul Scherrer Institut

PAUL SCHERRER INSTITUT



## Electrochemistry Laboratory

# Annual Report 2006

Hardcopies of this report are available from:  
Isabella Kalt (isabella.kalt@psi.ch)  
Paul Scherrer Institut  
5232 Villigen PSI  
Switzerland

A full version of this report is also available on the web:  
<http://ecl.web.psi.ch>

Paul Scherrer Institut  
Electrochemistry Laboratory  
5232 Villigen PSI  
Switzerland

Secretary  
Phone +41 (0)56 310 29 19  
Fax +41 (0)56 310 44 15

IMPRESSUM

**Publisher**

Electrochemistry Laboratory  
Paul Scherrer Institut  
5232 Villigen PSI

**Editorial Team**

Isabella Kalt  
Rüdiger Kötz  
Günther G. Scherer

**Printing**

Paul Scherrer Institut

ISSN 1661-5379

PSI Electrochemistry Laboratory – Annual Report 2006

© Paul Scherrer Institut

# CONTENT

**1 EDITORIAL**  
G.G. Scherer

**3 SCIENTIFIC CONTRIBUTIONS 2006**

**Fuel Cells - Catalysis**

**5** Investigating the kinetics of the  $H_{UPD}$  reaction on platinum electrodes

**6** Electrochemical surface reshaping of polycrystalline Pt: Morphology and cristallography

**7** On the measurement of the hydrogen unterpotential deposition in PEFCs

**9** Preparation of core-shell platinum-cobalt electrocatalysts for oxygen reduction

**10** Electro-oxidation of formic acid on  $Bi_2 PtIrO_7$  powder electrodes

**11** Fuel Cell performance of platinum/carbon co-sputtered electrodes

**12** DFT modeling of Ni over  $Al_2O_3(100)$  surface

**13 Fuel Cells - Membranes**

**15** Microstructured proton conducting membranes

**16** Kinetic studies on radiation grafted membranes for PEFC

**17** Radiation grafted membranes based on a trifluorostyrene derivative

**18** Effect of crosslinker on the fuel cell performance of styrene grafted poly (ethylene-*AL T*-tetrafluoroethylene) based membranes

**19** Fuel Cell durability of the radiation grafted PSI membrane under high  $H_2/O_2$  pressure and dynamic operating conditions

**20** Local degradation analysis of an aged fuel cell membrane

**21** Gas permeations in aged nafion membranes

**23 Fuel Cells - Diagnostics**

**25** Influence of oxygen partial pressure on channel-rib current distributions in PEFC

**26** Investigation of anisotropic material properties of gas diffusion media in PEFC

**27** Anisotropic transport properties of gas diffusion media for PEFC

**28** Local current density measurements in PEFC using segmented current collectors

**29** Modeling the low frequency response of air fed PEFCs

**30** Low frequency impedance response of air fed PEFCs

**32** Application of high resolution neutron imaging in PEFC diagnostic

**33** High power micro fuel cell employing micro-structured glassy carbon

**34** Cell interaction phenomena in polymer electrolyte fuel cell stacks

**36** Thermal analysis and optimization of a portable edge-air-cooled PEFC stack

**37 Batteries & Capacitors - Materials**

**39** Spray drying synthesis and electrochemical performance of lithium vanadates as positive electrode materials for lithium batteries

**41** Oxide nanoparticles as active material in lithium-ion batteries

**43** Synthesis and characterization of doped  $Li[Mn_{0.5-x/2}Ni_{0.5-x/2}Co_x]O_2$  cathode materials

- 45 Nitroxide radical polymers for organic radical batteries
- 47 Correlation between the active surface area of graphite materials and first lithium intercalation
- 49 **Batteries & Capacitors – Diagnostics**
- 51 A complete system for *in situ* X-ray diffraction measurements on electrochemical system at a synchrotron source
- 53 *In situ* X-ray diffraction of carbon for supercapacitors
- 55 Investigation of mesophase pitch derived carbons for high-energy supercapacitors
- 56 XPS study of nitrogen containing templated carbons for supercapacitors
- 57 Dilatometric study of lithium intercalation into graphite
- 58 Impedance spectroscopy on porous materials: A review and application to the study of graphite electrodes for lithium-ion-batteries
- 61 **THE ELECTROCHEMISTRY LABORATORY**
- 65 Structure
- 67 ECL-Personnel
- 68 Awards
- 69 Dissertations
- 70 Exchange Students
- 71 Seminars, Invited Speakers
- 73 Conferences, Workshops
- 74 Review Activities
- 75 Industrial Partners

77 Documentation

List of Projects, Teaching Activities, Contributions to Scientific Journals, Conferences, Patent Applications and Memberships

# EDITORIAL

According to the laboratory's philosophy, we carry out research and development of electrochemical energy conversion and storage systems at the materials, cell, and systems level. This comprehensive approach in the area of fuel cells, batteries, and supercapacitors is well esteemed by our industrial partners as well as by other companies and research laboratories. It also serves as a guideline for the education of our PhD-students and co-workers. Transfer of know-how from our laboratory to industry may also include transfer of people, either within a joint project or due to the fact that our people fit well into R&D needs and interest of companies. In this sense, the past year 2006 was a very successful one. Several of our young scientific co-workers and PhD-students, who finished their thesis during this year, were hired by prominent companies being active in research and development of electrochemical energy conversion and storage devices.

At the end of the year 2006 a minor reorganization of the laboratory took place, namely the integration of the Nanocat and SLS IR-Beam Line projects into the Supercapacitor Group. Starting January 1, 2007, this group will be renamed Interfaces and Capacitors Group. In a good tradition, the four research groups Fuel Cells, Fuel Cell Systems, Batteries, and now Interfaces and Capacitors will carry on the work as successfully as during the past years.

Within the present Annual Report 2006 of the Electrochemistry Laboratory, all groups communicate the progress made during the past year in various contributions. Again, topics range from materials development for the different electrochemical systems to the development of novel characterization methods adapted to the respective electrochemical system, i.e. fuel cell, battery, or capacitor. The success of our continuous efforts is well documented in our list of numerous peer reviewed publications, invited contributions to conferences, and talks and poster presentations at various conferences and workshops worldwide

With a fine tradition, the Electrochemistry Laboratory organized successfully a One-Day-Symposium with international participation. The 22<sup>nd</sup> One-Day-Symposium took place on May 11, 2006, addressing the subject of "Electrochemistry in Biology and Medicine", with contributions from R. Dutzler (University of Zürich, CH), P.L.T.M. Frederix (University of Basel, CH), P. Kern (EMPA Thun, CH), C. Ritter (Roche

Diagnostics GmbH, AT), S. Terrettaz (EPF Lausanne, CH), and R. Thull (University of Würzburg, DE), covering topics of electrochemical sensors in medicine, various methods of electrochemical investigations of ion transport across cell membranes, and the interaction of cells with micro- and nano-structured solid surfaces.

With great expectations, we look forward to the 23<sup>rd</sup> Symposium, which will take place on May 3, 2007, addressing the topic of "Electrocatalysis".

Again, we consider the past year 2006 a successful one. We will continue our effort to further contribute to the field of Electrochemistry and transfer our know-how to industrial partners as well as to support education of students and young scientists. Our work is carried out in the extended context of a sustainable energy development, within Paul Scherrer Institut and the Domain of the Swiss Federal Institutes of Technology

Günther G. Scherer



# SCIENTIFIC CONTRIBUTIONS 2006

FUEL CELLS

CATALYSIS



## INVESTIGATING THE KINETICS OF THE $H_{UPD}$ REACTION ON PLATINUM ELECTRODES

A. Reiner, T. Pajkossy<sup>1</sup>, H. Kuhn,  
A. Wokaun, G.G. Scherer  
+41(0)56 310 5165  
[andreas.reiner@psi.ch](mailto:andreas.reiner@psi.ch)

The Under Potential Deposition of Hydrogen ( $H_{UPD}$ ) is frequently used to quantitatively determine the electrochemically active Pt surface in polymer electrolyte fuel cells (PEFCs). A better knowledge about this reaction could possibly help in the understanding of the existing limitations and, as a consequence, directing efforts to evaluate the optimal Pt utilization in PEFC electrodes.

### Experimental

The experimental set-up and conditions have been described in detail in [1,2]. Pt electrodes with roughened- and feather-like morphology, prepared as reported in [3,4], were investigated.

### Results and Discussion

In order to extract kinetic parameters of the  $H_{UPD}$  reaction from impedance data [2], an equivalent circuit has to be designed. This circuit has to fulfill the following requirements: i) as few elements as possible, and ii) the exclusive incorporation of elements, which can be connected to a physical or chemical process.

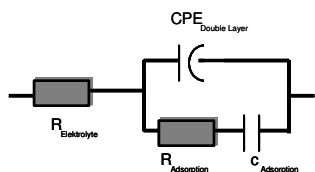


**Fig. 1:** Equivalent circuit, including an electrolyte resistance ( $R_{Electrolyte}$ ), a constant phase element for the double layer capacity ( $CPE_{Double\ Layer}$ ), a resistance for the hydrogen adsorption ( $R_{Adsorption}$ ), and a capacitor for adsorption ( $C_{Adsorption}$ ).

The equivalent circuit shown in figure 1 is the simplest one, representing the system under investigation and fulfils the above mentioned requirements. The resistance  $R_{EI}$  is associated to the ohmic resistance of the electrolyte, the constant phase element  $CPE_{DL}$  to the electrode-electrolyte double layer charging, the resistance  $R_{Ad}$  to the hydrogen adsorption step, and the capacitor  $c_{Ad}$  to the adsorption capacitance.

For electrodes with roughened and feather-like morphology, the upper diagram of figure 2 shows a linear dependence of the adsorption resistance on the applied potential [5]. As can be seen from Tab. 1, the corresponding exchange currents  $j_0$  are quite high, even compared to the *fast*  $H_2/H^+$  reaction in

1 M  $H_2SO_4$  on Pt, which yields values in the range of  $0.001\text{ A}\cdot\text{cm}^{-2}$ .

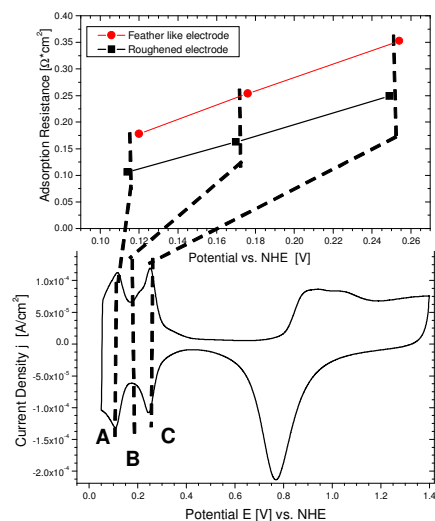


**Fig. 2:** Upper diagram: Dependence of the adsorption resistance on electrode potential. Lower diagram: Pt electrode cyclic voltammogram in 0.5 M  $H_2SO_4$ .

**Table 1:** Exchange current densities of the  $H_{UPD}$  reaction for electrodes with roughened and feather like morphology at different potentials, as described in the text.

Potential position	Exchange Current Density $j_0$ [ $A\cdot\text{cm}^{-2}$ ]	
	roughened	feather like
A	0.24	0.14
B	0.16	0.10
C	0.10	0.07

### Conclusions

Pt electrodes with roughened- and feather-like morphology allow to measuring the  $H_{UPD}$  adsorption resistance at different potentials. The determined values are quite low, and, therefore, the corresponding exchange current densities are high. This data may serve as a baseline for the respective characterization of Pt/solid electrolyte interfaces. In conclusion, due to the fast kinetics of  $H_{UPD}$  transport limitations are expected for such an interface.

### References

- [1] A. Reiner, B. Steiger, G.G. Scherer, A. Wokaun, *J. Power Sources* **156**, 28 (2006).
- [2] A. Reiner, H. Kuhn, A. Wokaun, G.G. Scherer, *PSI Electrochemistry Laboratory Annual Report 2005*, 47 (2006), ISSN 1661-5379.
- [3] A. Reiner, B. Steiger, G.G. Scherer, A. Wokaun, *PSI Scientific Report 2004*, **V**, 107 (2005).
- [4] X. Wei, A. Reiner, A. Wokaun, G.G. Scherer, this report.
- [5] A. Reiner, H. Kuhn, T. Pajkossy, A. Wokaun, G.G. Scherer, in preparation.

<sup>1</sup> Institute of Materials and Environmental Chemistry, Hungarian Academy of Science, Budapest, Hungary

# ELCTROCHEMICAL SURFACE RESHAPING OF POLYCRYSTALLINE PT: MORPHOLOGY AND CRYSTALLOGRAPHY

X. Wei, A. Reiner, E. Müller, A. Wokaun,  
G.G. Scherer  
+41(0)56 310 2474  
[xun.wei@psi.ch](mailto:xun.wei@psi.ch)

Thermally or potentially induced surface reconstruction has been observed on clean metal surfaces. If the rearrangement of surface atoms goes much further than atomic spacings, macroscopic changes, which are called surface reshaping, could happen to the surface morphology [1]. A drastic morphologic change was observed on the Pt electrode surface after electrochemical activation. The results of TEM investigation for the so called "Pt feathers" are presented here.

## Experimental

The preparation of the Pt disc electrode was reported before [2]. Cyclic voltammetry (CV) was carried out in 0.5 M sulfuric acid electrolyte using a conventional 3-electrode cell, including a Pt mesh counter electrode and normal hydrogen reference electrode (NHE). Electrochemical activation was done by cycling the electrode between 0.05 and 1.20V at a scan rate of 200 V/s. TEM characterization was carried out using a Philips CM 30 system.

## Results and Discussion

As reported before, electrochemically roughening of the Pt electrode surface leads first to the formation of some crystalline islands and then to rod like structures of about 1~3  $\mu\text{m}$  in length, which finally developed into a feather like morphology (FLM) with finer structures at nanometer scale [2]. An XPS study indicated that the feather structure is composed of Pt(0). SEM and TEM investigations provided both the morphologic details and crystallographic information. As shown in figure 1, the finer structures include a backbone, which is the central part of the FLM (marked with a dashed line), and needles, which grow around the side of the backbone (indicated by arrows).

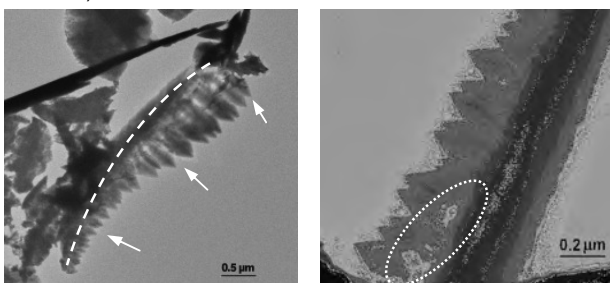


**Fig.1:** TEM image of a Pt FLM: overview (left);  
**Fig.2:** Part of a FLM with needles far from the backbone tip (right).

Near the backbone tips, needles are relatively small (100~200 nm in length) and tightly bound to the

backbone, while away from the tips, needles become bigger (up to  $\sim 1 \mu\text{m}$ ) and tend to break away from the backbone (marked with a cycle in figure 2). Both the backbones and the needles have even finer sub-structures (see figure 3, left). If a needle is given enough space to grow, its central part could develop into a secondary backbone, and the saw-like structure around the center could become secondary needles. This might be due to the step-wise development of this surface reshaping, which is further proved by the laminar structure between the backbone and the needles (figure 3, right).

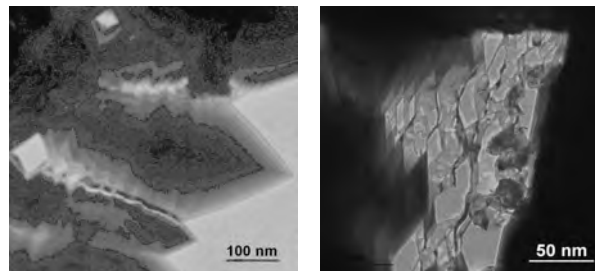


**Fig. 3:** Finer structure of a needle (left); laminar structure between needles and a backbone (right).

Electron diffraction analysis showed that most of the needles have identifiable crystallographic orientations (figure 4, left), and all needles of a feather aligned in one row appear to have the same crystal orientation; while the backbones present complicated ED patterns which are difficult to be interpreted so far (figure 4, right).

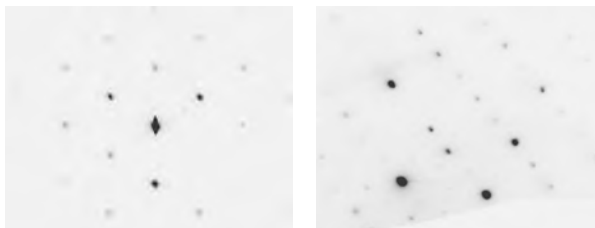


**Fig.4:** Electron diffraction patterns of one Pt FLM: needles (left) and backbone (right).

## Conclusions

The process of the Pt FLM formation is started from backbones in the form of small rods; and then needles start to grow around the backbones; later full-fledged needles tend to detach from the feather, which gives rise to the holes developed between the backbone and the ripe needles. Step-wise growth is observed in both backbones and needles. Most of the needles have identifiable crystallographic orientations, while the ED results of the backbones indicate a complicated growth process.

## References

- [1] A.S. Dakkouri, D.M. Kolb, in: A. Wieckowski (Ed.) Interfacial Electrochemistry, Marcel Dekker, 151 (1999).
- [2] A. Reiner, B. Steiger, G.G. Scherer, A. Wokaun, PSI Scientific Report 2004/Volume V, 107 (2005) ISSN 1423-7342.

## ON THE MEASUREMENT OF THE HYDROGEN UNDERPOTENTIAL DEPOSITION IN PEFCs

I.A. Schneider, A. Wokaun, G.G. Scherer  
+41(0)56 310 2795  
[ingo.schneider@psi.ch](mailto:ingo.schneider@psi.ch)

A high utilization of the platinum based catalysts used in polymer electrolyte fuel cell (PEFC) electrodes is important to keep the precious metal loading at low levels. The electrochemically available surface area (ECA) is used here as a quantitative measure to determine the catalyst utilization at anode and cathode of a PEFC. The ECA is determined using cyclic voltammetry (CV) in  $H_2/N_2$  operation mode of the cell [1].

Yet, an important aspect in  $H_{upd}$  measurements is the formation and re-oxidation of molecular hydrogen during the sweep. These reactions occur at low positive potentials, which overlap with the  $H_{upd}$  region and hamper an accurate determination of the ECA. In this context, one of the most important experimental parameters not scrutinized in the literature to date is the inert gas flow rate. In this work, we have investigated and characterized the peculiarities of voltammetric measurements in PEFCs associated with the convective nitrogen gas flow along the gas flow channels of the working electrode using a novel experimental technique. The method combines the use of sectioned gas diffusion electrodes with local voltammetric measurements in PEFCs [2].

### Experimental

The voltammetric measurements were performed in a nine-fold segmented linear PEFC ( $A_{cell}=63cm^2$ ) described elsewhere [3]. The electrodes of the outlet segment (seg. 9) can be operated in different modes, independently from the upstream segments (seg. 1-8). The MEA was manufactured using ETEK ELAT V2.1 gas diffusion electrodes (0.6mg Pt/cm<sup>2</sup>, 20wt% Pt/C) and a Nafion 112 membrane, using 250 $\mu$ m thick PTFE gaskets. For the CV measurements the working electrode (WE) was purged with fully humidified nitrogen gas using flow rates of  $V_{N_2}=0, 40, 100$  and 200 ml/min. Fully humidified hydrogen was fed with a constant gas flow rate of  $V_{H_2}=200$  ml/min to the other electrode serving as both counter and reference electrode. The voltammograms were recorded in a potential range of  $E=50mV-450mV$  using a sweep rate of  $v=20mV/sec$  at a cell temperature of  $T_{cell}=25^\circ C$ .

### Results and Discussion

The integral CVs of the cell are shown in figure 1 as a function of  $N_2$  gas flow rate  $V_{N_2}$ . The voltammogram at  $V_{N_2}=0ml/min$  exhibits a "butterfly like" shape. Yet, as a consequence of increasing gas flow rate, the cathodic hydrogen evolution current increases, whereas the hydrogen re-oxidation current disappears ( $E<80mV$ ).

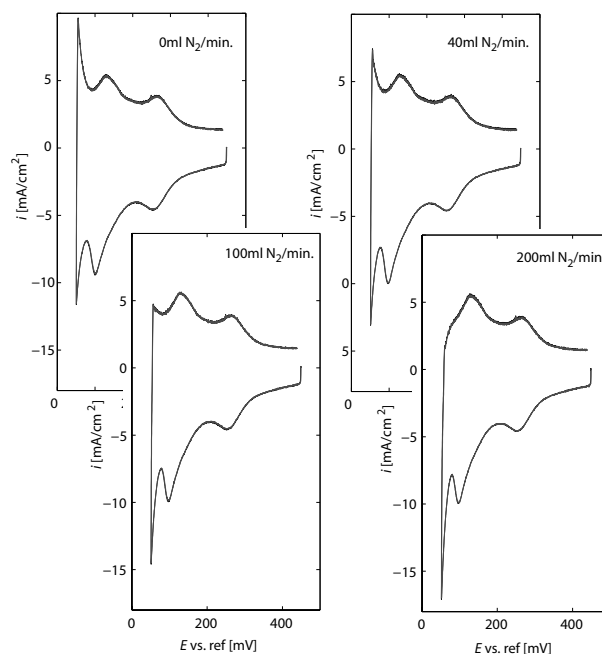


**Fig. 1:** Integral CVs of the linear PEFC at different  $N_2$  flow rates. The voltage sweep was applied to the overall cell.

The formation of molecular  $H_2$  at positive potentials (figure 1) is often subject to confusion. However, molecular  $H_2$  will be formed or oxidized at the working electrode at any given potential until the equilibrium activity as stated by the Nernst equation is reached.

Consequently, during CV measurements the  $H_2$  evolution current increases towards lower positive potential values. In a closed system ( $V_{N_2}=0ml/min$ ) molecular  $H_2$ , formed in the hydrogen reduction reaction, accumulates in the working electrode compartment and is re-oxidized in the anodic scan ("butterfly like" shape).

Yet, this is different in an open system ( $V_{N_2}>0ml/min$ ), where  $H_2$  is continuously removed from the system. The removed  $H_2$  must be compensated by formation of molecular  $H_2$  at the working electrode. This causes an additional cathodic current  $i_{H_2}$  in both the cathodic and the anodic sweep, which increases with the  $N_2$  gas flow rate. Consequently, the overall increasing cathodic current and the decreasing anodic current at  $E<80mV$  (figure 1) must be attributed to this effect, which is demonstrated in the experiment in figure 2.

In this experiment the potential sweep was performed solely in the upstream segments (seg. 1-8), whereas the outlet segment was operated at a constant potential of  $E=450mV$  to oxidize molecular hydrogen removed from segments 1-8 by the convective gas flow. The resulting  $H_2$  oxidation current is shown in figure 2a ( $i_{H_2}=-I_9/A_{1-8}$ ). The impact of the inert gas flow onto the voltammograms is greatly diminished after subtracting  $i_{H_2}$ , resulting in nearly congruent voltammograms (figure 2b).

The effects observed at low potentials in the integral voltammograms are actually the result of spatial inhomogeneities along the flow field caused by the flow of inert gas [4].

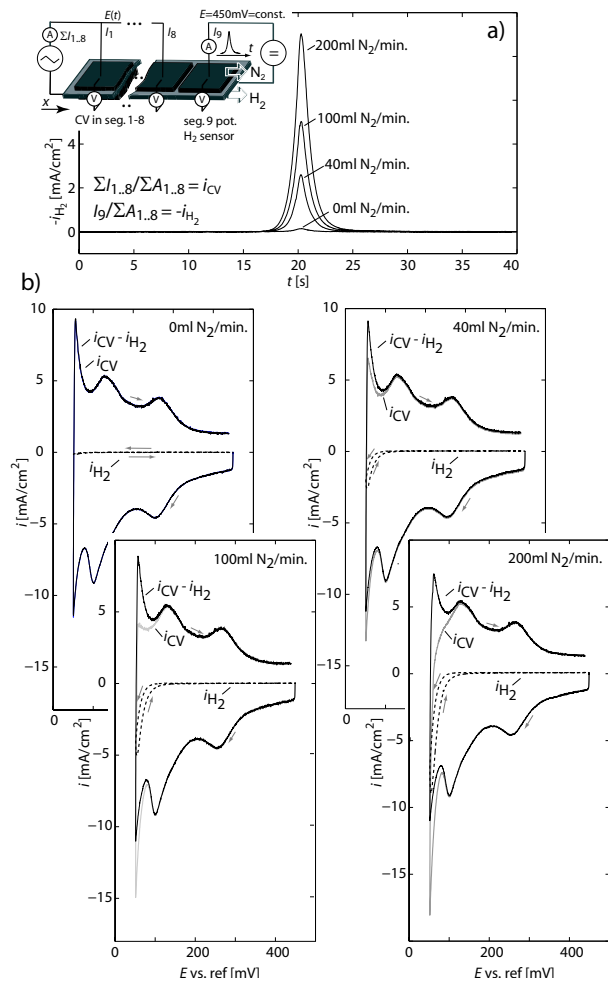


**Fig. 2:** a)  $H_2$  oxidation current  $-i_{H_2}=I_g/A_{1..8}$  ( $A$ : cell area) and, b) Integral CV of seg. 1-8 ( $i_{cv}$  vs.  $E$ ) and respective CV compensated for  $i_{H_2}$  caused by  $N_2$  gas flow ( $i_{cv}-i_{H_2}$  vs.  $E$ ).

As shown in figure 3 a large number of inlet segments exhibit high cathodic  $H_2$  reduction currents as a result of inert gas flow ( $V_{N_2}>0\text{ml/min}$ ) and low hydrogen activity in the gas phase (Fig 3b). The local cathodic hydrogen reduction currents decrease with increasing segment number as molecular hydrogen is formed in the  $H_2$  reduction reaction and accumulates in the nitrogen gas downstream the flow field (figure 3b). Finally, the local net flux of hydrogen approaches zero and overall, no hydrogen is added to or removed from a segment. As an important result, this segment and, of course, all segments of the cell downstream to this point almost show the “butterfly like” characteristic observed for the closed system (figure 3a). This effect is illustrated by the experiment shown in figures 3c, 3d.

In case A molecular  $H_2$  formed in segments 1-8 can accumulate in the inert gas. As a result, the voltammogram of the outlet segment at  $V_{N_2}=200\text{ml/min}$  (figure 3d) is virtually equal to the respective voltammogram for  $V_{N_2}=0\text{ml/min}$  (case A in figure 3c). In mode B no molecular hydrogen will accumulate and as a result of low hydrogen activity in the gas phase ( $V_{N_2}=200\text{ml/min}$ ) the voltammogram of the outlet segment (case B in figure 3d) exhibits high cathodic  $H_2$  reduction currents.

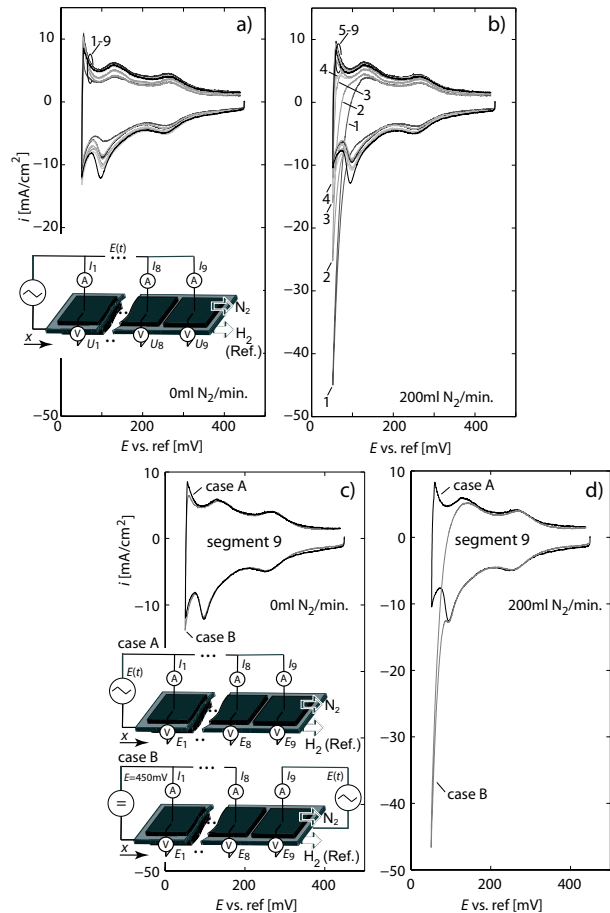


**Fig. 3:** a, b) Local CV of seg. 1-9 and, b, c) Effect of  $H_2$  formation and accumulation in segments 1-8 on the local CV of the outlet segment (seg. 9).

## Conclusions

The results reveal that the convective flow of inert gas usually employed in  $H_{upd}$  measurements in PEFCs leads to high cathodic hydrogen reduction currents in both the cathodic and the anodic sweep at lower positive potential values during the sweep and strong spatial inhomogeneities. The flow of inert gas should be minimized or even stopped during the measurement to allow molecular hydrogen to accumulate at the working electrode and to provide uniform reaction conditions along the flow field.

## References

- [1] S.S. Kocha, in Handbook of Fuel Cells, Wiley **3(3)**, 538 (2003).
- [2] I.A. Schneider, D. Kramer, A. Wokaun, G.G. Scherer, submitted (2006).
- [3] I.A. Schneider, D. Kramer, A. Wokaun, G.G. Scherer, Electrochem. Commun., accepted (2007).
- [4] I.A. Schneider, H. Fuchs, L. Gubler, A. Wokaun, G.G. Scherer, PSI Electrochemistry Laboratory Annual Report 2005, 8 (2006) ISSN 1661-5379.

## PREPARATION OF CORE-SHELL PLATINUM-COBALT ELECTRO-CATALYSTS FOR OXYGEN REDUCTION

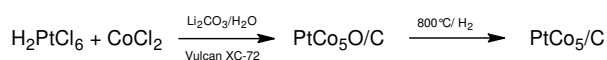
H. Schulenburg, A. Wokaun, G.G. Scherer  
+41(0)56 310 2125  
[hendrik.schulenburg@psi.ch](mailto:hendrik.schulenburg@psi.ch)

Among others, the commercialization of polymer electrolyte fuel cells for automotive applications is hindered by the high costs of Pt-based electro-catalysts [1]. Due to the sluggish kinetics of the oxygen reduction, most of the platinum is needed at the fuel cell cathode. The highest platinum mass activities are obtained with carbon supported platinum-cobalt catalysts, which consist of a cobalt rich core (PtCo<sub>5</sub>) and a platinum rich shell [2]. The preparation involves the deposition of a platinum monolayer on PtCo<sub>5</sub> nanoparticles by copper under potential deposition with subsequent displacement by platinum. The preparation of larger amounts of this catalyst doesn't seem to be straightforward, because of the cumbersome deposition of the platinum monolayer.

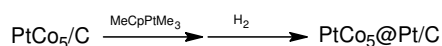
An alternative preparation route for platinum cobalt core-shell catalysts is presented here. A gas phase reaction is used for the preparation of the platinum monolayer onto carbon supported PtCo<sub>5</sub> nanoparticles.

### Experimental

PtCo<sub>5</sub>/C is prepared by basic hydrolysis of hexachloroplatinic acid and cobalt chloride in the presence of carbon black, followed by reduction and alloy formation at elevated temperatures.



According to STEM images, the particle size of the supported PtCo<sub>5</sub> nanoparticles is typically 3-10nm. Methylcyclopentadienylplatinum(IV)trimethyl (MeCpPtMe<sub>3</sub>) is used for the deposition of platinum onto PtCo<sub>5</sub> nanoparticles. More than one platinum layer can be deposited by repeating the reaction of PtCo<sub>5</sub> with MeCpPtMe<sub>3</sub> and reduction by hydrogen.



### Results and Discussion

Uncoated PtCo<sub>5</sub> nanoparticles show a fast dissolution of Co<sup>2+</sup> during cyclic voltammetry. After coating the particles four times with Pt, the dissolution of Co<sup>2+</sup> is stopped. This indicates that the PtCo<sub>5</sub> nanoparticles are covered with platinum and the Co-rich core is protected from dissolution. Rotating disc electrode measurements show an increase of the catalytic activity after the coating of PtCo<sub>5</sub> with platinum from MeCpPtMe<sub>3</sub> (figure1).

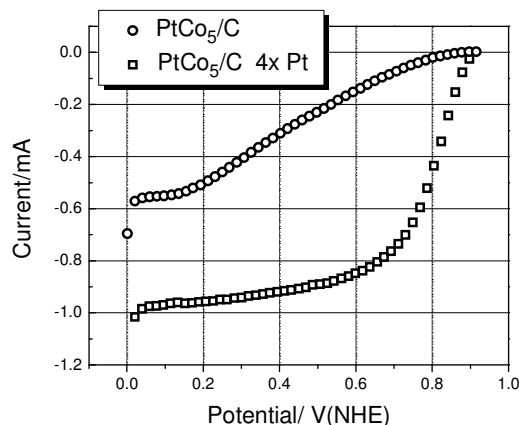


**Fig. 1:** Polarization curves of PtCo<sub>5</sub>/C before and after fourfold deposition of platinum. Anodic going scans, oxygen saturated 0,1M HClO<sub>4</sub>, 1600rpm, 5mV/s, room temperature, 0.02mg catalyst per electrode.

ICP-AES analysis of the fourfold coated catalyst gave a stoichiometry of PtCo<sub>0,4</sub>/C with a platinum loading of 44%. This corresponds to a mass activity of 31mA/mg<sub>Pt</sub> at 0,9V (RHE). The surface specific activity, determined by using the H<sub>upd</sub> area in the corresponding cyclic voltammogram, is 236μA/cm<sup>2</sup><sub>Pt</sub>, which is slightly higher compared to commercial Pt/C catalysts [1, 3]. The mass activity is below average commercial Pt/C catalysts. The determined stoichiometry of PtCo<sub>0,4</sub>/C and platinum deposition experiments on pure Vulcan XC-72 show that the metal is not only deposited on PtCo<sub>5</sub> nanoparticles, but also on the carbon support. This unwanted side reaction seems to be responsible for the moderate mass activity of the catalyst.

### Conclusions

Preparation of platinum cobalt core-shell catalysts for the oxygen reduction is possible, using a straightforward gas phase reaction. However, platinum is also deposited onto the carbon support. This has a negative impact on the mass activity of the catalyst. Optimized reaction conditions during the platinum deposition or the use of unsupported Co or PtCo<sub>x</sub> particles for Pt deposition may help to overcome this problem.

### References

- [1] H.A. Gasteiger, S.S. Kocha, B. Sompalli, F.T. Wagner, Appl. Catalysis **56**, 9 (2005).
- [2] J. Zhang, F.H.B. Lima, M.H. Shao, K.Sasaki, J.X. Wang, J. Hanson, R.R Adzic, J. Phys. Chem. B **109**, 22701 (2005).
- [3] U.A. Paulus, A. Wokaun, G.G. Scherer, T.J. Schmidt, V. Stamenkovic, N.M. Markovic, P.N. Ross, Electrochim. Acta **47**, 3787 (2002).

## ELECTRO-OXIDATION OF FORMIC ACID ON $\text{Bi}_2\text{PtIrO}_7$ POWDER ELECTRODES

X. Wei, A. Wokaun, G.G. Scherer  
+41(0)56 310 2474  
[xun.wei@psi.ch](mailto:xun.wei@psi.ch)

Formic acid oxidation (FAO) is considered as a model reaction for the mechanistic understanding of the electrooxidation of small organic molecules. In this report, the FAO was studied on pretreated  $\text{Bi}_2\text{PtIrO}_7$  powder electrodes. The voltammetric profiles provided kinetic insights into the FAO reaction.

### Experimental

The electrode preparation and the setup of the electrochemical measurements were introduced in Ref. [1]. The powder electrodes were reduced in Ar purged 0.5 M  $\text{H}_2\text{SO}_4$  by one cycle within different potential windows (see figure 1). Afterwards the FAO measurements were carried out in 0.5 M formic acid + 0.5 M  $\text{H}_2\text{SO}_4$  electrolyte.

### Results and Discussion

The pretreatment of  $\text{Bi}_2\text{PtIrO}_7$  electrodes to different negative potential limits is shown in figure 1. The study of methanol oxidation on the same electrodes has proved that the pyrochlore is methanol tolerant when the surface concentration of Pt(0) is lower than 23% (lower reducing limit at 0.10 V), as determined by XPS [1].

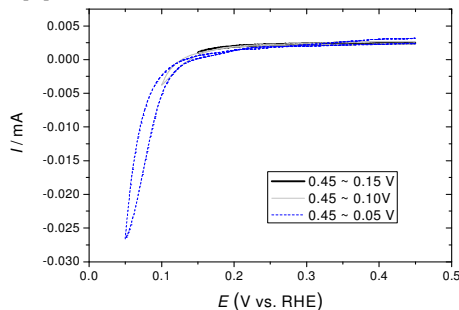


**Fig.1:** Current-potential curves for the reduction of  $\text{Bi}_2\text{PtIrO}_7$  powder electrodes to different lower vertex potentials. The scan rate was 0.5 mV/s.

FAO involves only 2 electrons. At the reduction potential windows where  $\text{Bi}_2\text{PtIrO}_7$  presents methanol tolerance (lower potential limit at 0.10 V and 0.05 V), FAO can still proceed. Most studies agree on the fact that FAO follows a dual path mechanism, which involves complete oxidation to form  $\text{CO}_2$  with a partial oxidation pathway to CO [2].

As shown in figure 2, the less reduced electrodes yield lower FAO currents. In the cathodic scan, the reaction is suppressed until the potential reaches 0.8 V, then the reaction rate is increased abruptly. The inhibition probably comes from strongly adsorbed water on the electrode at high potential range [3]. During the anodic sweep, a broad peak is detected in figure 2a and b at

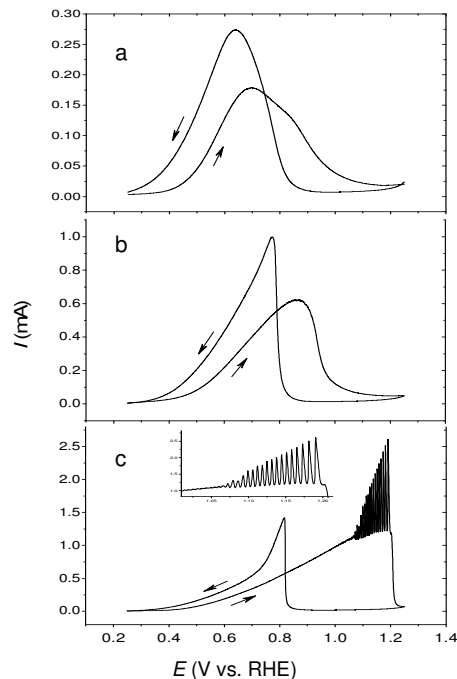


**Fig.2:** Linear sweep voltammograms of FAO on  $\text{Bi}_2\text{PtIrO}_7$  powder electrodes pre-treated at: a) 0.45 ~ 0.15 V; b) 0.45 ~ 0.10 V, c) 0.45 ~ 0.05 V. The scan rate was 10 mV/s.

0.5 V < E < 1.0 V, which is ascribed to FAO influenced by CO poisoning [4], while in figure 2c, the shift of the peak potential to ~1.2 V and the oscillatory behavior (see inserted figure) indicate that species other than CO are involved in the reaction. According to recent FAO studies, adsorbed bridge-bonded formates act as reaction blocking spectator species in FAO after the removal of CO [5]. For the less reduced electrodes, the formate adsorption is not favored due to the lack of abundant free Pt(0) sites.

### Conclusions

FAO involves less adjacent Pt(0) sites than methanol oxidation. The large difference between anodic and cathodic sweeps suggests that the electrode might become severely poisoned in the anodic sweep. The heterogeneously catalyzed dissociation of formic acid to water and adsorbed formate is a possible explanation for the observed current oscillations.

### References

- [1] N. Beck, ETH Zürich, Dissertation No. 16647 (2006).
- [2] A. Capon, R. Parsons, J. Electroanal. Chem., **45**, 205 (1973).
- [3] T. Iwasita, X.H. Xia, H.-D. Liess, W. Vielstich, J. Phys. Chem. B, **101**, 7542 (1997).
- [4] P. Strasser, M. Eiswirth, G. Ertl, J. Chem. Phys., **107**(3), 991 (1997).
- [5] Y.-X. Chen, M. Heinen, Z. Jusys, R.J. Behm, Langmuir, **22**(25), 10399 (2006).

## FUEL CELL PERFORMANCE OF PLATINUM/CARBON CO-SPUTTERED ELECTRODES

A. Reiner, A. Wokaun, G.G. Scherer  
+41(0)56 310 5165  
[andreas.reiner@psi.ch](mailto:andreas.reiner@psi.ch)

Polymer electrolyte fuel cell electrodes with a thin Pt catalyst layer localized near the membrane-electrode interface are believed to yield high Pt utilization [1]. Simultaneous deposition of Pt and C by co-sputtering creates Pt nanoparticles (1-2 nm) in a C matrix. Furthermore, this method can be used to deposit catalyst layers of several 100 nm thickness near the membrane-electrode interface [2,3].

### Experimental

The electrochemically active Pt surface was determined by Under Potential Deposition of Hydrogen ( $H_{UPD}$ ) in 0.5 M  $H_2SO_4$ . For fuel cell tests, a co-sputtered electrode, a Nafion 112 membrane, and a commercial Pt electrode (E-Tek, 0.5  $mg/cm^2$ ) were combined to form the respective membrane-electrode-assembly (MEA). The Pt loading of the co-sputtered electrodes (carbon cloth or carbon paper as substrate) was 0.075  $mg/cm^2$ .

### Results and Discussion

A large variety of specific electrochemical active surface values ( $cm^2/mg_{Pt}$ ) could be obtained by applying different sputter conditions (pressure, power) as well as by varying the thickness of the sputter layer and the substrate. Most of the co-sputtered electrodes have comparable or even superior values of the specific surface compared to the commercial electrodes, as displayed figure 1.

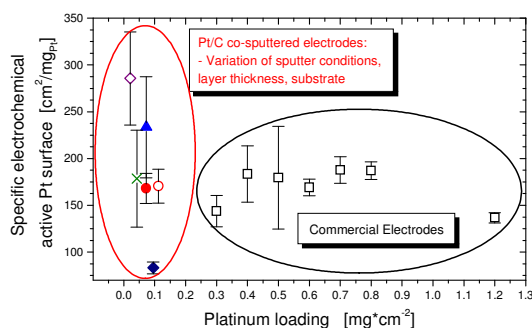


**Fig. 1:** Comparison of specific Pt surfaces of different co-sputtered and commercial E-Tek ELAT electrodes.

For first fuel cell experiments, the co-sputtered electrodes were used at the anode side. As can be seen from the results displayed in figure 2, the MEAs with a co-sputtered anode exhibit better mass activity characteristics than the conventional MEA. Furthermore, comparing the two MEAs utilizing a co-sputtered electrode, it becomes obvious that the MEA with the *ex situ* activated anode exhibits poorer performance than the MEA with the anode being activated within the fuel cell.

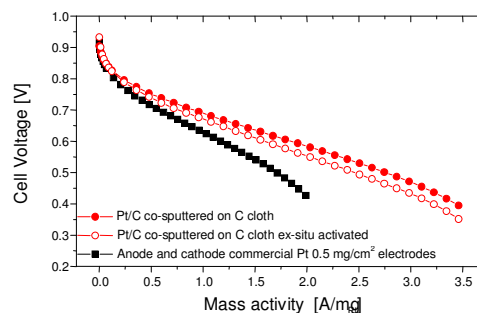


**Fig. 2:** Mass activities of a MEA with two commercial electrodes and combinations with a co-sputtered anode. Cell temperature: 80 °C,  $\lambda_{H_2}, \lambda_{O_2} = 1.5$ ,  $H_2$  humidified,  $O_2$  dry.

Alternatively, the co-sputtered electrode was placed at the cathode side. As the loading of the commercial anode exceeds that of the co-sputtered cathode by a factor of ~6, no limiting influence from the anode is to be expected. Hence, at high cell voltages the U(I) characteristics should be mainly determined by the cathode loading. The values for the cathode mass activity, as shown in figure 3, reveal that co-sputtered electrodes exhibit higher activities than the commercial combination.

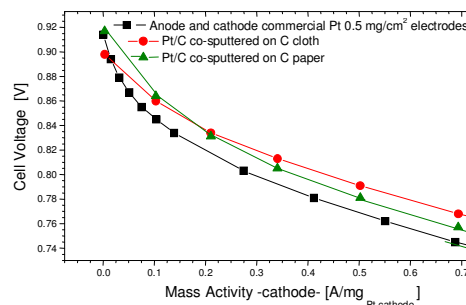


**Fig. 3:** Cathode mass activities of a conventional MEA and combinations with co-sputtered cathodes.

### Conclusions

Co-sputtering of Pt/C onto respective gas diffusion media offers the possibility to create catalyst layers, which show comparable or even superior values for the specific electrochemically active Pt surface than commercial electrodes. Moreover, first fuel cell tests reveal that co-sputtered electrodes, operating as anode or cathode, show a higher mass activity than the respective commercial electrode. Hence, this preparation method opens the possibility to utilize Pt more efficiently than in electrodes prepared by the (traditional) wet chemical process.

### References

- [1] J.O'M. Bockris, S. Srinivasan, Fuel Cells: Their Electrochemistry, McGraw-Hill, 271 (1969).
- [2] A. Reiner, W. Wei, M. Döbeli, M. Horisberger, A. Wokaun, G.G. Scherer, PSI Electrochemistry Laboratory Annual Report 2005, 46 (2006), ISSN 1661-5379.
- [3] A. Reiner, F. Hajbolouri, M. Döbeli, A. Wokaun, G.G. Scherer, Proc. 3rd European PEFC Forum, Lucerne, No. 109 (2005).

## DFT MODELING OF NI OVER $\text{Al}_2\text{O}_3(100)$ SURFACE

I. Czekaj, J. Wambach, A. Wokaun  
+41(0)56 310 4464  
[izabela.czekaj@psi.ch](mailto:izabela.czekaj@psi.ch)

The molecular structure of Ni/ $\gamma\text{-Al}_2\text{O}_3$  catalyst used during methanation of synthesis gas was investigated using DFT method with non-local functional. The several Ni-compounds such as Ni, NiO and Ni<sub>3</sub>C as well as  $\gamma\text{-Al}_2\text{O}_3$  surfaces were considered. Furthermore, geometric and electronic structure of Ni deposited on  $\gamma\text{-Al}_2\text{O}_3$  system was studied in details. The theoretical studies are presently used to help with understanding more detailed surface modifications during methanation and reasons of nickel particles detachment together with carbon whiskers formation in specific fixed bed conditions.

### Computational details

In our studies the Ni-compounds such as Ni, NiO and Ni<sub>3</sub>C as well as  $\gamma\text{-Al}_2\text{O}_3$  surfaces are modeled by clusters of different size and geometry. The electronic structure of all clusters is calculated by ab initio density functional theory (DFT) method (program code StoBe) using generalized gradient corrected functionals (RPBE) in order to account for electron exchange and correlation. Detailed analyses of the electronic structure in the clusters are carried out using Mulliken populations and Mayer bond order indices.

### Results and Discussion

The Ni/ $\gamma\text{-Al}_2\text{O}_3$  catalyst in different state of methanation consists of several Ni-compounds such as Ni, NiO and Ni<sub>3</sub>C (see figure 1), which was suggested by previous experimental studies [1, 2].

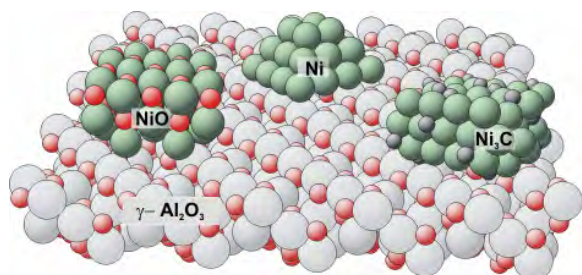


**Fig. 1:** Possible Ni- compounds at  $\gamma\text{-Al}_2\text{O}_3(100)$  surface.

Three investigated Ni-compounds were represented by clusters with more than 9 metal atoms, metallic Ni by Ni<sub>10</sub> cluster, Ni<sub>3</sub>C by Ni<sub>9</sub>C<sub>6</sub> cluster and NiO by Ni<sub>14</sub>O<sub>5</sub> cluster (see Figure 2).

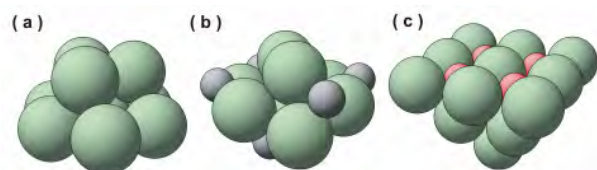


**Fig. 2:** Model of the Ni-compounds: (a) Ni<sub>10</sub> cluster for Ni (111) surface, (b) Ni<sub>9</sub>C<sub>6</sub> cluster for Ni<sub>3</sub>C(110) surface, (c) Ni<sub>14</sub>O<sub>5</sub> cluster for NiO (100) surface.

All findings about electronic structure suggest that nickel carbide is supposed to be less reactive than pure nickel or nickel oxide. Comparison of carbon monoxide adsorption at metallic Ni and Ni<sub>3</sub>C also confirms that nickel carbide is less reactive.

Figure 3 shows nickel deposition at Al<sub>15</sub>O<sub>40</sub>H<sub>35</sub> cluster, which represents (100) surface of  $\gamma\text{-Al}_2\text{O}_3$ . The nickel adsorbs at Al<sub>2</sub>O<sub>3</sub> (100) surface in hole position between surface oxygen centers with stabilization energy about 1.64eV (~37.8 kcal/mol) per Ni atom.

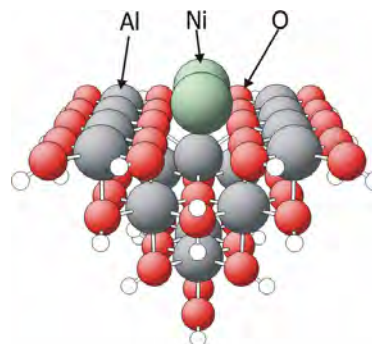


**Fig. 3:** Cluster of  $\gamma\text{-Al}_2\text{O}_3(100)$  surface with Ni-doped at hole position.

The nickel deposition influences electronic properties of Al<sub>2</sub>O<sub>3</sub> surface by modification of both oxygen and aluminum centers. Ni dopes electrons to the system, which leads to increase of negative charge of oxygen centers. Visible asymmetry in Ni deposition at Al<sub>2</sub>O<sub>3</sub> (100) surface suggests that Ni would prefer localization at AlO<sub>4</sub> tetrahedrons, which leads to local formation of NiAl<sub>2</sub>O<sub>4</sub> spinel.

### Conclusions

Comparison of electronic structure of Ni-compounds as well as adsorption of carbon monoxide suggests that nickel carbide is less reactive. Our studies of different nickel compounds and alumina support show good geometric compatibility between Al<sub>2</sub>O<sub>3</sub>, NiO and NiAl<sub>2</sub>O<sub>4</sub> systems.

Future theoretical studies of differences between electronic structure of Ni/Al<sub>2</sub>O<sub>3</sub> system and NiAl<sub>2</sub>O<sub>4</sub> spinel are planned for description of metal-support role in Ni-particle growth and detachment during methanation.

### References

- [1] I. Czekaj, F. Raimondi, J. Wambach, A. Wokaun, PSI Electrochemistry Laboratory Annual Report 2005, 42 (2006), ISSN 1661-5379.
- [2] F. Raimondi, M. Seemann, S. Biollaz, J. Wambach, A. Wokaun, PSI Scientific Report 2003, V, 116 (2004) ISSN 1423-7342.

FUEL CELLS

MEMBRANES



## MICROSTRUCTURED PROTON CONDUCTING MEMBRANES

P. Farquet, C. Padeste, S. Alkan-Gürsel,  
G.G. Scherer, H.H. Solak, A. Wokaun  
+41(0)56 310 2580  
[patrick.farquet@psi.ch](mailto:patrick.farquet@psi.ch)

Proton conducting membranes are subjected to very high mechanical stress when operated in the fuel cells [1]. Temperature, pressure, and water gradients can induce membrane tear leading to failure of the fuel cell. Selective irradiation of robust fluoropolymers through shadow masks followed by grafting of styrene and sulfonation is a promising method to obtain micro-structured proton conducting membranes with increased mechanical strength due to the shaded areas which remain un-grafted [2, 3].

### Experimental

ETFE films of 100 $\mu\text{m}$  thickness were exposed at ANKA (Angströmquelle Karlsruhe) at the LIGA3 beamline through high aspect ratio nickel shadow masks (figure 1) with 10-15 keV photons. The irradiated ETFE samples were then grafted for 16 h in a solution of 20 %<sub>vol</sub> of styrene in a 7/1 isopropanol/water solution. The grafted films were sulfonated by immersing samples in a 2 %<sub>vol</sub> chlorosulfonic acid / dichloromethane solution, then hydrolyzed overnight in a 4 g/l NaOH solution, and finally transformed into the protonated form by a 4h immersion in 2M H<sub>2</sub>SO<sub>4</sub>. The samples were dyed with methyl violet in order to visualize the microstructure definition under an optical microscope.

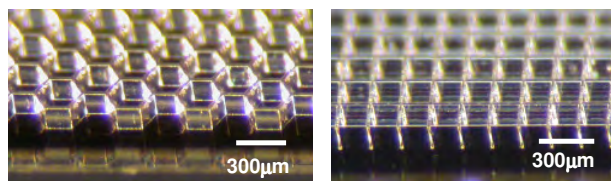


**Fig. 1:** Side view of nickel shadow masks: 85  $\mu\text{m}$  thick nickel honeycomb (left) and grid structures (right) were electroplated in a SU8 resist mold with 10  $\mu\text{m}$  structure width resulting in 93 % of open area.

### Results and Discussion

The use of synchrotron radiation coupled with the use of metallic filters enables the possibility to choose the desired photon energy range. Two requirements must be fulfilled to get well defined grafted microstructures. First, the nickel shadow masks should have a maximum of absorption within the chosen photon energy range in order to avoid any grafting in the shaded areas. Second, the ETFE base polymer should absorb only a small fraction of the delivered photons in this energy range in order to avoid radical density gradients between the front side and the rear side of the exposed films. Calculations showed that high photon absorption by the mask and homogenous grafting could be achieved with 10-15 keV photons (figure 2).

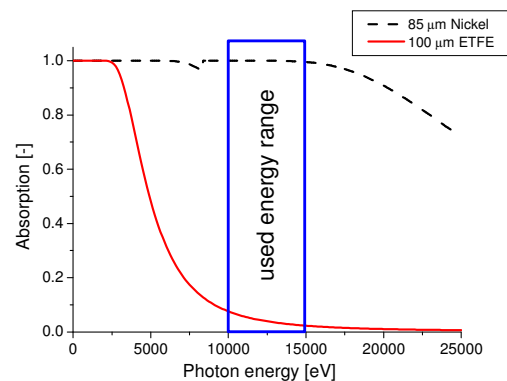


**Fig. 2:** Calculated absorption of different energy photons in 100  $\mu\text{m}$  ETFE and 85  $\mu\text{m}$  thick Ni structures.

Grafting reactions showed an increasing of degree of grafting up to 100 % with increasing dose and high conductivity. High contrast between exposed and shaded parts was observed with optical microscopy (figure 3). The pattern shapes are conserved after the irradiation, grafting, and sulfonation steps. Furthermore, we did not observe any difference in grafting density between the front side and the rear side of the exposed films.

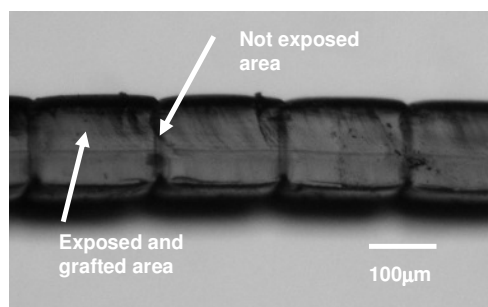


**Fig. 3:** Cross-section of a grafted, sulfonated and dyed proton-conducting membrane exposed through a 85  $\mu\text{m}$  thick Ni grid with 15  $\mu\text{m}$  features and 90% of open area.

### Conclusions

High fluence and coherence of synchrotron light allows fast exposures at LIGA beamlines through Ni shadow masks. The synthesized microstructured membranes showed clear distinction between grafted and non-grafted parts. Further characterization of the microstructured membranes with TEM and SEM are in preparation.

### References

- [1] L. Gubler, S. Alkan Gürsel, G.G. Scherer, Fuel Cells **5**, 317 (2005).
- [2] H.P. Brack, C. Padeste, M. Slaski S. Alkan, H.H. Solak, JACS **126**, 1004 (2004).
- [3] S.A. Gürsel, C. Padeste, H.H. Solak, G.G. Scherer, Nucl. Instr. Meth. Phys. Res. B **236**, 449 (2005).

## KINETIC STUDIES ON RADIATION GRAFTED MEMBRANES FOR PEFC

F. Wallasch, M. Slaski, L. Gubler,  
A. Wokaun, G.G. Scherer  
+41(0)56 310 2132  
[frank.wallasch@psi.ch](mailto:frank.wallasch@psi.ch)

Proton-conducting membranes with enhanced chemical and mechanical stability are of paramount importance for the further improvement of fuel cell performance. Enhanced chemical stability of sulfonated poly-styrene side chains, grafted into pre-irradiated backbone polymers (ETFE, FEP), can be obtained by exchanging the  $\alpha$ -hydrogen, which is prone to be radically attacked [1], by a methyl group, e.g., using  $\alpha$ -methylstyrene (AMS) as a monomer [2]. In this preparation, a co-monomer, methacrylonitrile (MAN) is employed [3]. The use of only small amounts of divinylbenzene (DVB) as a crosslinking agent leads to extended lifetimes of the resulting membranes in fuel cells. The influence of crosslinker on the grafting kinetics and its influence on the properties of the AMS/MAN grafted membranes is not well understood. A simplified kinetic approach [4] was used to study the time dependence of the degree of grafting ( $X_G$ ) of the grafting reaction of an AMS/MAN mixture, without as well as with crosslinker (0.5 % (v/v) DVB).

### Experimental

The grafting reactions were carried out at 50 °C with pre-irradiated FEP films (DuPont, thickness 25  $\mu\text{m}$ , dose 25 kGy) in isopropanol and 20 % water, using 30 % (v/v) of the monomers in a molar ratio  $R_m$  of AMS to MAN of 1.5. In the case of crosslinking, DVB (0.5 %, v/v) was added to the solution. The reactions were stopped after different times and the degree of grafting was calculated from the mass change.

$$X_G = \frac{m_{\text{grafted}} - m_{\text{irrad.}}}{m_{\text{irrad.}}} \cdot 100\%$$

The reaction profiles ( $X_G$  versus time) were fitted with a simplified kinetic model, which neglects changes in concentrations and reaction rates during the reaction, termination by chain transfer, and the presence of inhibitors or radical scavengers. The used fitting equation (see below) was obtained after mathematical evaluation and simplification from the terms for the rate of termination  $r_t$  of polymer based radicals  $P\cdot$  and the rate of polymerization  $r_{p0}$  as changes of  $X_G$ .

$$X_G = \frac{r_{p0}}{\gamma} \ln(1 + \gamma(t - t_0)) = P1 \cdot \ln(P2 + P3 \cdot t)$$

For the fitting, the parameters  $P1 = r_{p0} / \gamma$ ,  $P2 = (1 - \gamma t_0)$ , and  $P3 = \gamma$  were estimated by at least 100 iterations.

## Results and Discussion

The data points and the fitted curves are shown in figure 1 and the calculated reaction rate constants summarized in table 1.

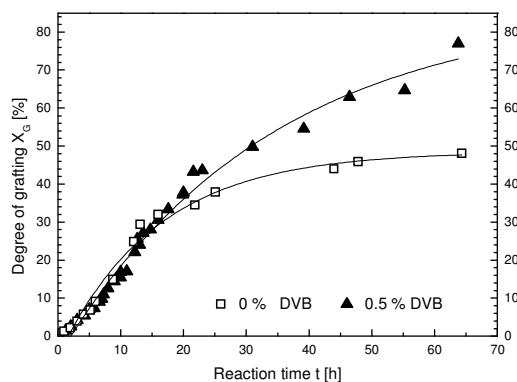


**Fig. 1:** Reaction profiles of the uncrosslinked and the crosslinked (0.5 % DVB) poly (AMS-co-MAN) grafted films

	$r_{p0} / \text{t}^{-1}$	$t_0 / \text{h}$	$\gamma / \text{t}^{-1}$
0 % DVB	5.24	1.60	0.30
0.5 % DVB	2.91	2.16	0.06

**Table 1:** Calculated reaction parameters.

The initial polymerization rate  $r_{p0}$  decreases upon the addition of the crosslinker, while the delay time  $t_0$  increases. According to the grafting front mechanism [5], the crosslinker impedes the penetration of the monomers into the film by reducing the swelling and therefore the diffusion within the film. The radical lifetime  $\gamma$  drops by using DVB, which may be due to the lower probability of crosslinked chains for termination by recombination.

### Conclusions

The kinetics of the graft polymerization reactions in the presence or absence of 0.5 % DVB, respectively, can be approximated by this simplified model. The temperature dependence of the grafting process and the related chain length distribution, the chemical constitution of the grafted polymer, e.g., the distribution of the monomers over the film thickness, and the influence of crosslinking on the properties of the membranes are the subject of the ongoing work.

### References

- [1] A. Pachenko, H. Dilger, E. Möller, T. Sixt, E. Roduner, *J. Power Sources* **127**, 325 (2004).
- [2] L. Gubler, M. Slaski, A. Wokaun, G.G. Scherer, *Electrochem. Commun.* **8**, 1215 (2006).
- [3] M. Slaski, Dissertation ETH Zürich, Nr. 16995 (2007).
- [4] T. Rager, *Helv. Chim. Acta* **86**, 1966 (2003).
- [5] H.-P. Brack, H. G. Bührer, L. Bonorand, G.G. Scherer, *J. Mat. Chem.* **10**, 1795 (2000).

## RADIATION GRAFTED MEMBRANES BASED ON A TRIFLUOROSTYRENE DERIVATIVE

S. Alkan Gürsel<sup>1</sup>, Z. Yang<sup>1</sup>, B. Choudhury<sup>1</sup>,  
M.G. Roelofs<sup>1</sup>, G.G. Scherer  
+41(0)56 310 2797  
[selmiye.alkan@psi.ch](mailto:selmiye.alkan@psi.ch)

The synthesis of cost-competitive polymer electrolyte membranes for fuel cells by radiation induced grafting is an attractive option. Our laboratory has reported on styrene grafted poly (tetrafluoroethylene-co-hexafluoropropylene) and poly (ethylene-*alt*-tetrafluoroethylene) (ETFE) based membranes, crosslinked with divinyl benzene [1,2]. In this study, we investigated the use of a novel derivative of  $\alpha,\beta$ -trifluorostyrene ( $p\text{-CF}_2=\text{CFC}_6\text{H}_4\text{OCF}_2\text{CF}_2\text{SO}_2\text{F}$ , monomer Z), a substituted styrene monomer with protected  $\alpha$ -position, for the preparation of alternative membranes of higher chemical stability, instead of styrene [3,4].

### Experimental

Monomer Z was synthesized as described in [4]. A series of membranes was prepared by grafting of Z into pre-irradiated ETFE base film (25  $\mu\text{m}$ ) in inert atmosphere followed by hydrolysis of the sulfonyl fluoride with base. Emulsion and solution grafting methods and grafting in alcohol/water mixture were performed. The resulting membranes were characterized *ex-situ* for the identification of fuel cell relevant membrane properties, and some of them were evaluated in fuel cells.

### Results and Discussion

It was determined that higher irradiation doses and longer reaction times were required to achieve reasonable graft levels, since monomer Z has a considerably lower reactivity compared to styrene (figure 1).

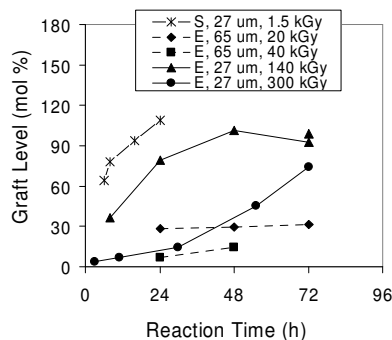


**Fig. 1:** Comparison of Z grafting by the emulsion method at 70 °C (E,) films of different thickness ( $\mu\text{m}$ ) and different pre-irradiation doses (kGy,) and styrene grafting in an alcohol/water mixture at 60 °C (S).

These membranes exhibit water uptake up to 70% and *ex-situ* conductivities, which increased with increasing graft level (table 1).

**Table1:** Membranes tested in single fuel cells characterized by fuel cell relevant properties: Graft Level (GL), Ion Exchange Capacity (IEC), Water Uptake, and *ex-situ* Conductivity

Membrane	GL (mass %)	IEC (meq/g)	Water uptake (mass%)	Conductivity (S/cm)
1	225	2.15 $\pm$ 0.05	72.2 $\pm$ 1.8	0.30 $\pm$ 0.02
2	106	1.49 $\pm$ 0.09	30.1 $\pm$ 0.1	0.08 $\pm$ 0.01
3	229	2.11 $\pm$ 0.09	71.2 $\pm$ 1.4	0.27 $\pm$ 0.04
4	104	1.29 $\pm$ 0.06	24.5 $\pm$ 0.3	0.08 $\pm$ 0.02

Over the complete current density range, the best performance was obtained for membrane #1. The ohmic cell resistance, which is mainly determined by the resistance of the membrane, is shown in lower part of figure 2. Membrane #3 exhibits the lowest membrane resistance of less than 100  $\text{m}\Omega\text{ cm}^2$  and all other membranes have lower area resistances than Nafion® 112 (figure 2).

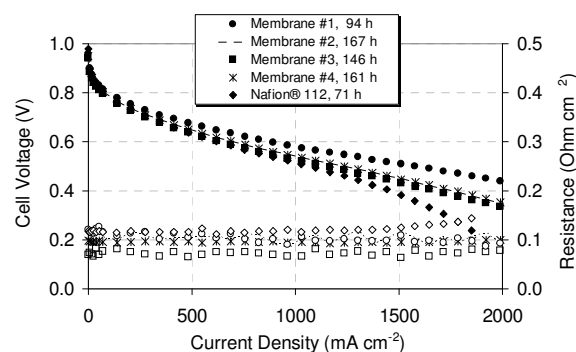


**Fig. 2:** Single cell performance of radiation grafted membranes based on the monomer Z compared with Nafion® 112. Electrodes: E-TEK 0.6  $\text{mg cm}^{-2}$ , cell temperature 60 °C, reactants  $\text{H}_2/\text{O}_2$ :1.5/9.5, pressure 1  $\text{bar}_a$ , gases fully humidified.

### Conclusions

Despite the relatively high pre-irradiation dose used during the preparation of the membranes and in addition excluding hot pressing (to improve the contact between membrane and electrodes), Z based membranes exhibited comparable or better performance than Nafion® 112 membranes in fuel cells.

### References

- [1] L. Gubler, S.A. Gürsel, G.G. Scherer, Fuel Cells 5, 317 (2005).
- [2] L. Gubler, N. Prost, S.A. Gürsel, G.G. Scherer, Solid State Ionics 176, 2449 (2005).
- [3] Z. Yang, M.G. Roelofs, S. Alkan Gürsel, G.G. Scherer, WO Pat. 2006102672 A1 (2006).
- [4] S. Alkan Gürsel, Z. Yang, B. Choudhury, M.G. Roelofs, G.G. Scherer, J ECS 153(10), A1964 (2006).

<sup>1</sup> DuPont Research and Development, Wilmington, USA

# EFFECT OF CROSSLINKER ON THE FUEL CELL PERFORMANCE OF STYRENE GRAFTED POLY (ETHYLENE-*ALT*-TETRAFLUOROETHYLENE) BASED MEMBRANES

H. Ben youcef, S. Alkan Gürsel, M. Arcaro, L. Gubler, A. Wokaun, G.G. Scherer  
+41(0)56 310 4188  
[hicham.ben-youcef@psi.ch](mailto:hicham.ben-youcef@psi.ch)

Poly(tetrafluoroethylene-*co*-hexafluoropropylene (FEP) based membranes developed at PSI by the radiation grafting process were optimized in a previous study for their fuel cell performance. Thereby, the membrane prepared with 10% divinylbenzene (DVB) as the crosslinker was found to exhibit optimum performance [1]. In this study, the influence of the DVB concentration on the fuel cell performance of related radiation grafted membranes, however based on poly(ethylene-*alt*-fluoroethylene) ETFE, has been studied.

## Experimental

ETFE (25  $\mu\text{m}$ ) based membranes were prepared in the presence of styrene and DVB with a fixed degree of grafting (DOG) of 25%, as described previously [2]. Selected membranes with different DVB concentration in the initial grafting solution (0%, 5%, 8%, 10%, and 15%) were tested in single fuel cells up to 160h. Membranes were hotpressed with electrodes (E-TEK/Pt: 0.5  $\text{mg}/\text{cm}^2$ ) to form membrane electrode assemblies (MEA). Membranes were tested *ex situ* for their fuel cell relevant properties. The *in situ* characterization of the MEAs was carried out by means of current-voltage measurements and electrochemical impedance spectroscopy.

## Results and discussion

The ion exchange capacity (IEC) for the crosslinked ETFE based membranes with different DVB concentrations and the *ex situ* conductivity at room temperature in the fully water swollen state were determined.

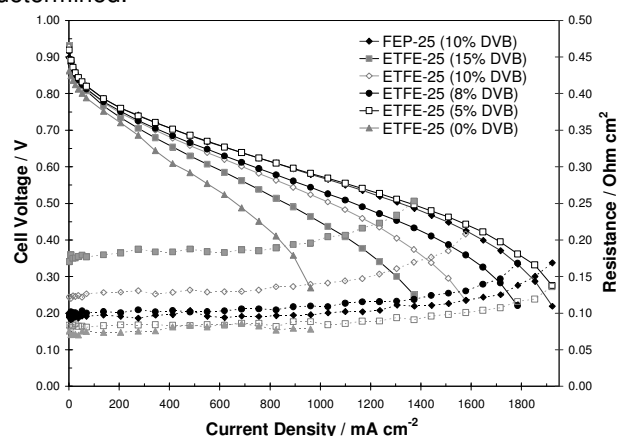


**Fig. 1:** Single cell performance using radiation grafted membranes based on ETFE with different DVB concentrations, compared to standard FEP based

membrane. Cell temperature 80 °C, reactants  $\text{H}_2/\text{O}_2$  stoich. of 1.5/1.5.

There is no significant change in IEC of the membranes up to 15% DVB concentration. In fact, the observed values were around 1.7 meq/g for the membranes up to 10% DVB, while a slight decrease was measured for 15% with value of 1.6 meq/g.

The conductivity decreases with increasing DVB concentration up to 15% DVB. Indeed, the obtained value for the uncrosslinked membrane was ~100 mS/cm, and then the measured values dropped to 62, 31, 26, and 29 mS/cm for the membranes with 5, 8, 10, and 15% DVB, respectively.

The membrane electrode assembly (MEA) performance data in single cells and the ohmic resistance of (crosslinked) ETFE membranes (0%, 5%, 8%, 10%, and 15% DVB in grafting solution) and the standard crosslinked FEP membrane as reference are presented in figure 1. The MEA with the ETFE based membrane (5% DVB) shows a comparable performance to the FEP based membrane, whereas, the performance of MEAs with ETFE based membranes (0%, 8%, 10%, 15%) was inferior.

In order to elucidate the origin of the differences in performance, the MEAs were analysed by means of electrochemical impedance spectroscopy (EIS) and the extracted data are presented in table 1.

Film	DOG (%)	DVB (%)	$R_{\Omega}(\text{pulse})$ $\text{m}\Omega \text{ cm}^2$	$R_{\Omega}(\text{ac-imped})$ $\text{m}\Omega \text{ cm}^2$	$R_{\text{pol}}(\text{ac-imped})$ $\text{m}\Omega \text{ cm}^2$
ETFE-25	25.6	0	84	94	411
ETFE-25	25.8	5	84	95	184
ETFE-25	25.2	8	104	121	195
ETFE-25	24.1	10	136	142	193
ETFE-25	27.3	15	188	197	195
FEP-25	18.0	10	104	113	166

**Table.1:** Comparison between the ohmic resistance and the polarization resistance @0.5  $\text{A}/\text{cm}^2$ .

The ohmic resistance  $R_{\Omega}$  determined by both methods (current-pulse experiments and ac-impedance) follows the same trend and increases with the increase of the DVB content. The polarization resistance  $R_{\text{pol}}$  behaves differently with the crosslinker content. Indeed, the  $R_{\text{pol}}$  increases slightly for the membranes from 5% to 8% DVB and then no significant change is observed with further increase of the DVB content. The high  $R_{\text{pol}}$  value observed for the uncrosslinked membrane is due to the degradation occurring already after 165h of testing time.

From the results of this investigation, we can conclude that the ETFE based membranes with 5% DVB (in grafting solution) shows the best performance in fuel cells and exhibits the lowest ohmic resistance loss.

## References

- [1] T. J. Schmidt, K. Simbeck, G. G. Scherer, J. Electrochem. Soc. **152(1)**, A93 (2005).
- [2] H. Ben youcef, S. Alkan Gürsel, G. G. Scherer, A. Wokaun, PSI Electrochemistry Laboratory Annual Report 2005, 31 (2006) ISSN 1661-5379.

## FUEL CELL DURABILITY OF THE RADIATION GRAFTED PSI MEMBRANE UNDER HIGH H<sub>2</sub>/O<sub>2</sub> PRESSURE AND DYNAMIC OPERATING CONDITIONS

L. Gubler, G.G. Scherer  
+41(0)56 310 2673  
lorenz.gubler@psi.ch

The lifetime of a polymer electrolyte fuel cell (PEFC), in particular the functionality and integrity of the proton exchange membrane (PEM), is highly dependent on the operating conditions. Whereas lifetimes of 5'000 h and more can be obtained for the PSI Membrane at typical operating conditions of 80 °C cell temperature and constant load, lifetime is observed to be reduced to 3'000 h using a protocol with intermittent load changes to open circuit voltage (OCV) [1]. In order to allow qualification of different membranes and membrane electrode assemblies (MEAs) within shorter time, durability experiments using radiation grafted membranes prepared at PSI were carried out in cells of 100 cm<sup>2</sup> under harsh operating conditions over a period of 1'000 h.

### Experimental

In a 2-cell stack of technical relevance with 100 cm<sup>2</sup> active area, an MEA based on a radiation grafted PSI membrane (25 μm FEP base film, graft level 17%) and a Nafion<sup>®</sup> 112 based MEA were tested simultaneously to allow direct back-to-back comparison. The PSI membrane, being only 35 μm thick compared to Nafion<sup>®</sup> 112 (60 μm), was protected in the edge of the active area using a 25 μm Kapton<sup>®</sup> subgasket on both anode and cathode side. The stack was operated under harsh conditions using H<sub>2</sub>/O<sub>2</sub> reactants at a pressure of 2.5 bar<sub>a</sub>, and a dynamic load protocol with current density ranging from zero to 0.7 A/cm<sup>2</sup>. Cell temperature was 70-75 °C. The chemical state of the membranes was monitored by high frequency (HF) resistance measurement at 2 kHz. Degradation is associated with an increase in resistance. The separator functionality of the electrolyte membranes was assessed via intermittent electrochemical determination of H<sub>2</sub> crossover.

### Results and Discussion

The performance of the two cells in the stack was assessed periodically every week. The MEA based on the PSI membrane showed, in contrast to the Nafion<sup>®</sup> 112 cell, no performance decay after 1'129 h on test (figure1). The polarization curve is, however, merely a crude means to assess the state of the MEA. More meaningful diagnostic tools are aimed at probing the different functionalities of the electrolyte membrane: Loss of sulfonic acid groups due to chemical degradation will lead to an increase in the HF resistance of the cell. For both types of MEA, the resistance change is fairly small (after some initial increase for the Nafion<sup>®</sup> 112 cell) (Fig.2a). Yet, H<sub>2</sub> crossover shows an increase during the time on test for both MEAs, indicating slow but gradual

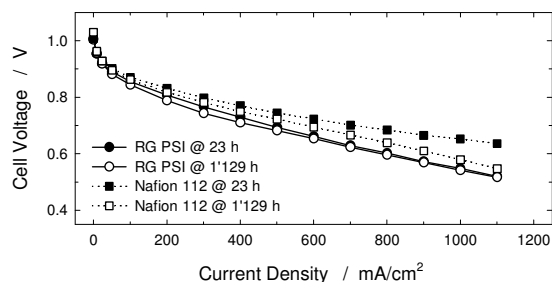


**Fig. 1:** Performance of the cell with radiation grafted (RG) PSI membrane after different operating times. Cell temperature 71-76 °C, reactants H<sub>2</sub>/O<sub>2</sub> at a stoichiometry of 1.5/1.5, gas inlet dewpoint 40 °C, pressure 2.5 bar<sub>a</sub>.

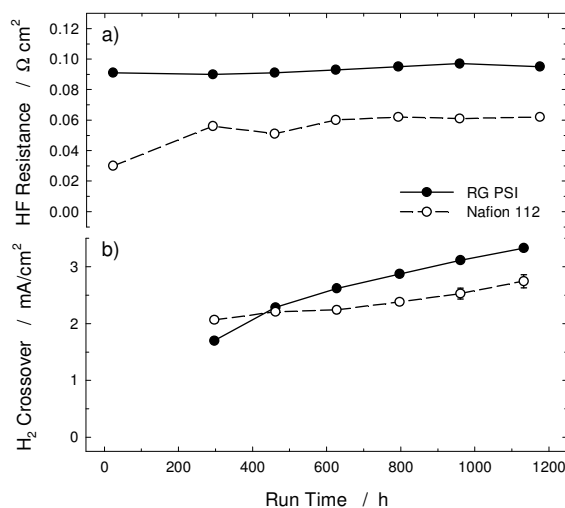


**Fig. 2:** Characterization of a) the chemical integrity of the membrane electrode assemblies by high frequency (2 kHz) resistance measurement, and b) the mechanical integrity by determination of the hydrogen crossover rate.

deterioration of the integrity of the membranes. This might be related to gradual changes in the polymer structure due to the periodic changes in the hydration state of the membrane, caused by the changes in cell current [2]. Eventually, tears or pinholes may be formed in the membrane. Although the changes in membrane integrity were small enough not to have an impact on performance during the total accumulated time on test, it is not unlikely that mechanical MEA failure might be expected at some point.

### Conclusions

A 1'000 h durability test under aggressive operating conditions was successfully completed, without decrease in electrochemical performance of the radiation grafted PSI membrane. Monitoring of the integrity of the MEA indicates, however, gradual mechanical membrane deterioration, also for the Nafion<sup>®</sup> 112 based benchmark MEA.

### References

- [1] L. Gubler, M. Arcaro, G.G. Scherer, PSI Electrochemistry Laboratory Annual Report 2005, 29 (2006) ISSN-1661-5379.
- [2] M. Crum, W. Liu, ECS Transactions **3**, 541 (2006).

## LOCAL DEGRADATION ANALYSIS OF AN AGED FUEL CELL MEMBRANE

L. Gubler, R. Müller<sup>1</sup>, G.G. Scherer  
+41(0)56 310 2673  
lorenz.gubler@psi.ch

Durability of the polymer electrolyte fuel cell (PEFC) is limited to a large extent by the degradation of the components and materials in the membrane electrode assembly (MEA), especially under practical operating conditions involving realistic load profiles and start/stop cycles. The functionality of the electrolyte membrane is particularly critical, as it serves also as separator between anode and cathode for electrons and reactants. It is therefore important to identify correlations between membrane degradation and impacts of cell design on a local scale. Radiation grafted membranes developed at PSI have shown fuel cell lifetimes of several thousand hours [1]. Analysis of local degradation yielded large differences, which can be attributed to cell design and gas inlet/outlet positions [2]. In this study, a cell design with anticipated uniform distribution of reactant gases is used.

### Experimental

A PSI membrane was aged *in situ* artificially over 690 h under aggressive conditions in a cell of 10 cm<sup>2</sup> active area. After disassembly of the cell and the MEA, the extent of local degradation was analyzed using transmission FTIR spectroscopy by quantifying the intensity of the S=O stretching vibration at 1'039 cm<sup>-1</sup> of the sulfonic acid group. Loss of this function translates into a decrease in proton conductivity and thus cell performance.

### Results and Discussion

The residual concentration of sulfonic acid groups in the membrane was mapped at different positions (Fig. 1). Areas located underneath a land of the current collector / flow field could be differentiated from areas associated with flow field gas channels. The figure also shows the pathway for H<sub>2</sub>/O<sub>2</sub> supply to the cell.

The extent of degradation was subsequently calculated from the ratio of the S=O band intensity in the respective area to the intensity in reference areas outside the active area (figure 2).

Two insights can be gained from these results:

- Degradation in the channel area is about twice as high as degradation in the land area. This might be a consequence of higher local H<sub>2</sub>/O<sub>2</sub> concentration next to the membrane in the channel areas of the flow field.
- Higher degradation is observed on the O<sub>2</sub> inlet side of the cell. This calls for optimization of the cell design to provide more uniform conditions.

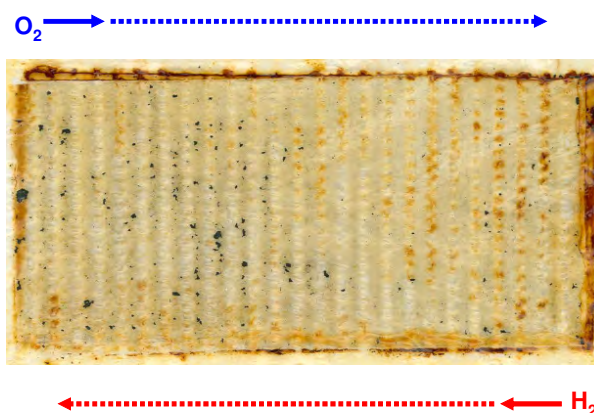


**Fig. 1:** Appearance of the aged FEP (25 μm) based radiation grafted membrane after aging for 690 h at various operating conditions: 0 - 1 A/cm<sup>2</sup>, 78-95 °C, 1 - 3 bar<sub>a</sub>. O<sub>2</sub> enters the cell from the top left, and is then distributed over the width of the flow field; vice-versa for H<sub>2</sub>.

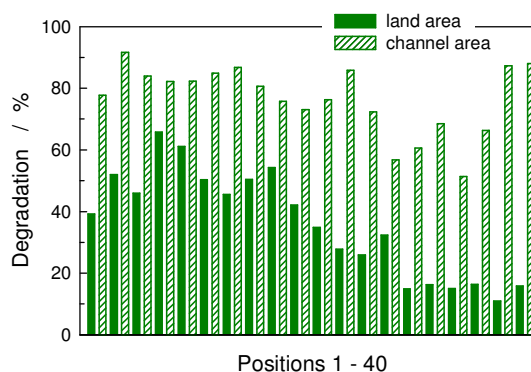


**Fig. 2:** Local degradation analysis using FTIR spectroscopy of the membrane shown in figure 1. Channel and land areas of the fuel cell flow field can be discriminated.

As it was shown that substantial differences in current density between channel and land areas can occur, even when using O<sub>2</sub> as reactant [3], it is likely that there is a correlation between local sub-mm operating conditions and rate of membrane degradation. Forthcoming experiments are expected to yield further insight into this phenomenon.

### Conclusions

The understanding of fuel cell membrane degradation on a local scale is important to correlate aging mechanisms with local operating conditions (temperature, current density, H<sub>2</sub>/O<sub>2</sub> and H<sub>2</sub>O concentration, etc.). Furthermore, results may help in improving cell design to yield more homogeneous operating conditions over the active area.

### References

- [1] L. Gubler, H. Kuhn, T.J. Schmidt, G.G. Scherer, H.P. Brack, K. Simbeck, *Fuel Cells* **4**, 196 (2004).
- [2] M. Slaski, L. Gubler, G.G. Scherer, A. Wokaun, *PSI Electrochemistry Annual Report 2004*, 114 (2005).
- [3] S.A. Freundberger, M. Reum, A. Wokaun, F.N. Büchi, *Electrochem. Commun.* **8**, 1435 (2006).

<sup>1</sup> University of Applied Forest Sciences, Rottenburg, Germany

## GAS PERMEATION IN AGED NAFION MEMBRANES

G. Schuler, F.N. Büchi  
+41(0)56 310 5396  
[gabriel.schuler@psi.ch](mailto:gabriel.schuler@psi.ch)

Although some remarkable PEM fuel cell durability test results have been published, degradation is still a major problem. One critical part of PEM fuel cells in terms of degradation is the membrane. It is known, that gas permeation lowers membrane lifetime, but the mechanisms are still not fully understood [1]. Besides emission rate measurements of membrane constituents, gas permeation data is an indicator of the actual state of the membrane with the advantage of possible real time measurement. Most investigations of membrane degradation used artificial or small laboratory cells. As operating conditions strongly influence cell degradation, data from cells of real applications are very important. Therefore in the present study integral electrochemical hydrogen permeation measurements of new and aged cells have been conducted. This data provides a basis for future degradation investigations in model cells of technical size.

### Experimental

The investigated cells consisted of graphitic serpentine flow fields with an active area of 200 cm<sup>2</sup>, Nafion 112 membranes and Toray 090 gas diffusion layers. New cells were preconditioned on the laboratory test bench during 24h at 0.5 A/cm<sup>2</sup> before the gas permeation measurements. Aged cells were field-tested for several hundred hours in a real world application. Single cells were used for the subsequent permeation measurements, using the classical electrochemical measurement setup described in [2]. The parameter study included temperature and pressure variations. Permeation measurements under pressure variations were conducted in symmetric and pressure difference configurations.

### Results

Hydrogen permeation measurement of new cells gave clear results with small measurements uncertainties. In contrast to this, the measurements of aged cells were very sensitive to pressure fluctuations.

**Table 1:** Parameter study of hydrogen permeation in new and aged cells. Base case temperature 65 °C.

Parameter	New Cell	Aged cell
T var. [mA/cm <sup>2</sup> *K]	+ 0.017	-
p var. symmetric [mA/cm <sup>2</sup> *bar]	+0.5	-
p variation H <sub>2</sub> [mA/cm <sup>2</sup> *bar]	+0.6	+33
p variation N <sub>2</sub> [mA/cm <sup>2</sup> *bar]	+0	nonlinear decrease

Due to this, reliable measurements of aged cells were only feasible in hydrogen or nitrogen overpressure modes (Tab.1). In new cells the influence of cell temperature on the permeation rate is less significant as compared to the effect of hydrogen pressure. As expected, hydrogen permeation increases in the hydrogen overpressure mode in both, aged and new cells. The permeation rate with hydrogen overpressure in aged cells is by up to a factor 55 higher as compared to new cells (Tab.1). Figure 1 illustrates the difference in hydrogen permeation rate between new and aged cells. Interestingly, under nitrogen overpressure only aged cells show a decrease of the hydrogen permeation.

### Conclusions

The overall hydrogen permeation rate is the sum of diffusive and convective permeation through the membrane. While in new cells the permeation is purely diffusive, from the pressure difference measurements we can conclude that in aged cells the major part of the permeation is convective. We suppose that the membrane of the aged cells is locally degraded and has holes in the range of micrometers. This leads to locally increased gas permeation. Beside the negative effect of efficiency loss, the gas permeation seems to directly influence membrane degradation [1].

The information obtained from the conducted integral measurements is limited. In order to gain more profound information about the relationship of gas permeation, membrane degradation and cell performance local information, ideally in an on-line configuration is needed.

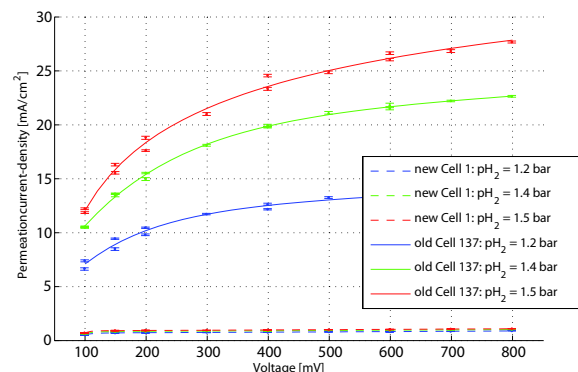


**Fig. 1:** Hydrogen permeation of aged and new cells in hydrogen overpressure mode, nitrogen pressure 1 bar, cell temperature 65 °C, gas fluxes 0.13 nl/s.

### References

- [1] V.O. Mittal, H.R. Kunz, J. Fenton, J. Electrochem. Soc. **9**, A299 (2006).
- [2] S.S. Kocha, Handbook of Fuel Cells, Wiley, **3(3)**, 538 (2003).



FUEL CELLS

DIAGNOSTICS



## INFLUENCE OF OXYGEN PARTIAL PRESSURE ON CHANNEL-RIB CURRENT DISTRIBUTIONS IN PEFC

M. Reum, S.A. Freunberger, F.N. Büchi  
+41(0)56 310 2127  
[mathias.reum@psi.ch](mailto:mathias.reum@psi.ch)

Diffusion of reactant gases through the porous structure of electrodes has been identified as one of the limiting processes in PEFC operation [1]. Measurement of the local current distribution on the scale of channels and ribs is a useful tool to gain insight on the impact of these limitations.

Under the ribs, long diffusion pathways through the gas diffusion layer (GDL) have to be taken in account. Additionally, oxygen concentration is significantly lowered near the gas outlet of an air fed cell. A new method for measuring the local currents on a sub-millimeter scale [2] was applied to study these relations. The results show, how the current distribution across channel and rib reacts on the decrease of oxygen supply to this critical cell regions.

### Experimental

A diagnosis cell – representing a small section of a technical flow field with channel and rib widths of 2.0 mm each – was employed. The cell was operated with a nitrogen/oxygen mixture on the cathode, in which the O<sub>2</sub> fraction was varied between 5 and 100 Vol-%. This way depletion of oxygen along a virtual channel can be simulated while recording the local current density using the method described in [2]. Reactants were fed in excessive stoichiometries in order to ensure homogeneous conditions along the short channel. The absolute gas pressure was 1.5 bar, the operation temperature 65 °C.

### Results and Discussion

The graphs in figure 1 show the behavior of the local current density in the middle of the rib and in the middle of the channel as function of the integral current density.

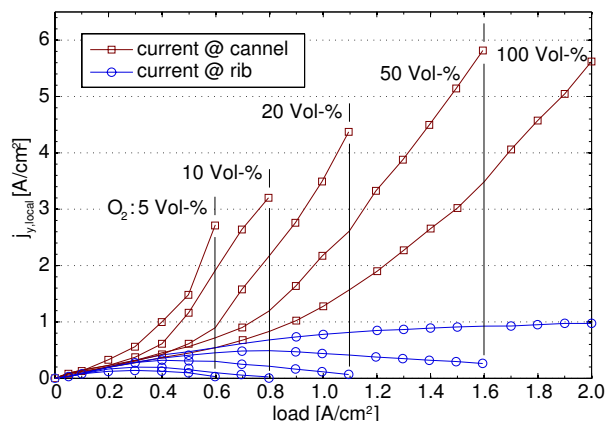


**Fig. 1:** Local current densities at the middle of the channel and the middle of the rib for different oxygen fractions (constant flow,  $rh = 0.35$ ).

It can be seen that an inhomogeneity between the two local currents is developing similarly for all oxygen fractions. However with lower oxygen fractions, the strong partition between channel and rib is shifting to lower integral current densities. Differences are seen in the development of the rib current. For a cell operated with 100 % oxygen, the rib current is stagnating after half of the maximum load, while the current in the middle of the channel is increasing to about 300% of the integral load. Cells operated with 50 % oxygen or less, however, show a maximum of the rib current and in the cases of 10 and 5 % oxygen even a total inhibition of the current generation under the rib is observed.

Comparison of the current distributions at constant voltage (e.g. 500 mV, see figure 2) simulates the development along an oxidant feed channel. While a mostly homogeneous distribution is observed with high O<sub>2</sub> partial pressure, a distinct peak is developing for lowered oxygen fractions in the middle of the channel. This peak is evolving simultaneously with a decrease of the rib currents close to zero.

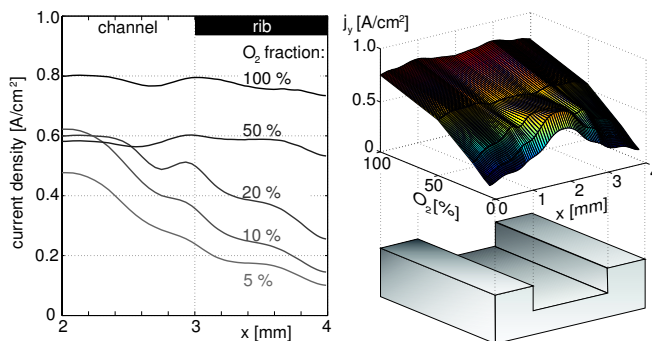


**Fig. 2:** Comparison of current distributions, recorded in the same cell for decreasing oxygen fractions at 0.5 V (constant flow).

### Conclusions

Lowering oxygen partial pressure in the cathode reactant gas causes significant changes in the current distribution across channel and rib. The shifting of current generation to the channel area is considered a consequence of oxygen starvation under the flow field land. Since complete inhibition of local current production is observed at high loads, the diffusivity of O<sub>2</sub> through the porous electrode can be considered a major limiting factor for cell areas exposed to a depleted reactant gas. Consequently, the results on the sub-millimeter scale play an important role to assess local losses and open up the possibility for optimizing PEFC structures and materials.

### References

- [1] K.T. Jeng, S.F. Lee, G.F. Tsai, C.H. Wang, J. Power Sources **138**, 41 (2004).
- [2] S.A. Freunberger, M. Reum, J. Evertz, A. Wokaun, F.N. Büchi, J. Electrochem. Soc. **153**, A2158 (2006).

## INVESTIGATION OF ANISOTROPIC MATERIAL PROPERTIES OF GAS DIFFUSION MEDIA IN PEFC

M. Reum, S.A. Freunberger, J.Kübler<sup>1</sup>,  
R. Bächtold<sup>1</sup>, F.N. Büchi  
+41(0)56 310 2127  
[mathias.reum@psi.ch](mailto:mathias.reum@psi.ch)

Gas Diffusion Layers (GDL) in polymer electrolyte fuel cells serve as reactant distributors and current collectors. Therefore, their combined mechanical and electrical properties are of interest for fuel cell operation.

The electric resistivity of carbon paper is investigated for its dependence on compression and orientation of the carbon fibres. These studies are required to generate input data for in-situ measurement of the current distribution on a sub-millimeter scale in PEFC [1]. The goal is to account for the compression effect when considering the resistance of a GDL under mechanical load. The link between this strain, anisotropic material structure and electrical properties is one of the crucial error sources in the modelling of accurate current distributions, albeit it is often neglected (e.g.[2]).

### Experimental

First, the in-plane (x-direction) and through-plane (y-direction) conductivities of the carbon paper “Toray TGP-060” were investigated using a 4-point resistance measurement technique. Due to the “stacked fibre” structure of the material, a strong anisotropy of more than one order of magnitude can be observed between the x- and y-plane (figure 1a). Subsequently, the GDL’s strain was recorded when exposed to compressive stress (see stress-strain curve in figure 1b). When the stress-strain curve flattens, also the conductivity in the y-plane stagnates. This indicates that GDL resistivity is a function of the contact points of carbon fibres in the material bulk, which can only increase with clamping force to a certain limit.

### Computational

The experimentally determined material properties are used to simulate the situation of a compressed GDL in an operating fuel cell. The distribution of bulk conductivity corresponds to the distribution of compressive forces, which vary strongly across channel and rib. Therefore, the software tool “ANSYS<sup>®</sup>” was used to calculate local conductivity on the basis of the mechanical characteristics obtained from the F-x curve.

The compressed domain, together with the calculated pressure distribution at the interface of flow field rib and GDL, is shown in figure 2a. A sharp peak is observed at the rib edge, which is caused by the bending of the GDL into the channel. On the basis of the pressure distribution the compression at any coordinate in the material bulk is obtained from

ANSYS<sup>®</sup>. Figure 2b shows the conductivity distribution in the cross section of the GDL, which is varying up to a factor of 4 throughout the domain.

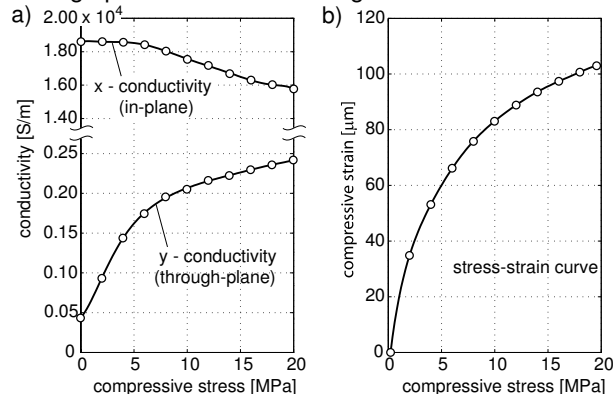


**Fig. 1:** Properties of GDL “Toray TGP-060” carbon paper: a) Electrical: conductivities x- and y-plane, b) Mechanical: stress-strain (F-x) curve.

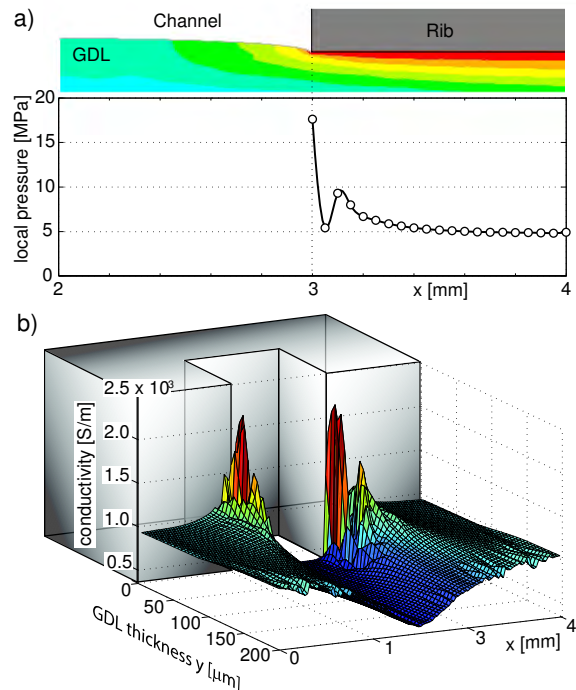


**Fig. 2:** a) Scheme of compressed GDL (displacement 50 μm) with calculated pressure distribution, b) Distribution of conductivity (y-plane) in GDL bulk.

### Conclusions

It has been shown that the GDL local electrical conductivity is in conjunction with the material’s structure and mechanical load. By combination of resistance measurements and numerical simulations of mechanical properties, the local anisotropic GDL conductivity is obtained. Based on this data, even a compressed GDL can be used as a shunt resistor to acquire current density distributions from measured voltage boundary conditions, as described in [1].

### References

- [1] S.A. Freunberger, M. Reum, J. Evertz, A. Wokaun, F.N. Büchi, J. Electrochem. Soc. **153**, A2158 (2006).
- [2] W. Sun, B.A. Peppley, K. Karan, J. Power Sources **144**, 42 (2005).

<sup>1</sup> High Performance Ceramics, EMPA Dübendorf

## ANISOTROPIC TRANSPORT PROPERTIES OF GAS DIFFUSION MEDIA FOR PEFC

R. Flückiger, S. Freunberger, D. Kramer,  
A. Wokaun, G.G Scherer, F.N. Büchi  
+41(0)56 310 4189  
[reto.flueckiger@psi.ch](mailto:reto.flueckiger@psi.ch)

Gas diffusion layers (GDL) in PEFCs are collecting current from the catalyst layers and simultaneously allow access of gases to the reaction zone. This gas diffusion is strongly hindered under the ribs of the flowfield at high current densities. The result is a voltage loss due to mass transport limitations. In order to model this phenomena the GDL materials have to be characterized appropriately in terms of effective diffusivity  $D_{eff}$ .

Current PEFC models use direction and compression independent effective diffusivities. Others make use of pore network models [1] or random fibre models [2] to describe the relationship between porosity  $\epsilon$  and relative effective diffusivity  $D_{eff}/D$ . However, these models are only valid for purely spherical or fibrous structure. They do not take into account the influence of different carbon structures, PTFE wet-proofing or micro porous layers (MPL). Therefore measuring  $D_{eff}/D$  and subsequent fitting was considered to be the most promising approach to characterize technical GDLs.

### Results and Discussion

The applied method is based on EIS of electrolyte immersed samples and was already presented by S. Freunberger and D. Kramer [3].

Figure 1 compares different approximations used in literature with in-plane measurements of GDL materials. The diagonal represents a theoretical material with a tortuosity of 1 independent of porosity. The comparison shows that the models generally predict a better diffusivity than the experiments.

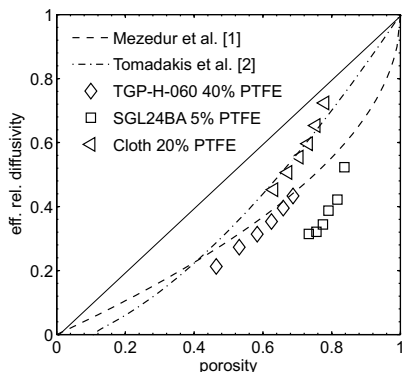
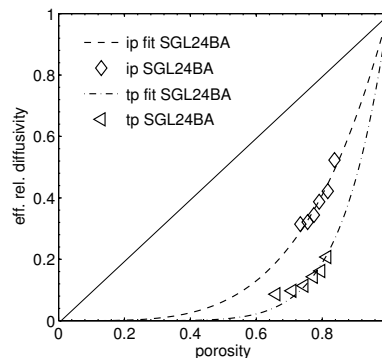


**Fig. 1:**  $D_{eff}/D$  for different literature-models compared to in-plane measurements of TGP-H-060 40% PTFE, SGL24BA 5% PTFE and Carbon Cloth 20% PTFE.

E-TEK's Carbon Cloth with 20% PTFE shows the highest  $D_{eff}/D$ . The pores of this cloth are relatively large and the PTFE is not blocking the diffusion path. Toray's carbon paper TGP-H-060 with 40% PTFE

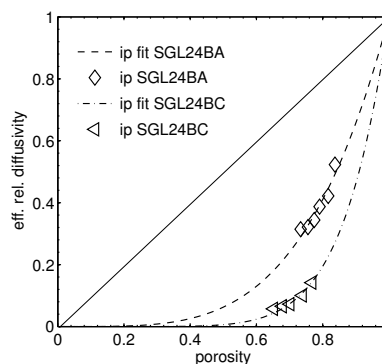
has a better  $D_{eff}/D$  than SGL's carbon paper with only 5% PTFE. This indicates that the two substrates with 0% PTFE have significantly different pore structures.

Figure 2 shows the in-plane and through-plane measurements of SGL24BA. The smaller  $D_{eff}/D$  for the through-plane direction can be explained by the predominant in-plane alignment of the carbon fibers resulting in an in-plane alignment of the pores.



**Fig. 2:** In-plane (ip) and through-plane (tp)  $D_{eff}/D$  of SGL24BA. Curves are fitted with pore network model [2].

Figure 3 illustrates the effect of MPL on the in-plane  $D_{eff}/D$  of SGL24. Although the MPL is only about 20 $\mu$ m thick and forms a parallel diffusion resistance its influence is significant. This is because the MPL is penetrating into the porous structure of the GDL and blocking the diffusion paths.



**Fig. 3:** In-plane  $D_{eff}/D$  of SGL24BA (without MPL) and SGL24BC (with MPL). Curves are fitted with pore network model [1].

### Conclusion

Measuring effective diffusivities with the method based on EIS of electrolyte immersed samples is straight forward. It is able to capture the influence of different carbon substrates, the PTFE content and the MPL-coating.

### References

- [1] M. Mezedur, M. Kaviany, W. Moore, *AIChE Journal*, **48**, 15 (2002).
- [2] M.M. Tomadakis, S.V. Sotirchos, *AIChE Journal*, **39**, 397 (1993).
- [3] S.A. Freunberger, D. Kramer, F.N. Büchi, G.G. Scherer, *PSI Electrochemistry Laboratory Annual Report 2005*, 26 (2006) ISSN 1661-5379.

## LOCAL CURRENT DENSITY MEASUREMENTS IN PEFC USING SEGMENTED CURRENT COLLECTORS

A. Tsukada, T. Gloor, F.N. Büchi  
+41(0)56 310 2661  
[akinori.tsukada@psi.ch](mailto:akinori.tsukada@psi.ch)

In a large fuel cell, the current density distribution over the bipolar plate is not at all homogenous, in particular when the gases are not fully humidified. Furthermore condensed water can obstruct the flow channels, which leads to the alleviation of the local electrochemical reactions. As a matter of fact, a flow field on the bipolar plate has generally several bends (meanders) and in certain conditions, condensed water can block the gas passages [1, 2].

### Experimental

The cell setup comprises a polymer electrolyte fuel cell with a 28-fold segmented cathode current collector (figure 1). It was developed based on previous work [3] and allows the testing of complete cells, previously operated in real world applications., Current passing through each segment can be monitored by means of Hall sensors. The active area of the cell is 200 cm<sup>2</sup>. The cell is supplied with pure hydrogen and oxygen at different pressures (1.5 and 2.5 bar<sub>a</sub>), stoichiometric ratio (1.2 to 1.5) and dewpoints (70°C or less than 20°C). It is operated at a constant temperature of 75°C. Total currents are varied from 50 to 200 A.

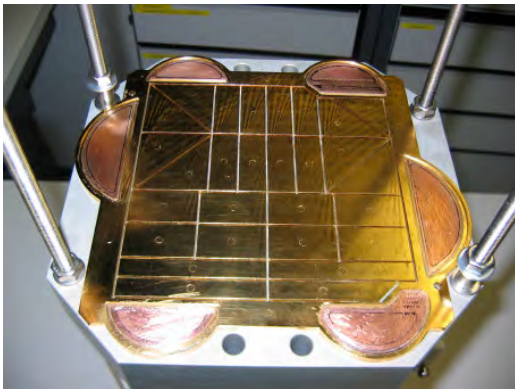


**Fig.1:** 28-fold segmented, gold-coated cathode current collector.

### Results and Discussion

Very inhomogeneous current densities are measured along the flow field with a new membrane-electrode-assembly (MEA), when hydrogen and oxygen are not humidified, particularly at the gas entrances (Nr. 1 to 8) (see figure 2). Further, before each bend in the flowfield a current alleviation is observed (Nr. 7, 15, 20, 24 & 27), which could be caused by obstruction of condensed water. The gas tries to overcome flowing through the porous gas diffusion layer. In the bend the current production is therefore lowered [1].

An aged MEA has been tested and compared with the new one at a total current of 50 Amp. (figures 2 & 3) The aged cell shows a different current distribution. The current density is higher at the gas entrances and the variation of the curve is now rather the opposite of the humidified one. This is particularly visible between segments 5 and 16. Furthermore, the humidification does not improve the cell performance.

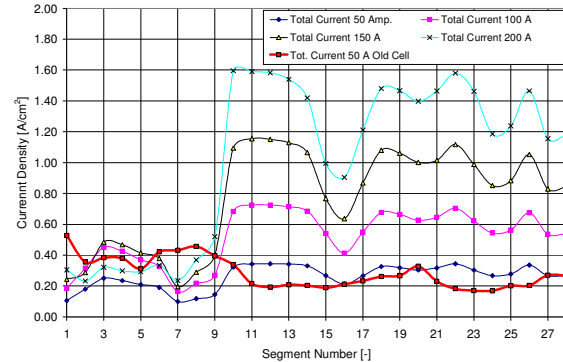


**Fig.2:** Current density along segmented collector:  $\lambda_{H_2/O_2} = 1.5/1.5$ ;  $p = 1.5 \text{ bar}_a$ ,  $T_{dew} = 20/20^\circ\text{C}$ .

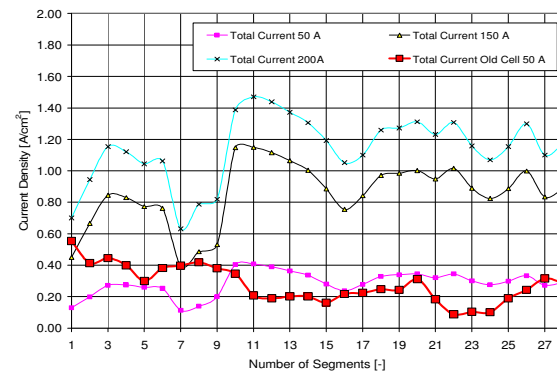


**Fig.3:** Current density along segmented collectors:  $\lambda_{H_2/O_2} = 1.5/1.5$ ;  $p = 2.5 \text{ bar}_a$ ,  $T_{dew} = 70/70^\circ\text{C}$ .

### Conclusions

Better acquaintance of the bend effect of the flow field is important to obtain a more homogeneous current distribution. At the same time premature degradation of the MEA, i.e. due to local hot spots, needs to be further investigated. A closer local examination of damaged regions could be of great importance.

### References

- [1] K. Yoshizawa, K. Ikezoe, Y. Tasaki, D. Kramer, E.H. Lehmann, G.G. Scherer, ECS Transactions, **3**, 397 (2006).
- [2] T.A. Trabold, J.P. Owejan, D.L. Jacobson, M. Arif, P.R. Huffman, Int. J. Heat Mass Transfer, **49**, 4712 (2006).
- [3] F.N. Büchi, A.B. Geiger, R.P. Neto, J. Power Sources, **145**, 62 (2005).

## MODELING THE LOW FREQUENCY RESPONSE OF AIR FED PEFCs

D. Kramer, I.A. Schneider, A. Wokaun,  
G.G. Scherer  
+41(0)56 310 4140  
[denis.kramer@psi.ch](mailto:denis.kramer@psi.ch)

Several sophisticated, mechanistic models are available in the literature to describe the impedance response of air-fed PEFCs in a rigorous mathematical approach. All these models have two common attributes: they are one-dimensional and rely on finite diffusion of oxygen through the porous structures of the MEA [1,2]. Recently, we have shown that oxygen concentration oscillations can be detected in the cathodic effluent during impedance measurements, disproving the assumption of confinement to the GDL [3]. As a consequence, the local impedance response of an air-fed PEFC must not be seen as solely defined by local processes [4]. The oxygen concentration oscillations evoked upstream of and transported within the cathodic flow field to a given point, which is the ac equivalent of the oxygen depletion along the channels in dc mode [5], have to be considered whilst developing a model for air-fed PEFCs operated under technically relevant stoichiometries.

### Model

A steady-state impedance model is developed where the boundary condition of oxygen concentration oscillations at the GDL-channel interface is found from mass conservation (semi-finite diffusion), rather than forcing a zero amplitude (finite diffusion). Further on, the model accounts for the propagation of oxygen concentration oscillations by the convective flow within the cathodic flow field. Placing emphasis on effects stemming from this ac analogue of oxygen depletion, effects originating from morphology and finite conductivity of membrane and electrode are neglected for the sake of simplicity.

### Results

The diagrams a) to c) show the calculated impedance response for two stoichiometric ratios (SRs) at an average current density of 500 mA/cm<sup>2</sup>. Diagram a) compares the sum spectra, calculated from the local spectra of diagram b) and c). The spectra with circles result from the full model, whereas the spectra shown by lines are calculated with the assumption of finite diffusion. For both SRs, a distinct, second low frequency loop forms only under the assumption of semi-finite diffusion in conjunction with oxygen depletion along the channel. Diagram d) shows the amplitude of the oxygen concentration oscillations at the GDL-channel interface as a function of position. In the case of higher SR, this curve is monotonically increasing. In the case of lower SR, however, a maximum is passed at about  $z = 0.5$ . This is in agreement with the local spectra shown in diagram c), where a

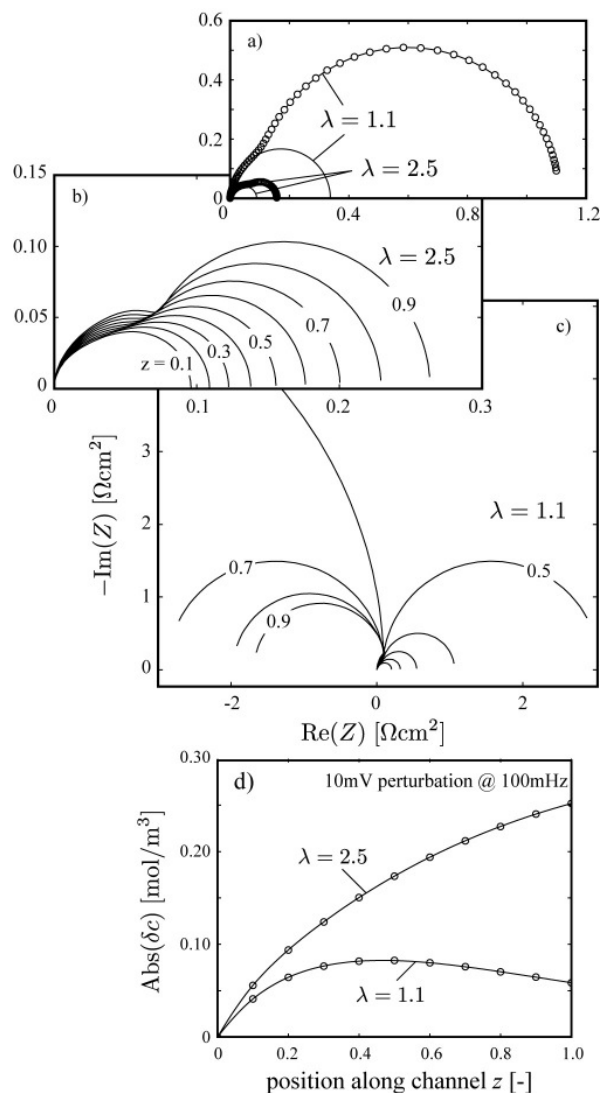


**Fig 1:** Calculated impedance spectra showing the impact of semi-finite diffusion and oxygen depletion.

negative-going low frequency loop is observed in the local spectra for  $z > 0.5$ . Both effects (negative-going loop and attenuated concentration oscillation amplitude) are a consequence of the ac voltage associated with the oxygen concentration oscillations within the channel exceeding the actual perturbation voltage.

### References

- [1] T.E. Springer, T.A. Zawodzinski, M.S. Wilson, S. Gottesfeld, *J. Electrochem. Soc.* **143** (2), 587 (1996).
- [2] F. Jaouen, G. Lindbergh, *J. Electrochem. Soc.* **150** (12), A1699 (2003).
- [3] I.A. Schneider, S. Freunberger, D. Kramer, A. Wokaun, G.G. Scherer, *J. Electrochem. Soc.* **154** (4), B383 (2007).
- [4] D.J.L. Brett, S. Atkins, N.P. Brandon, V. Vesovic, N. Vasileiadis, A. Kucernak, *Electrochem. Solid-State Lett.* **6** (4), A63 (2003).
- [5] I.A. Schneider, D. Kramer, A. Wokaun, G.G. Scherer, *J. Electrochem. Soc.*, accepted.

## LOW FREQUENCY IMPEDANCE RESPONSE OF AIR FED PEFCs

I.A. Schneider, D. Kramer, A. Wokaun,  
G.G. Scherer  
+41(0)56 310 2795  
[ingo.schneider@psi.ch](mailto:ingo.schneider@psi.ch)

When performing ac impedance spectroscopy in a PEFC operated on pure hydrogen and air at technical air flow rates a low frequency capacitive arc occurs in the spectrum of the overall cell ( $f_{\text{mod}} < 10\text{Hz}$ ). The arc has been attributed to the finite diffusion of oxygen through nitrogen in the backing layer [1]. Yet, we have shown recently that oxygen concentration oscillations are built up in the cathode gas channels of a technical air fed PEFC during ac impedance measurements ( $f_{\text{mod}} < 10\text{Hz}$ ), which disproves this assumption [2]. This observation becomes even more important, since the oscillations cause a sinusoidal ac voltage response downstream the flow field [2]. As an important result, local processes and upstream processes in the gas channels must contribute to the local ac impedance response of a technical air fed PEFC. Yet, due to the spatial separation of these processes their contribution to the local impedance response of a PEFC can be mutually excluded, if the ac current is applied only locally.

In this work, we have investigated and characterized the specific contribution of processes occurring in the cathode flow field to the ac impedance response of a technical  $\text{H}_2/\text{air}$  PEFC by using a novel experimental technique, which combines the use of sectioned electrodes with local ac measurements in PEFCs [3].

### Experimental

The impedance measurements were performed in a linear nine fold segmented  $\text{H}_2/\text{air}$  PEFC operated under fully humidified conditions. The electrodes (anode and cathode) of the outlet segment (test segment) are electrically separable (figure 1). The outlet segment (seg. 9) can be operated in different modes independently from the upstream segments (seg. 1-8).

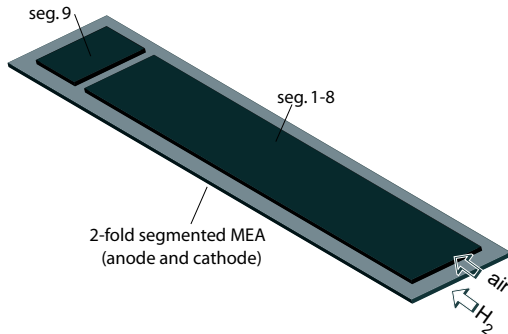


**Fig. 1:** 2-fold segmented MEA (ETEK V2.1 electrodes, Nafion 112 membrane)  $A_{\text{cell}}=63\text{cm}^2$ . Experimental conditions:  $I_{\text{cell}}=31.5\text{A}$ ,  $T_{\text{cell}}=70\text{ }^\circ\text{C}$ ,  $\lambda_{\text{H}_2}=1.5$ ,  $T_{\text{air}}=T_{\text{H}_2}=80\text{ }^\circ\text{C}$ ,  $T_{\text{hum\_air}}=T_{\text{hum\_H}_2}=80\text{ }^\circ\text{C}$ ,  $f_{\text{mod}}=100\text{mHz}-5\text{kHz}$  (15pts/dec).

## Results and Discussion

Integral and local spectra of the PEFC are shown in figure 2 for  $\lambda=3.5$  and  $\lambda=1.1$ . The size of the low frequency loop strongly increases towards lower  $\lambda$  values in the integral spectra (figure 2a). In the local spectra the arc diameter increases as oxygen is depleted towards the air outlet (figure 2b). However, at low air stoichiometry (figure 2c) the local spectra taken in the outlet region (seg. 7-9) show negative polarization resistance values at low frequencies. This effect is hidden in the respective integral spectrum (figure 2a).

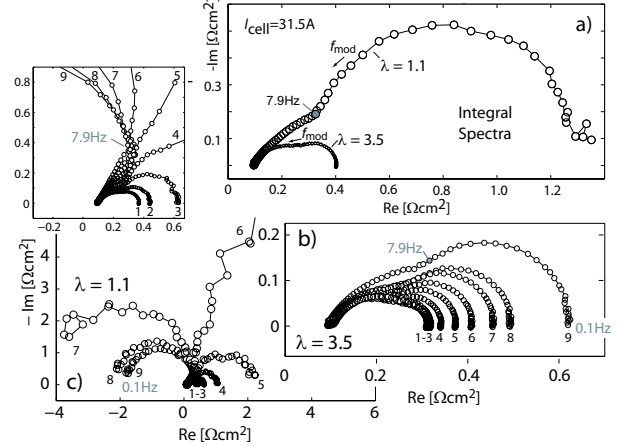


**Fig. 2:** (a) Integral and (b, c) local impedance spectra of the linear PEFC. Number of local spectrum denotes PEFC segment. The ac current was applied to the overall cell.

According to the results shown in figure 2 it seems feasible to attribute the occurrence of the low frequency loop to increasing polarization losses due to oxygen depletion along the cathode flow field. This can be experimentally proven using the setup in figure 1.

On the one hand, only local processes in the outlet segment will contribute to the local ac impedance response if the ac current is applied locally in this segment (seg. 9). As can be seen in figure 3, neither the positive nor the negative resistance low frequency loop observed for  $Z_{\text{local+upstr}}$  under same steady state conditions occur in this case in the local impedance spectra of  $Z_{\text{local}}=\eta_{\text{local}}/i_{\text{mod}}$  taken in the outlet segment.

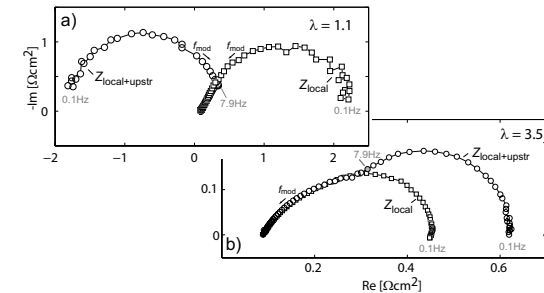


**Fig. 3:** Local impedance spectra of the outlet segment at a given  $\lambda$ . The ac current was either applied to the overall cell ( $Z_{\text{local+upstr}}$ ) or locally to the outlet segment ( $Z_{\text{local}}$ ).

Consequently, the occurrence of the low frequency does not originate from a hindrance of oxygen diffusion in the pores of the backing layer, since the local steady state conditions are equal at a given  $\lambda$ . On the other hand, only upstream processes contribute to the local ac response, if the ac modulation signal  $\eta_{\text{mod}}$  is applied solely to the upstream segments (seg. 1-8). The fractional ac polarization voltage  $\eta_{\text{up}}=K\eta_{\text{mod}}$  caused by upstream depletion of oxygen can be experimentally determined in a given frequency range, in case that the outlet segment is operated in constant current mode [3]. The frequency response of  $1/(1-K)$  is shown in figure 4a.

Yet, if both, local and upstream processes contribute to the local ac impedance response of the outlet segment the ac polarization voltage  $\eta_{\text{mod}}$  must be equal to the sum of  $\eta_{\text{local}}=Z_{\text{local}}i_{\text{mod}}$  and  $\eta_{\text{up}}=K\eta_{\text{mod}}$  [3]. Consequently, the local cell impedance  $Z_{\text{local+upstr}}$  is given by  $Z_{\text{local}}/(1-K)$ . The calculated local impedance spectra shown in figures 4b, 4c are in good agreement with the experimentally obtained 'reference' spectra for  $Z_{\text{local+upstr}}$  shown in figure 3. This gives experimental proof that the occurrence of the low frequency loop in  $\text{H}_2/\text{air}$  PEFC spectra must be attributed to depletion of oxygen in nitrogen along the cathode gas channels.

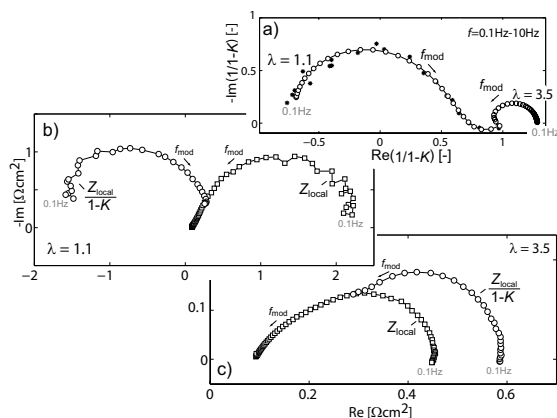


**Fig. 4:** (a) Frequency response of  $1/1-K$  (b, c) Experimentally obtained spectra  $Z_{\text{local}}$  and calculated local impedance spectra  $Z_{\text{local+upstr}}=Z_{\text{local}}/(1-K)$  of the outlet segment.

The unique characteristics observed in the local impedance spectra of a  $\text{H}_2/\text{air}$  PEFC (figure 5a) depend on the fraction of  $\eta_{\text{mod}}$  covered by  $\eta_{\text{up}}$ . The ratio  $K=\eta_{\text{up}}/\eta_{\text{mod}}$  determines the fractional ac polarization voltage  $\eta_{\text{local}}=\eta_{\text{mod}}-\eta_{\text{up}}$  which ultimately drives the local ac current  $i_{\text{mod}}$  at a given air stoichiometry  $\lambda$ .

As can be seen in figures 5a, 5b the polarization resistance observed at low frequencies is positive while the ratio  $|\eta_{\text{up}}|/|\eta_{\text{mod}}|$  is smaller than unity ( $\lambda>1.4$ ). In this case  $\eta_{\text{local}}$  and  $i_{\text{mod}}$  are in phase to  $\eta_{\text{mod}}$  (1 in figure 5c). The local ac current becomes minimal for  $|\eta_{\text{up}}|/|\eta_{\text{mod}}|\approx 1$  (2 in figure 5c) and the polarization resistance tends towards an infinite value ( $\lambda\approx 1.4$ ). As the ratio  $|\eta_{\text{up}}|/|\eta_{\text{mod}}|$  exceeds unity ( $\lambda<1.4$ ) the ac polarization voltage  $\eta_{\text{local}}$  and consequently  $i_{\text{mod}}$  are out of phase to  $\eta_{\text{mod}}$  (3 in figure 5c) and a

capacitive loop in air fed PEFC impedance spectra negative polarization resistance is observed at low frequencies.

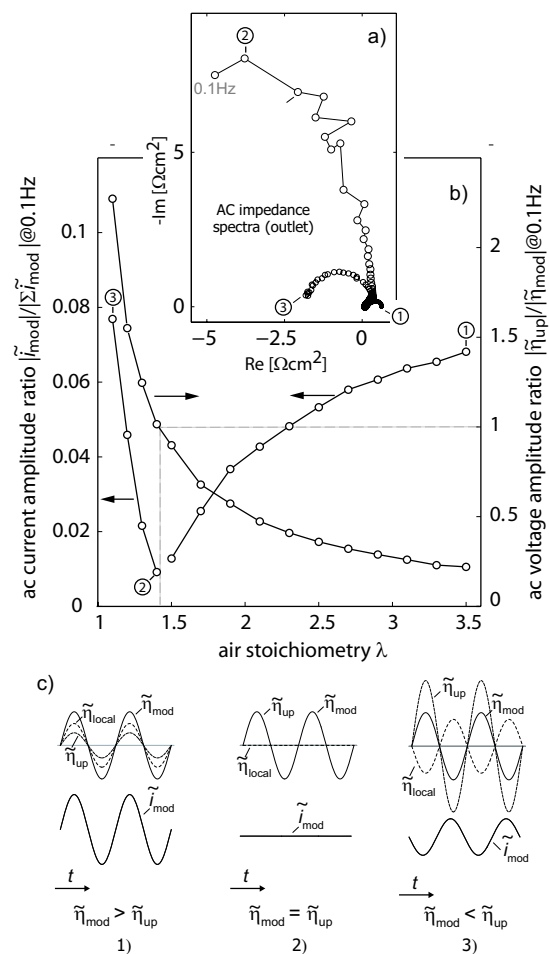


**Fig. 5:** (a) Local impedance spectra  $Z_{\text{local+upstr}}$  of the outlet segment (b) Ac voltage and ac current amplitude ratio (@100mHz) vs air stoichiometry (c) Sketch to explain the negative/positive polarization resistance at low frequencies.

## Conclusions

The results give experimental proof that the occurrence of a low frequency capacitive loop in  $\text{H}_2/\text{air}$  PEFC impedance spectra does not originate from a hindrance of oxygen diffusion in the pores of the GDL but must be attributed to another processes, namely depletion of oxygen in nitrogen along the cathode gas flow channels. The occurrence of this loop is indicative of a limitation of the local cell performance by concentration polarization losses, caused by oxygen depletion along the cathode flow channels.

## References

- [1] T.E Springer, T.A. Zawodzinski, M.S. Wilson, S. Gottesfeld, J. Electrochem. Soc. **143**, 587 (1996).
- [2] I.A. Schneider, S.A. Freunberger, D. Kramer, A. Wokaun, G.G. Scherer, J. Electrochem. Soc. **154**, B382 (2007).
- [3] I.A. Schneider, D. Kramer, A. Wokaun, G.G. Scherer, submitted to JES (2006).

## APPLICATION OF HIGH RESOLUTION NEUTRON IMAGING IN PEFC DIAGNOSTICS

P. Boillat, G. Frei, Y. Tasaki<sup>1</sup>, Y. Ichikawa<sup>1</sup>,  
D. Kramer, E. Lehmann, G.G. Scherer,  
A. Wokaun  
+41(0)56 310 2743  
[pierre.boillat@psi.ch](mailto:pierre.boillat@psi.ch)

Neutron radiography has proven to be a powerful method to detect and quantify liquid water in the flow fields and gas diffusion media of Polymer Electrolyte Fuel Cells (PEFC) [1]. Although *through plane* imaging is now a well established method, *in plane* imaging (membrane parallel to the neutron beam) sets strong requisites in terms of spatial resolution and calls for constant improvement. The introduction of a new detector system at the ICON beamline [2] of the SING spallation neutron source constituted an important step in that direction. Additionally, several techniques of anisotropic resolution enhancement were successfully applied to fuel cells, as described below.

### Anisotropic resolution enhancements

The typical dimensions of a polymer electrolyte fuel cell in parallel and across the membrane plane differ by at least one order of magnitude. Therefore, a high spatial resolution is only required in the direction across the membrane.

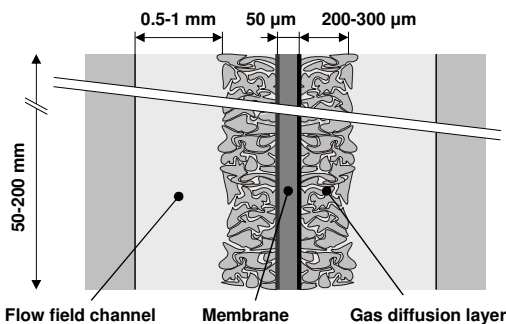


**Fig. 1:** Typical dimensions along and across the membrane of a PEFC

A first important factor limiting the spatial resolution of neutron radiography is the effect of beam divergence, which is characterized by the ratio of the aperture of the neutron source to the distance between the object and the aperture (L/D ratio). Increasing the L/D ratio implies either increasing the distance to the aperture or reducing the aperture diameter. In both cases, the neutron flux is reduced (and, therefore, the needed exposure time increased) proportionally to the square of the L/D ratio. By using a neutron aperture in the form of a slit, the neutron flux is only reduced proportionally to the L/D ratio. This anisotropic enhancement thus provides an optimal trade-off between spatial and time resolution. Another major limitation comes from the detector

itself. Traditionally, the detector system with highest resolution applicable for fuel cell imaging is an imaging plate. The introduction of the new CCD based micro-tomography setup allowed to dramatically improve the spatial resolution. Further improvement is achieved due to the fact high resolution is only needed in one direction. Hence, orienting the detector in a tilted position additionally produces a magnifying effect

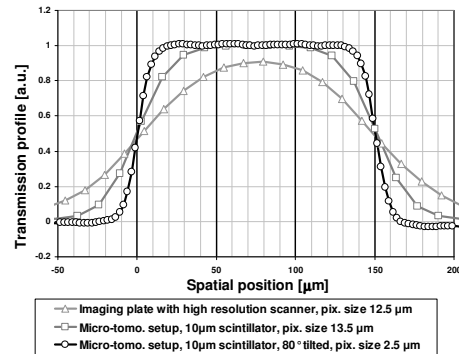


**Fig. 2:** Profiles with different detectors across a 150 µm wide test object. The scale is normalized so the integral surfaces under all curves are the same.

### Applications to fuel cell diagnostics

The higher spatial resolution obtained is beneficial to both, *in plane* as well as *through plane* imaging. For the latter, a higher spatial resolution allows to better separate the channel and land areas of the fuel cell, and, therefore, to assess better the presence of an inhomogeneous water distribution between these two areas. For *in plane* measurements, the high spatial resolution possible now allows to evaluate the distribution profile of the liquid water across the membrane electrodes assembly (MEA). The images of dry cells, utilizing different techniques (Fig. 3), illustrate the magnitude of the improvements provided by the new micro-tomography setup and the anisotropic resolution enhancements.

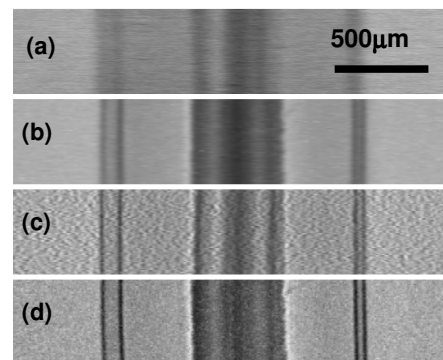


**Fig. 3:** In-plane imaging of dry fuel cells (horizontal and vertical scales are not the same): (a) imaging plate (b) micro-tomo setup with 10µm scintillator (c) imaging plate, tilted (d) micro-tomo setup, tilted.

### References

- [1] J. Zhang, D. Kramer, R. Shimoi, Y. Ono, E. Lehmann, A. Wokaun, K. Shinohara, G.G. Scherer, *Electrochim. Acta*, **51**, 2715 (2006).
- [2] G. Kühne et al, *Swiss Neutron News* **28**, 20 (2005).

<sup>1</sup> Nissan Motor Co. Ltd., Yokosuka-shi, Japan

## HIGH POWER MICRO FUEL CELL EMPLOYING MICRO-STRUCTURED GLASSY CARBON

B.C. Seyfang, M. Kuhnke<sup>1</sup>, T. Lippert,  
G.G. Scherer, A. Wokaun  
+41(0)56 310 2092  
[bernhard.seyfang@psi.ch](mailto:bernhard.seyfang@psi.ch)

A novel, simplified concept for micro fuel cells is introduced that combines the necessary functions in only three parts: Two Glassy Carbon based plates containing micro-structured flow fields and a catalyst coated membrane. The preparation of the micro-structures consists of a sequence of processing steps, i.e. Sputtering, Laser Ablation, and Reactive Ion Etching. After assembling the individual parts, fuel cell tests were carried out and a maximum power density of 415 mW/cm<sup>2</sup> was obtained.

### Experimental

The particular micro-structuring process has been described by Kuhnke et al. [1-3]. At the gas inlets, the flow fields have eleven channels, which then are merged to six and finally to three channels. The channels are 140 μm deep; the width is 60 μm at the bottom and 100 μm from edge to edge. The whole micro-structured area is 1 cm<sup>2</sup>. Two of those plates were assembled together and a catalyst coated membrane (Nafion 112, Pt-loading 0.18 mg/cm<sup>2</sup> (anode), 0.25 mg/cm<sup>2</sup> (cathode), Paxitech, France) was sandwiched in-between (figure 1). The geometric catalyst area is 1 cm<sup>2</sup>; the electrochemically active area, as determined by CV (H<sub>upd</sub>), yields 59 cm<sup>2</sup>/cm<sup>2</sup><sub>geo</sub> on the anode and 84 cm<sup>2</sup>/cm<sup>2</sup><sub>geo</sub> on the cathode side, respectively. The micro fuel cell was operated with both, undiluted hydrogen (9 sccm, λ = 1.3 at 1 A/cm<sup>2</sup>) and oxygen (6 sccm, λ = 1.7 at 1 A/cm<sup>2</sup>). The gases had a relative humidity of 80%; the cell temperature was 50°C.

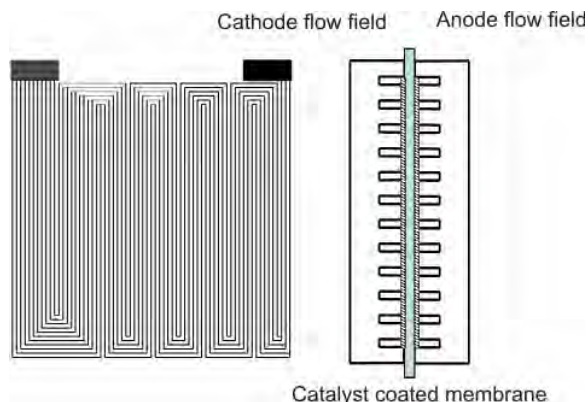


**Fig. 1:** Top view of a micro-structure including merged flow field channels; principle of the micro fuel cell (cross sectional view).

## Results and Discussion

Fuel cell tests were carried out, resulting in a typical polarization curve as shown in figure 2.

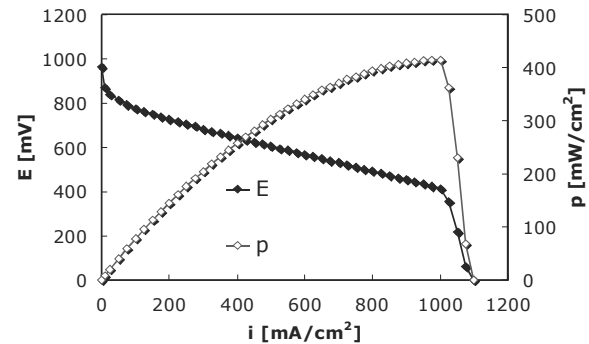


**Fig. 2:** Polarization curve and power density. Conditions:  $T = 50^\circ\text{C}$ ; rel. humidity 80%;  $\text{H}_2$ : 9 sccm,  $\lambda = 1.3$  at  $1\text{A}/\text{cm}^2$ ;  $\text{O}_2$ : 6 sccm,  $\lambda = 1.7$  at  $1\text{A}/\text{cm}^2$ .

The system of merged flow field channels was introduced to have a sufficient liquid water removal from the channels during operation. The gas flows are reduced along the channel pathway by consumption of the gases, due to the electrode reactions. So the gas velocity is kept in the same order of magnitude by reduction of cross sectional area, i.e. the number of parallel channels. During operation no water accumulation could be observed.

The power density yields a maximum of 415 mW/cm<sup>2</sup> at 425 mV (395 mW/cm<sup>2</sup> at 500 mV), which exceeds all values for power densities of micro PEFCs (active area < 5 cm<sup>2</sup>) published so far [4].

The fuel cell was operated for 19 days with a minimum power density of 325 mW/cm<sup>2</sup>, what is up to 80% of the maximum value.

### Conclusions

First results obtained with a novel, simplified concept for a micro fuel cell reveal power densities in the range of >400mW/cm<sup>2</sup>. A set of analytical methods will be used in the future to obtain a deeper understanding of the limiting effects, such as influence of liquid water or active sites, diffusion or degradation. Due to the rather simple principle of this micro fuel cell, it might also be a powerful tool to examine phenomena observed in technical PEFCs.

### References

- [1] M. Kuhnke, G. Dumitru, T. Lippert, E. Ortelli, G.G. Scherer, A. Wokaun, JLMN-J. Laser Micro/Nanoengineering **1**, 67 (2006).
- [2] M. Kuhnke, T. Lippert, E. Ortelli, G. G. Scherer, A. Wokaun, Thin Solid Films **453-454**, 36 (2004).
- [3] M. Kuhnke, T. Lippert, G. G. Scherer, A. Wokaun Surf. Coat. Technol. **200**, 730 (2005).
- [4] N.T. Nguyen, S. H. Chan, J. Micromech. Microeng. **16**, R1 (2006).

<sup>1</sup> Robert Bosch GmbH, 72703 Reutlingen, Germany

## CELL INTERACTION PHENOMENA IN POLYMER ELECTROLYTE FUEL CELL STACKS

S. A. Freunberger, I.A. Schneider, M. Hofer,  
F.N. Büchi  
+41(0)56 310 2410  
[stefan.freunberger@psi.ch](mailto:stefan.freunberger@psi.ch)

Fuel cells stacks in the commonly used bipolar arrangement comprise multiple stacked single cells. Bipolar plates (BPP) serve as electrical connectors between the alternate poles of two adjacent cells. This bipolar stacking of fuel cells connects them in series electrically and in parallel for the reactant and coolant flows. Therefore, all cells in a stack have to carry the same total current while not necessarily receiving the same media flows. Resulting differences in local current have to be redistributed between the cells. Hence, potential gradients along the BPP will occur that in turn influence the cells current distribution. By this, disturbances in single cells spread out to several neighboring cells.

Electrochemical impedance spectroscopy (EIS) is used to assess mass transfer and flooding effects and was therefore extended for stack diagnostics, e.g. [1]. The effort to use EIS in stacks to monitor cell failure [2], however, is tremendously error prone as inevitable differences between the cells heavily distort the spectra as we show in this article.

### Experimental

The experiments described here were performed in a specialized 2-cell stack of cells with linear flow field with an active area of 200 cm<sup>2</sup> and 0.4 m channel length [3]. Individual media supply allows for independent operation of the cells. The flow field plates were made from Sigracet BMA 5 graphite (SGL carbon) with partial segmentation in the outer flow field plates where current is measured in 10 segments with Hall sensors. For the locally resolved EIS measurements the setup by Schneider et al. [4] was used.

### Results and Discussion

The most probable cause for coupling phenomena arises from different reactant flows due to the parallel media supply of the cell. The current density distribution is most sensitive to air flow and therefore coupling phenomena are investigated in the following by means of air stoichiometry differences.

Figure 1 shows the current density distributions, the local voltage, and the resulting in-plane current for one cell at constant air stoichiometry  $\lambda_{\text{air}} = 3$  and the other cell varied from  $\lambda_{\text{air}} = 3$  to 1.2. The latter (anomalous) cell takes a bigger fraction of the total polarization at the air outlet and the cell voltage drops there (figure 1b). The driving force for the adjacent cell is therefore reduced as compared with its isolated iso-potential operation. In turn the current density drops and couples to the disturbed cell (figure 1a).

The extent of current density coupling is governed by the resulting in-plane current with the occurring potential gradient in the BPP (figures 1b+c).

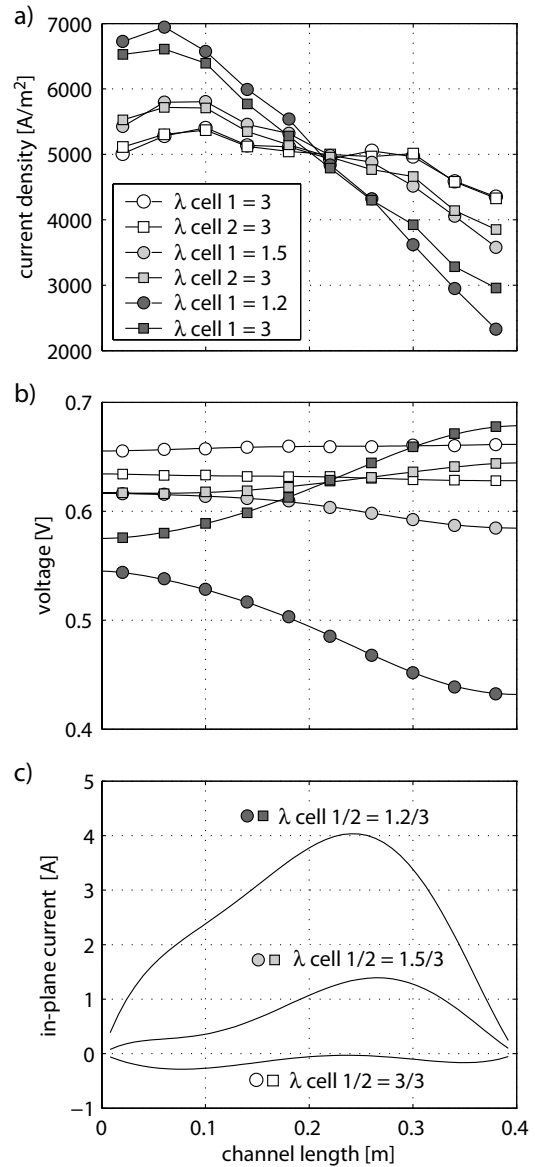
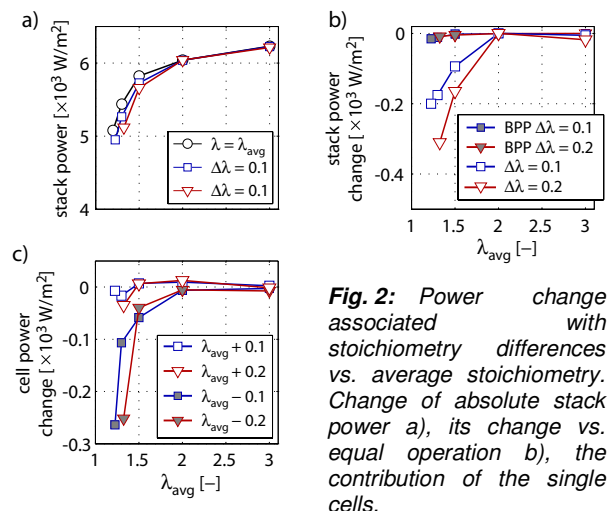


**Fig. 1:** Reduction of the air stoichiometry in one cell with constantly operated other cell. Distributions of a) current density, b) cell voltage, and c) in-plane current in the bipolar plate.  $T_{\text{cell}} = 70 \text{ }^\circ\text{C}$ ,  $r.H.(H_2, \text{air}) = 100\%$ ,  $p = 1 \text{ bar}_a$ .

A particularly relevant case in real stacks is deviations of individual cell air stoichiometries around the average stack stoichiometry  $\lambda_{\text{avg}}$ . Figure 2 analyzes the effect of such deviations on cell and stack power in dependence of the stack stoichiometry. The stoichiometry of the two cells is  $\lambda = \lambda_{\text{avg}} \pm \Delta\lambda$  with  $\Delta\lambda$  being 0, 0.1, and 0.2. Stack power drops significantly below an average stoichiometry of  $\lambda = 2$  with minor contributions of power losses due to in-plane current in the bipolar plate (filled symbols in figure 2b). In figure 2c the cell power is referenced to its value at iso-potential operation, i.e. equal operation of both cells. It shows that the major losses arise in the cell with reduced air flow; i.e. the cell where polarization increases along

the flow path. This is in contrast to a theoretical study that predicts increasing cell power with increasing polarization along the air flow path [5]. The reverse polarization profile as it applies to the other cell leads to virtually no power change for the potential gradients that appear with  $\lambda_{\text{air}} \geq 1.5$ . Stronger non-uniform polarization with its maximum at the inlet, as it appears at  $\lambda_{\text{air}} < 1.5$  in the cell with increased flow leads to a power loss too. The losses due to those air stoichiometry variations sum up to about 5% of the total power at  $\lambda_{\text{avg}} = 1.2$ .



### Implications for Impedance Measurements

Non-uniform polarization and altered current density in a cell due to a differently operated adjacent cell as shown above for the DC case have considerable impact on local and integral EIS spectra in the individual cells of the stack (figure 3c). The base case is the two cells operated identically at  $\lambda_{\text{air}} = 2.5$  (figure 3a) with the typical features of high and low frequency capacitive loops [6]. The spectra change significantly when the cell adjacent to the measured cell is operated with reduced air stoichiometry of  $\lambda_{\text{air}} = 1.2$  (figure 3b). The spectra are mainly influenced by the adjacent cell in the low frequency part below  $\approx 10$  Hz. This is because the impact of integral current deflection, which is the same for both cells, on the current distribution depends on  $\lambda_{\text{air}}$  and modulation frequency. At high frequencies the current profile (cf. figure 1a) oscillates nearly parallel up and down irrespective of  $\lambda_{\text{air}}$ . At low frequencies and  $\lambda_{\text{air}}$ , however, the modulation current close to the outlet may become very large and out of phase [6]. The associated redistribution in the bipolar plate changes therefore both the modulation voltage and current in the measured cell as compared to the iso-potentially operated cell.

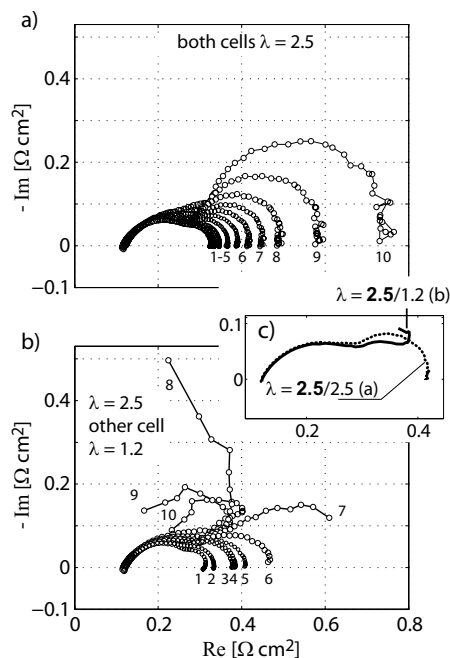


**Fig. 3: Reaction of the local and integral cell spectra on unequally operated adjacent cell.** Numbers indicate segment position from inlet. a) Local spectra of one cell for equally operated cells. b) Distortion of the local spectra due to reduced stoichiometry in the adjacent cell. c) Impact of the stoichiometry in the adjacent cell on the integral cell spectrum.

### Conclusions

The mechanism and effect of practically relevant flow anomalies has been studied in a specialized stack. Non-uniform polarization has been found to reduce cell power. Power losses by in-plane current are found to be negligible. Furthermore, we have revealed, that low frequency features in stack spectra are heavily error-prone. Virtually homogeneous operation of all cells is vital for meaningful spectra.

### References

- [1] B.X. Andraeus, Dissertation EPF Lausanne Nr. 2598 (2002).
- [2] N. Fouquet, C. Doulet, C. Nouillant, G. Dauphin-Tanguy, B. Ould-Bouamama, J. Power Sources **159**, 905 (2006).
- [3] S.A. Freunberger, M. Santis, I.A. Schneider, A. Wokaun, F.N. Büchi, J. Electrochem. Soc. **153**, A396 (2006).
- [4] I.A. Schneider, H. Kuhn, A. Wokaun, G.G. Scherer, J. Electrochem. Soc. **152**, A2092 (2005).
- [5] S.M. Senn, D. Poulidakos, Electrochem. Comm. **7**, 773 (2005).
- [6] I.A. Schneider, S.A. Freunberger, D. Kramer, A. Wokaun, G.G. Scherer, J. Electrochem. Soc., in press.

# THERMAL ANALYSIS AND OPTIMIZATION OF A PORTABLE, EDGE-AIR-COOLED PEFC STACK

R. Flückiger, A. Tiefenauer<sup>1</sup>, M. Ruge<sup>2</sup>,  
C. Aebi<sup>3</sup>, A. Wokaun, F.N. Büchi  
+41(0)56 310 41 89  
[reto.flueckiger@psi.ch](mailto:reto.flueckiger@psi.ch)

Internally humidified, edge-air-cooled PEFC stacks are promising for portable systems in terms of specific power and specific cost. Their main drawback are thermal power limitations due to limited heat removal. The aim of this study was to minimize the cooling limitation with a simultaneous cost and weight reduction by optimization of the stack geometry.

## Stack Design

The stack design is based on the concepts of internal humidification [1], punching of carbon-based bipolar plates [2] and edge-air-cooling. The bipolar plate is composed from a separator plate and two perforated plates for each flowfield. The separator plate acts simultaneously as a cooling rib as showed in figure 1. For the separator and flowfield plates SIGRAFLEX<sup>®</sup> from SGL Carbon was used. This material is a good electric ( $\sigma=16'000\text{S/m}$ ) and excellent thermal conductor ( $\kappa=290\text{W/(mK)}$ ).

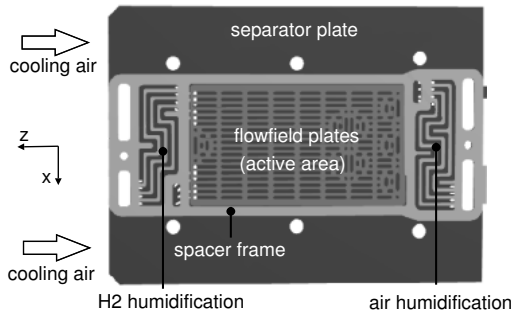


**Fig. 1:** Top view of an open cell with the separator plate extended over the active area and the spacer frame with the hydrogen and air humidification flowfields.

## Model

A thermal FE-model was developed and validated against experimental temperature distributions (figure 2). The model includes anisotropic heat conduction and heat convection by the cooling air. Cell voltage, liquid water fraction and limiting temperature were determined experimentally for improved accuracy. Complex flowfield structures were approximated with the Numerical Volume Averaging Method [3] to reduce computational cost. These simplifications resulted in an effective reproduction of the cooling limitation which allowed for extensive optimization studies.

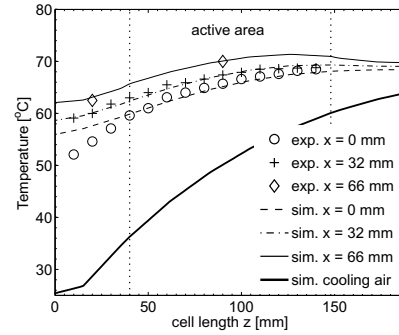


**Fig. 2:** Comparison of experimental and simulated temperature profiles along the cooling air.  $j=3880\text{A/m}^2$ ;  $U=0.67\text{V}$ .

## Results and Discussion

Figure 3 illustrates the specific cost as a function of active area and separator plate thickness. There is a clear minimum along the active-area-axis. Bigger active areas have higher heat removal limitations and consequently the expensive MEA material is not well utilized. Therefore large active areas are not preferable in terms of specific cost. While the separator plate thickness, has only a small influence on the specific cost, it mainly determines the specific power.

As a result of the optimization study specific power was improved by +86% with simultaneous reduction of specific cost by -35%.

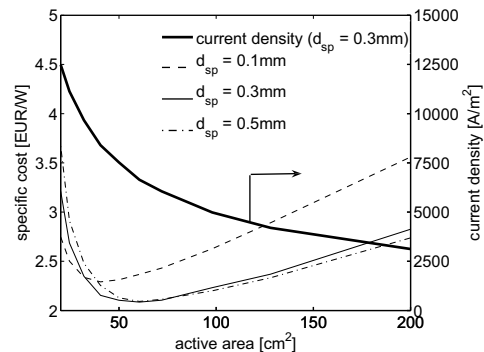


**Fig. 3:** Specific-cost curves as a function of active area for different separator plate thicknesses (current density is plotted for a separator plate thickness of  $d_{sp}=0.3\text{mm}$ ).

## Conclusions

Light-weight and low-cost PEFC stacks are feasible with an edge-air-cooling concept. However, even when highly heat conductive materials are used, the concepts suffer from a limited power output due to heat removal restrictions. An extensive thermal analysis allows for significant improvements.

## References

- [1] M. Santis, D. Schmid, M. Ruge, S. Freunberger, F. N. Büchi, *Fuel Cells*, **4**, 214 (2004).
- [2] M. Ruge, M. Höckel, *Proc. 3<sup>rd</sup> European Polymer Electrolyte Fuel Cell Forum*, Lucerne, Switzerland, B096 (2005).
- [3] M. Roos, E. Batawi, U. Harnisch, T. Hocker, *J. Power Sources*, **118**, 86 (2003).

<sup>1</sup> Center for Computational Physics, ZHW, Winterthur  
<sup>2</sup> Fuel Cell Laboratory, HTI, Biel  
<sup>3</sup> CEKA Elektrowerkzeuge AG, Wattwil

# BATTERIES & CAPACITORS

## MATERIALS



# SPRAY DRYING SYNTHESIS AND ELECTROCHEMICAL PERFORMANCE OF LITHIUM VANADATES AS POSITIVE ELECTRODE MATERIALS FOR LITHIUM BATTERIES

N. Tran, M. Holzapfel, K. Bramnik<sup>1</sup>,  
H. Hibst<sup>1</sup>, J. Pröls<sup>1</sup>, N. Mronga<sup>1</sup>, P. Novák  
+41(0)56 310 4542  
[nicolas.tran@psi.ch](mailto:nicolas.tran@psi.ch)

Vanadium oxides are considered as good candidates for the positive electrode of lithium-metal batteries because they offer both high reversible capacity and good cycleability in a potential range below 4V vs. Li where no side reaction due to electrolyte degradation is expected. Among those oxides the lithium trivanadate  $\text{Li}_{1+x}\text{V}_3\text{O}_8$  ( $x=0.1-0.2$ ) raises interests because it has demonstrated reversible capacities at least double than that of lithium cobalt oxide [1]. Their electrochemical performances depend on the material size and morphology [2-3]. To address this issue, lithium vanadates were synthesized by a spray drying method, which allows to form spherical aggregates at low drying temperature [4].

The samples have been characterized by XRD, SEM,  $S_{\text{BET}}$ , and electrochemical tests in lithium cells.

## Experimental

Three moles of ammonium metavanadate  $\text{NH}_4\text{VO}_3$  (99 wt %, GfE GmbH) were mixed together with 1.1 moles of  $\text{LiOH}\cdot\text{H}_2\text{O}$  (55 wt %, Chemetall GmbH) in distilled water preheated at 90 °C. The resulting yellow solution was stirred for 15h at 90 °C (pH = 8.0) and then spray-dried with air using a *Mobile minor 2000* type device (entrance temperature=330 °C, output temperature=107 °C). The light brown powder was then calcined at a selected temperature for 1h and cooled down at room temperature. We synthesized three " $\text{Li}_{1+x}\text{V}_3\text{O}_8$ " materials by the spray drying technique, by heat treatment at 320 °C (sample A), at 585 °C (sample B) and at 585 °C in the presence of carbon (sample C), respectively.

XRD patterns were recorded in the  $2\theta = 5-65^\circ$  range using a Bruker D4-Endeavor diffractometer. SEM images were collected using a *JEOL* microscope. Specific surface area of the samples was measured according to the BET method with a *Gemini V2365* device.

Composite positive electrodes were prepared by a conventional solvent route where acetonitrile (99.9%, Sigma) was used as the dispersing medium. The  $\text{Li}_{1+x}\text{V}_3\text{O}_8$ , carbon black, and binder powders were dispersed in the solvent under magnetic stirring for 5 hours. The solvent quantity was 4 mL for 500 mg of the rest, i.e.,  $\text{Li}_{1+x}\text{V}_3\text{O}_8$ +CB+binders. The slurry was spread on an aluminum foil and then dried at room temperature for 2 hours. Electrode disks (1.3 cm<sup>2</sup>)

were cut, dried at 50 °C under vacuum for 1h, and transferred in an argon filled glove box ( $\text{H}_2\text{O} < 2$  ppm) for cell assembly. The working electrodes consisted of 86 % active material, 10.5 % Super P carbon black (TIMCAL), 3.5 % of a (1:1) polymeric binder mixture of PVdF-HFP (Kynar 2801, Atochem) and PEO ( $M_w = 300.000$ , Sigma). Hermetically sealed laboratory cells were used in which working and counterelectrode (metallic lithium) were pressed together (2 kg/cm<sup>2</sup>) against a glass fiber separator soaked with the electrolyte (EC:DMC 1:1 with (1M)  $\text{LiPF}_6$ ). The mass loading was 4-10 mg of active material per cm<sup>2</sup>. All voltages given in the text are expressed vs.  $\text{Li}^+/\text{Li}$ . The cycling was performed in the 2.0V-3.3V potential window in a galvanostatic mode followed by a potentiostatic mode until the current reached C/50. All composite electrodes were tested assuming the same theoretical capacity of 320 mAh/g. For the long term cycling tests, the charge and discharge rates were equal to C/3. For the rate capability tests, the current rate was increased from C/10 to 8C.

## Results and Discussion

The XRD patterns of the three samples are shown in Figure 1.

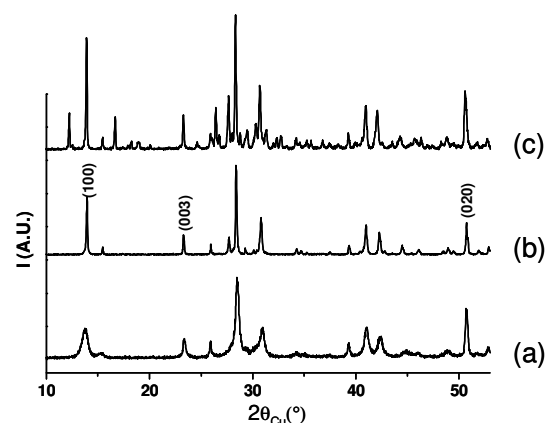


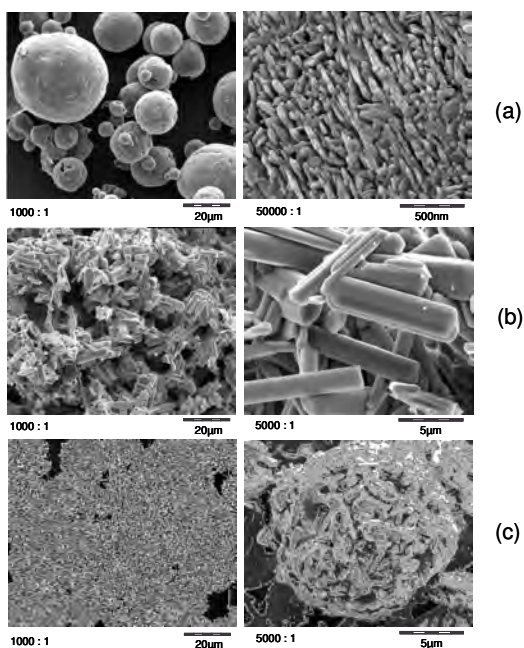
**Fig. 1:** XRD ( $\text{CuK}\alpha$ ) patterns of lithium vanadates synthesized in different conditions: (a) at 320 °C, (b) at 585 °C, and (c) at 585 °C with carbon.

XRD patterns for sample (a) and (b) indicated the presence of a single phase: all the reflections could be attributed to the  $\text{Li}_{1+x}\text{V}_3\text{O}_8$  phase. For sample (a), the broadness of the (100), (020), and (003) reflections are clearly different, which suggests an anisotropic shape of the crystallites in this sample. The XRD pattern of sample (c) can clearly not be explained by a single phase. The pattern analysis indicates the presence of  $\text{Li}_{1+x}\text{V}_3\text{O}_8$ ,  $\text{LiV}_2\text{O}_5$  and  $\text{Li}_{0.30}\text{V}_2\text{O}_5$  phases, which confirms that a carboreduction occurred in this synthetic condition leading to lithium vanadates with the vanadium element at different oxidation states

SEM pictures of the samples are shown in figure 2. Sample (a) exhibits a quite heterogeneous size distribution (5-40  $\mu\text{m}$ ) of spherical dense agglomerates consisting itself of nano rods ( $S_{\text{BET}} = 13.3 \text{ m}^2/\text{g}$ ). Sample (b) shows well defined

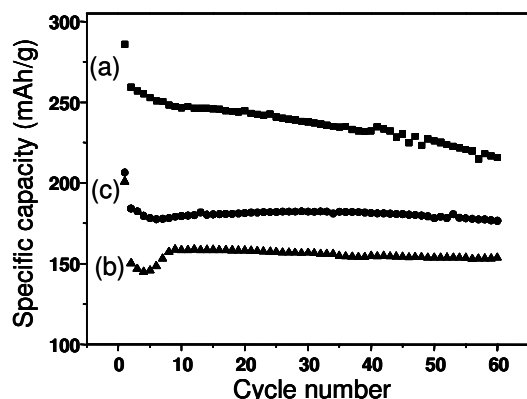
<sup>1</sup> BASF Aktiengesellschaft, Research and Development, Ludwigshafen, Germany

macro rods (10  $\mu\text{m}$  long and 2  $\mu\text{m}$  thick;  $S_{\text{BET}} = 3.3 \text{ m}^2/\text{g}$ ). In contrast, sample (c) that was calcined at the same temperature as sample (b) consists of spherical porous spheres (10  $\mu\text{m}$ ; ( $S_{\text{BET}} = 9.1 \text{ m}^2/\text{g}$ )).



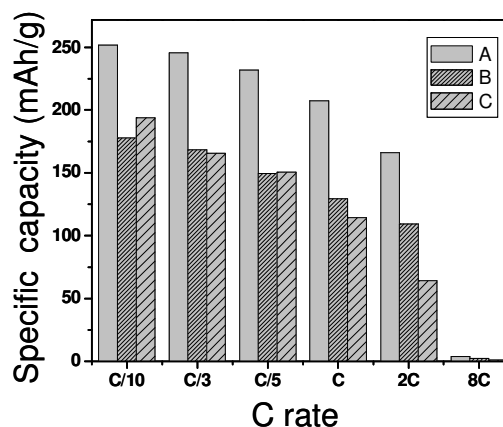
**Fig. 2:** SEM pictures of the lithium vanadates synthesized under different conditions: (a) at 320  $^{\circ}\text{C}$ , (b) at 585  $^{\circ}\text{C}$ , and (c) at 585  $^{\circ}\text{C}$  with carbon.

Figure 3 shows the galvanostatic discharge capacity vs. cycle number for the discussed three kinds of vanadium oxides. The sample heated at 320  $^{\circ}\text{C}$  exhibits a discharge capacity of 260 mAh/g at the second cycle but only 220 mAh/g at the 60<sup>th</sup> cycle. The discharge capacity of the two other samples calcined at 585  $^{\circ}\text{C}$  is initially much lower but the cycling is much more stable.



**Fig. 3:** Galvanostatic discharge capacity at the C/3 rate for lithium vanadates synthesized under different conditions: (a) at 320  $^{\circ}\text{C}$ , (b) at 585  $^{\circ}\text{C}$ , and (c) at 585  $^{\circ}\text{C}$  with carbon.

The addition of carbon during calcination resulted in a significant improvement of the reversible capacity at the C/3 rate for the sample heat treated at 585  $^{\circ}\text{C}$ .



**Fig. 4:** Rate capability experiments for lithium vanadates synthesized under different conditions: (a) at 320  $^{\circ}\text{C}$ , (b) at 585  $^{\circ}\text{C}$ , and (c) at 585  $^{\circ}\text{C}$  with carbon.

As shown in figure 4, the sample (a) exhibits a higher rate capability than the other samples, which may be due to the shortest diffusion path for  $\text{Li}^+$  ions in the nanorods constituting the aggregates for sample (a). Sample (c) is superior to sample (b) at very slow C rates but is revealed slower at higher rates. Despite the porous aggregates of sample (c) and their spherical shape, the electrochemical performances for sample (c) were found lower than sample (a). It is believed that the presence of extra phases in sample (c) retarded its electrochemical performance at high rates.

## Conclusions

Spherical lithium vanadates were successfully synthesized by spray drying and subsequent calcination at 320  $^{\circ}\text{C}$  and at 585  $^{\circ}\text{C}$ , respectively, in the presence of carbon. The discharge capacity at the C/3 rate for the sample calcined at 320  $^{\circ}\text{C}$  was much higher but with poorer cycle life than for the sample calcined at 585  $^{\circ}\text{C}$  with carbon. The sample synthesized for comparison, a lithium vanadate prepared at 585  $^{\circ}\text{C}$  without carbon, exhibited rod shaped particles with lower electrochemical performance. The spherical shape and the porosity of the oxide aggregates are thus believed to explain partly the improvement in the reversible capacity at low rates for the sample heat treated at 585  $^{\circ}\text{C}$  with carbon.

## References

- [1] G. Pistoia, F. Pasquali, M. Tocci, R.V. Moshtev, V. Manev, *J. Electrochem. Soc.* **132**, 281 (1985).
- [2] S. Jouanneau, A. Le Gal La Salle, A. Verbaere, D. Guyomard, *J. Electrochem. Soc.* **152** (8) A1660 (2005).
- [3] S. Jouanneau, A. Verbaere, S. Lascaud, D. Guyomard, *Solid State Ionics*, **177**, 311 (2006).
- [4] J. Gao, C. Jiang, C. Wan, *J. Power Sources* **125**, 90 (2004).

## OXIDE NANOPARTICLES AS ACTIVE MATERIAL IN LITHIUM-ION BATTERIES

T.J. Patey, J. Ufheil, F. Ernst<sup>†</sup>, R. Büchel<sup>†</sup>,  
S.E. Pratsinis<sup>†</sup>, P. Novák  
+41(0)56 310 4071  
[timothy.patey@psi.ch](mailto:timothy.patey@psi.ch)

Oxide nanoparticles in electrodes present various advantages and disadvantages over electrodes using oxide microparticles in lithium-ion batteries. Potential advantages include higher charge and discharge rates, whereas a disadvantage could be a decrease in performance due to increasing electrode/electrolyte reactions [1]. These events occur due to the increase in specific surface area of nanoparticles over microparticles, creating a larger interface between electrolyte and electrochemically active material. With energy storage becoming an increasingly important issue for high-powered devices, use of lithium-ion batteries for these applications will require a larger interface between electrolyte and active material. For use of Li-ion batteries in electric vehicles, use of oxide nanoparticles as active material could be one method to increase the power density for this application [2].

Flame spray pyrolysis (FSP) has been identified as a scalable process to synthesize oxide nanoparticles at high production rates [3-4]. This process can produce electrochemically active oxide nanoparticles with a spinel unit cell structure such as  $\text{LiMn}_2\text{O}_4$ ,  $\text{LiFe}_5\text{O}_8$ ,  $\text{Li}_4\text{Ti}_5\text{O}_{12}$ . Ernst et al. demonstrated that FSP is a potentially cost-effective process to producing electrochemically active nano spinel materials of controlled composition, crystallinity, and morphology [5].

### Experimental

Electrodes containing the oxide nanoparticles as active material are prepared so as to reliably measure the electrochemical characteristics of the nanoparticles. The current preparation technique involves dispersing a mixture of oxide nanoparticles and two types of carbon black (Super P and Ensaco 350, Timcal SA) [10:1:1] within an organic solution of N-methylpyrrolidone (NMP, Fluka.). This suspension is then added to a solution composed of 10 wt. % polyvinylidene fluoride (SOLEF PVDF 1015, Solvay) dissolved in NMP and [5.7:1], forming a viscous slurry. The slurry is doctor bladed at a thickness of 350  $\mu\text{m}$  on an aluminum foil and dried to remove the NMP, forming the electrode used to electrochemically characterize the nanoparticles. These nanoparticles are produced by flame spray pyrolysis (FSP) as described in other work [5].

Efforts are being made to optimize the electrode preparation technique. In the ideal electrode, the active material is in contact with both the electrolyte and the electrical network of the electrode.

Parameters such as electrode porosity, electrical conductivity, and dispersion of nanoparticles in a suspension are under investigation. The electrode engineering plays a vital role in electrochemical characterization of nanoparticles.  $\text{TiO}_2$  is being used as a model material as it does not noticeably react with the electrolyte between potentials of 1 and 3 V vs.  $\text{Li/Li}^+$ .

### Results and Discussion

Electrodes containing little active mass are prepared to determine whether the oxide nanoparticles are well dispersed throughout the electrode. In one case,  $\text{TiO}_2$  (AK1) and carbon black (Super P) were mixed into NMP by a turbo-stirrer at a ratio of 1 to 4.7, respectively. This suspension was used to make an electrode, and a scanning electron micrograph (SEM) image of this electrode is seen in figure 1.

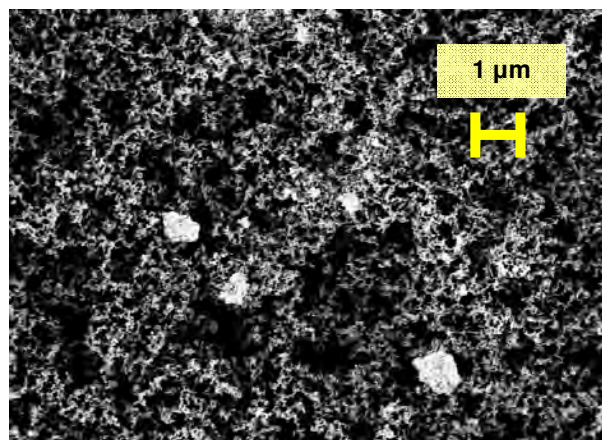


**Fig. 1:** SEM image of  $\text{TiO}_2$  (AK1, lighter shaded clumped agglomerates) and carbon black (Super P, darker shaded branch-like aggregates) within an electrode.

In figure 1, clumped aggregates of  $\text{TiO}_2$  are seen within a medium of branch-like aggregates of carbon black. The clumped aggregates are composed of  $\text{TiO}_2$  nanoparticles having a predominant particle size of ca. 20 nm. Because a significant volume of  $\text{TiO}_2$  is present within the clumped aggregates and not in contact with the carbon black, a significant proportion of the  $\text{TiO}_2$  has poor electrical contact with the electrode. For the purpose of material characterization, this situation is not ideal, as a significant amount of the  $\text{TiO}_2$  does not contribute to the electrochemical energy storage of the system.

For future characterization, preparation of the electrode should be optimized for characterization of the material itself. This is important so that the potential performance of new oxide nanoparticles for application in lithium-ion batteries can be better understood.

An initial study on the flame synthesis of  $\text{Li}_{0.4}\text{V}_2\text{O}_5$  is presented. A SEM image of this powder is seen in figure 2.

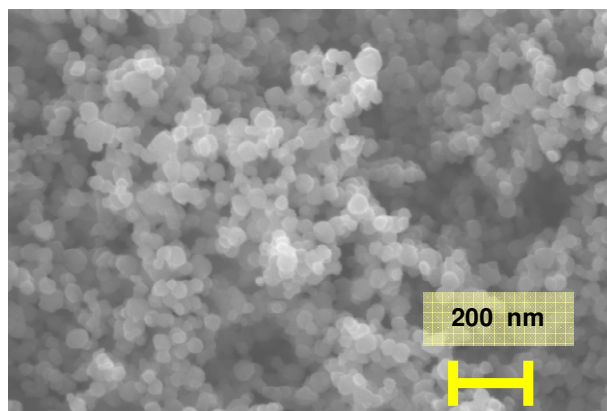


**Fig. 2:** SEM image of FSP-produced  $\text{Li}_{0.4}\text{V}_2\text{O}_5$ .

Separate electrodes containing FSP-produced  $\text{Li}_{0.4}\text{V}_2\text{O}_5$  nanoparticles and  $\text{V}_2\text{O}_5$  microparticles (Riedel-de Haën) were prepared. These  $\text{V}_2\text{O}_5$  microparticles were dissolved into the precursor used to synthesize the nanoparticles. The electrochemical properties were tested and the cycling discharge capacities of both materials are displayed in figure 3.

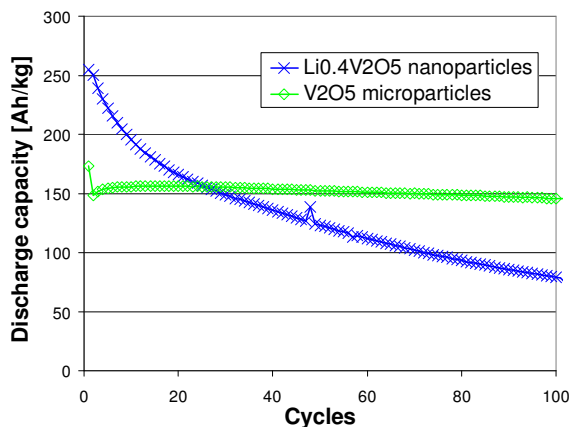


**Fig. 3:** Cycling behaviour of  $\text{Li}_{0.4}\text{V}_2\text{O}_5$  (FSP-produced) and  $\text{V}_2\text{O}_5$  (Riedel-de Haën) powders; electrolyte 1 M  $\text{LiPF}_6$  in EC/DMC (1:1, w/w); potential limits of 1.5 and 4 V and currents of  $\pm 100 \text{ mA g}^{-1}$  active mass.

Figure 3 shows that the lithiated nanoparticles have an initially higher capacity, but after about 20 cycles, the discharge capacity decreases below that of the microparticles used to synthesize them. In comparison, the microparticles are more stable. This is likely to do to the improved electrical and physical contact between these particles.

## Conclusions

Reliable measurement of oxide nanoparticles as active material will require optimization of the electrode preparation process. This will aid in the study of the potential impact of nanoparticles in lithium-ion batteries.

Oxide nanoparticles have an initially higher discharge capacity than their microparticle counterparts, however, the capacity of the nanoparticles sharply

decreases. This decline is likely due to both material degradation and loss of electrical contact during cycling. The magnitudes of each of these contributions are not fully understood. Further study of the materials and of the engineering of the electrodes is required.

## References

- [1] A.S. Arico, P. Bruce, B. Scrosati, J.M. Tarascon, W. Van Schalkwijk, *Nature Materials* **4**, 366 (2005).
- [2] T. Kawamura, M. Makidera, S. Okada, K. Koga, N. Miura, J. Yamaki, *J. Power Sources* **146**, 27 (2005).
- [3] L. Madler, H.K. Kammler, R. Mueller, S.E. Pratsinis, *J. Aerosol Sci.* **33**, 369 (2002).
- [4] R. Mueller, L. Madler, S. E. Pratsinis, *Chem. Eng. Scie.* **58**, 1969 (2003).
- [5] F.O. Ernst, H.K. Kammler, A. Roessler, S.E. Pratsinis, W.J. Stark, J. Ufheil, P. Novak, *Mater. Chem. Phys.*, article in press (2007).

## SYNTHESIS AND CHARACTERIZATION OF DOPED $\text{Li}[\text{Mn}_{0.5-x/2}\text{Ni}_{0.5-x/2}\text{Co}_x]\text{O}_2$ CATHODE MATERIALS

W. Scheifele, J. Reim<sup>1</sup>, H. Rentsch<sup>1</sup>, P. Novák  
+41(0)56 310 2471  
[werner.scheifele@psi.ch](mailto:werner.scheifele@psi.ch)

Layered cathode materials based on a Li-Mn-Ni chemistry promise several advantages over the widely used  $\text{LiCoO}_2$  - better electrochemical performance, improved safety, and lower cost. In early studies the effect on electrochemical performance of Mn:Ni ratio and synthesis conditions were investigated, but most of the materials lacked practical usefulness [1,2,3]. In 2001, Novák et al. were successful in stabilizing the oxide by introducing aluminum [4]. The  $\text{Li}[\text{Mn}_{0.5}\text{Ni}_{0.4}\text{Al}_{0.1}]\text{O}_2$  showed high charge capacity and excellent cycling stability even at elevated temperatures.

We now investigated similar layered cathode materials of the general formula  $\text{Li}[\text{Mn}_{0.5-x/2}\text{Ni}_{0.5-x/2}\text{Co}_x]\text{O}_2$  with  $x < 1/3$ . The materials were synthesized by a simple and cost-effective production route. We were specifically interested if the expected reduction of electrochemical performance due to lower cobalt content could be counteracted by the introduction of dopants. In a systematic study, we tried to introduce a broad range of dopants with different valence states and varying ionic radii: +2: Mg, +3: B, Al, Y, In, La, +5: Nb and Ta.

### Experimental

**Synthesis procedure:** The lithium complex oxides were synthesized by a solid state method. Commercial oxides, hydroxides, and/or carbonates of the respective elements were used. Lithium carbonate, a nickel compound, a manganese compound, a cobalt compound, and a compound of the doping element (boric acid, aluminum hydroxide, gallium oxide, magnesium hydroxide, niobium (V) oxide or tantalum (V) oxide, respectively) were mixed together in the appropriate ratio and fired at 1000 °C for 10 h in air. After cooling, the product was crushed and ball-milled to a powder with a particle size of  $d_{90} < 20 \mu\text{m}$ . Phase identity and purity of the products was checked using powder XRD.

**Electrochemical characterization:** Test electrodes comprising aluminum foil current collectors were prepared by the standard doctor blade technique starting from N-methylpyrrolidone-based slurries of active material. The composition of the electrodes was as follows: 85.7% of active mass, 4.75% of a poly-isobutene binder (Oppanol<sup>®</sup> B200, BASF AG, Ludwigshafen, Germany), and 9.55% mixture of carbon black (15% Ensaco<sup>®</sup> 250, Hubron Ltd, Manchester, England) and graphite (85% TIMREX<sup>®</sup> MB15, TIMCAL SA, Bodio, Switzerland).

The oxides were tested against lithium metal as counter electrode in titanium-based cells. The electrolyte used was battery grade ethylene carbonate and dimethyl carbonate (1:1) with 1M  $\text{LiPF}_6$  and was obtained from Ferro Corp. (Independence, OH, USA). The electrochemical measurements were conducted in combined galvanostatic-potentiostatic protocol. First, classical galvanostatic (constant current) cycling with a specific current of 30 mA/g in the beginning, increasing up to 600 mA/g during further cycling (cf. Figure 3) was performed until an upper voltage limit of 4.4 V vs.  $\text{Li}/\text{Li}^+$  and a lower voltage limit of 3.0 V vs.  $\text{Li}/\text{Li}^+$ , respectively, for the charge and discharge. At the end of each charge step a potentiostatic step followed, with a reduction of the current at the fixed upper potential limit down to a value of 3 mA/g, to complete the charging.

### Results and Discussion

One goal of this work was to establish a simple and low-cost production route for  $\text{Li}[\text{Mn}_{0.5-x/2}\text{Ni}_{0.5-x/2}\text{Co}_x]\text{O}_2$  type compounds. We chose the composition with  $x = 0.1$ ,  $\text{LiMn}_{0.45}\text{Ni}_{0.45}\text{Co}_{0.1}\text{O}_2$  (1), as the base and reference compound for our studies. We focused on solid state methods using metal oxides, hydroxides, and carbonates as precursor compounds. Single-phase products were obtained after one firing step at 1000 °C. Prerequisite is the proper choice of reactive raw materials in combination with the appropriate mixing technology. In the course of our work, we could show that our method is also applicable to other compositions, namely for  $x \leq 1/3$ .

Scanning electron microscopy was carried out to determine particle sizes and morphology (figure 1). Primary particles are mainly between 0.5 and 3  $\mu\text{m}$ , which are somehow agglomerated. This is in accordance with particle size measurements by laser granulometry giving typical values of  $d_{10}$  of ca. 1  $\mu\text{m}$ ,  $d_{50}$  of ca. 2-4  $\mu\text{m}$ , and  $d_{90}$  of 10-15  $\mu\text{m}$ .

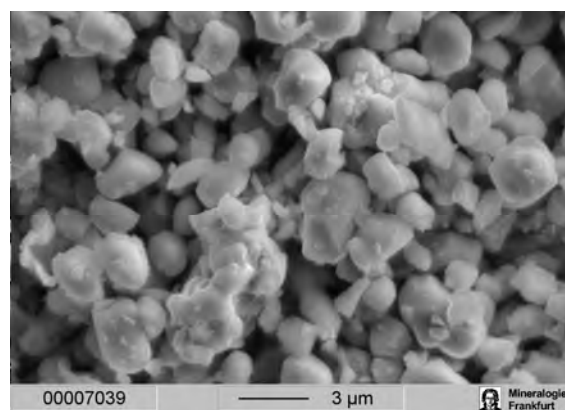


Fig. 1: SEM picture of compound 8.

<sup>1</sup> Ferro GmbH, Frankfurt/Main, Germany

In our doping study we tried to introduce 1 or 5 mol% of the selected dopants into our reference composition 1. This means, we applied our synthesis method to a series of low Co containing compounds  $\text{Li}[\text{Mn}_{0.45}\text{Ni}_{0.45}\text{Co}_{0.1}]{_{1-y}}\text{M}_y\text{O}_2$  with  $y = 0.01$  and  $0.05$ , respectively. In a first step, it was verified by powder XRD if the doping element M was incorporated into the host structure or not. The Rietveld method was used to determine the lattice constants of the target compound and to calculate the phase compositions if more than one phase was present.

Yttrium, indium, and lanthanum could not be introduced into the structure. As raw materials,  $\text{Y}_2\text{O}_3$ ,  $\text{In}_2\text{O}_3$ , and  $\text{La}(\text{OH})_3$  were used. In case of yttrium,  $\text{LiYO}_2$  and  $\text{Y}_2\text{O}_3$ , in case of indium,  $\text{Li}(\text{Ni}_{0.5}\text{In}_{0.5})\text{O}_2$ , and in case of lanthanum,  $\text{La}_2\text{Li}_{0.5}\text{Co}_{0.5}\text{O}_4$  and  $\text{LaNiO}_3$  were detected as secondary phases in quantitative amounts, respectively. For the case of boron, only the 1 % doped material could be synthesized. If higher B doping was tried, XRD revealed  $\text{Li}_3\text{BO}_3$  as a secondary phase. On the other hand, magnesium, aluminum, gallium, niobium, and tantalum could be incorporated into the structure up to 5 mol%.

**Table 1:** Overview of prepared samples of the doping series  $\text{Li}[\text{Mn}_{0.45}\text{Ni}_{0.45}\text{Co}_{0.1}]{_{1-y}}\text{M}_y\text{O}_2$  and discharge capacities [mAh/g] after 4th and 30th cycle (3.0-4.4 V / CCCV / 30 mA/g)

Comp.	M	y	Ionic radius [Å]	Discharge Capacity 4 <sup>th</sup> cycle [mAh/g]	Discharge Capacity 30 <sup>th</sup> cycle [mAh/g]
1	-	0		146	137
2	B	0.01	0.27	146	140
3a	Al	0.01	0.55	147	138
3b	Al	0.05	0.55	136	127
4a	Ga	0.01	0.62	145	138
4b	Ga	0.05	0.62	137	107
5a	Mg	0.01	0.63	141	134
5b	Mg	0.05	0.63	118	113
6	Nb	0.01	0.64	148	146
7	Ta	0.01	0.64	147	143

We attribute this mainly to size effects. Table 1 lists the effective ionic radii of the relevant elements [5]. All radii refer to a coordination number of six, for  $\text{Ni}^{2+}$  and  $\text{Co}^{3+}$  ions the low-spin states were assumed.  $\text{Y}^{3+}$ ,  $\text{In}^{3+}$ , and  $\text{La}^{3+}$  ions are too big, while  $\text{B}^{3+}$  is too small, and  $\text{Mg}^{2+}$ ,  $\text{Ga}^{3+}$ ,  $\text{Nb}^{5+}$ , and  $\text{Ta}^{5+}$  fit perfectly into the transition metal layer.

Compounds 1, 2, 3a, 3b, 4a, 4b, 5a, 5b, 6, and 7 were electrochemically tested in half-cells in the voltage range 3.0-4.4 V. Table 1 shows the measured discharge capacities in the 4th and 30th cycle. The undoped material 1 starts at 146 mAh/g and shows only a moderate cycling stability. The 1 % doped materials show approximately the same starting values in the 4th cycle. Doping with 1 % B shows a slightly positive effect on cycling stability, while doping with 1 % Al and Ga show nearly no effect, and doping with 1 % Mg even shows a negative effect. On the other hand, doping with 1 % Nb improves the cycling stability significantly: from the 4th to the 30th cycle, only a loss of 2 mAh/g is

observed. The effect of 1 % Ta doping is not as high as that of Nb, but the compound still performs better than the comparative samples. Doping with 5 % of Al, Ga, and Mg deteriorates the electrochemical performance markedly. For the most promising composition 6, a discharge capacity of 148 mAh/g (4th cycle, rate: 30 mA/g) was achieved while maintaining the good cycling stability.

In a second step we studied the influence of higher Co amounts. This, in addition to improvements in the synthesis conditions, resulted in a significant increase of charge capacity. Using our solid state route compounds like  $\text{Li}[\text{Mn}_{0.42}\text{Ni}_{0.42}\text{Co}_{0.16}]{_{0.99}}\text{Nb}_{0.01}\text{O}_2$  ( $x = 0.16$ ,  $y = 0.01$ ,  $M = \text{Nb}$ , 8) were synthesized and, for comparison, also undoped  $\text{Li}[\text{Mn}_{1/3}\text{Ni}_{1/3}\text{Co}_{1/3}]\text{O}_2$  ( $x = 1/3$ ,  $y = 0$ , 9). For the compound 8, a high initial discharge capacity of 162 mAh/g (@30 mA/g), excellent cycling stability, and very good rate capability is observed. As expected, doubling of Co content as in 9 further improves the electrochemical performance at high rates. This is illustrated in figure 2.

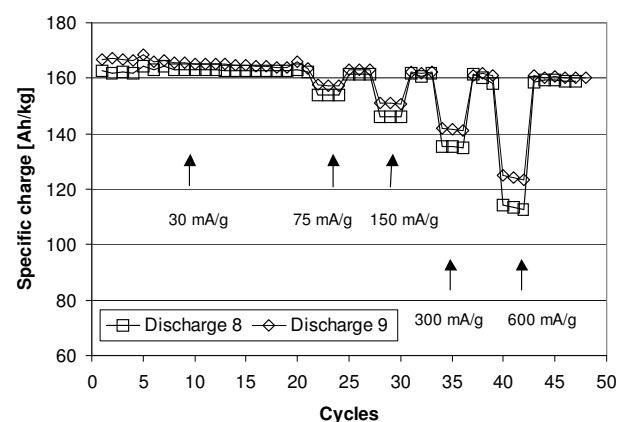


**Fig. 2:** Cycling behavior and rate capability tests of samples 8 and 9 (3.0-4.4 V vs. Li / CCCV).

## Conclusions

Layered cathode materials of the general type  $\text{Li}[\text{Mn}_{0.5-x/2}\text{Ni}_{0.5-x/2}\text{Co}_x]\text{O}_2$  with excellent electrochemical performance were prepared by a cost-effective solid state route. They are characterized by high discharge capacities and excellent cycling stabilities. We demonstrated the beneficial effect of introducing Nb and Ta to low Co containing compounds ( $x \ll 1/3$ ).

## References

- [1] E. Rossen, C.D.W. Jones, J.R. Dahn, *Solid State Ionics*, **57**, 311 (1992).
- [2] D. Caurant, N. Baffier, V. Bianchi, G. Grégoire, S. Bach, *J. Mater. Chem.*, **6**, 1149 (1996).
- [3] M.E. Spahr, P. Novák, B. Schnyder, O. Haas, R. Nesper, *J. Electrochem. Soc.*, **145**, 1113 (1998).
- [4] P. Novák, R. Nesper, M. Coluccia, F. Joho, A. Piotto Piotto, *Abstract Lithium Battery Discussion Electrode Materials*, Arcachon, France, 56 (2001).
- [5] R.D. Shannon, *Acta Cryst.*, **A32**, 751 (1976).

## NITROXIDE RADICAL POLYMERS FOR ORGANIC RADICAL BATTERIES

J. Vetter, P. Nesvadba<sup>1</sup>, L. Bugnon<sup>1</sup>  
C. Morton<sup>1</sup>, P. Novák  
+41(0)56 310 2457  
[petr.novak@psi.ch](mailto:petr.novak@psi.ch)

Persistent nitroxide radicals, most known example being 2,2,6,6-tetramethylpiperidine-N-oxyl (TEMPO), show a unique redox behavior. One-electron reduction leads to hydroxylamine anions whereas one-electron oxidation generates oxoammonium cations [1] (figure 1) that form stable salts. The reversible oxidation of nitroxides to oxoammonium cations (and their back-reduction into nitroxides) can be utilized in the recently emerged organic radical battery [2-6] (ORB).

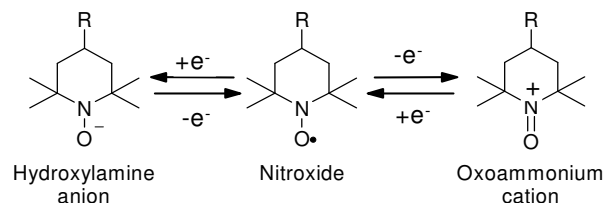


**Fig. 1:** Redox behavior of nitroxide radicals.

The setup of an ORB is similar to that of a classical secondary Li-ion battery [7], however, the cathode material (e.g. LiCoO<sub>2</sub>) used in Li-ion batteries is replaced by a suitable nitroxide compound. Among the advantages of ORB's is the absence of heavy metals making them environmentally benign and more safe, and fast charging and discharging at a high voltage (~3.6 V) practically identical to that of Li-ion batteries.

### Polymer synthesis

Low solubility in the electrolyte is a key requirement for battery materials, and it is currently best fulfilled with TEMPO moieties bound to a polymeric backbone as in, e.g., Poly(4-methacryloyloxy-2,2,6,6-tetramethylpiperidin-N-oxyl) (PTMA). Conventional synthesis of PTMA by polymerization of the corresponding amine monomer and subsequent oxidation of the amino group, however, yields only 60–80% radical content. By group-transfer-polymerization (GTP) of the pre-formed nitroxide monomer, a polymer with 100% radical content (GTP-PTMA) was obtained [8]. Synthesis in the presence of a bifunctional monomer (without a nitroxyl group) yielded an insoluble polymer (X-GTP-PTMA) with a calculated radical content of 94.3%.

### Electrochemical testing

Electrodes comprised of the powdered nitroxide, graphite (TIMREX<sup>®</sup> KS6, TIMCAL Ltd.), carbon black (Ensaco 250, TIMCAL Ltd.), and a binder (PVdF

6020, Solvay SA) in the ratio (by wt.) 27:46:8:19 were coated on Al foil. The electrodes were dried for 12 h at 120 °C in vacuum and then transferred into an argon-filled glovebox (H<sub>2</sub>O, O<sub>2</sub>, N<sub>2</sub> < 5 ppm) for cell assembly without exposure to air. Their geometric surface area was 1.33 cm<sup>2</sup>. Laboratory test cells with a coin-cell-type design [9] were assembled with a lithium metal counter and reference electrode and a glass fiber separator soaked with the electrolyte. Ethylene carbonate (EC) / dimethyl carbonate (DMC) 1:1, 1M LiPF<sub>6</sub> was used as the electrolyte. Electrochemical tests were performed at 25.0(±0.1) °C on a BATSMAL battery measurement system (Astrol Electronic AG). Cyclic voltammetry (CV) was carried out at a sweep rate of 0.1 mV s<sup>-1</sup>. Galvanostatic cycling experiments were performed between 3.0 and 4.0 V vs. Li/Li<sup>+</sup>.

### Results and Discussion

The suitability of the new PTMA for the application as active material in the positive electrode of organic radical batteries [2-6] was tested in half-cells vs. metallic lithium. Electrodes were prepared from PTMA, conductive carbon, and PVdF binder, with an aluminum foil current collector. In cyclic voltammetry (CV) vs. metallic Li, a single, sharp, highly reversible redox couple at a potential of ca. 3.6 V (vs. Li/Li<sup>+</sup>) was identified (figure 2). This redox potential is very similar to the potential of commonly used oxide materials (e.g., LiCoO<sub>2</sub>) for the positive electrode in lithium-ion batteries. The traces of seven consecutive CV cycles of a X-GTP-PTMA composite electrode shown in figure 2 are almost indistinguishable, showing that the redox reaction is very reversible with no or very little side reactions and/or deactivating processes.

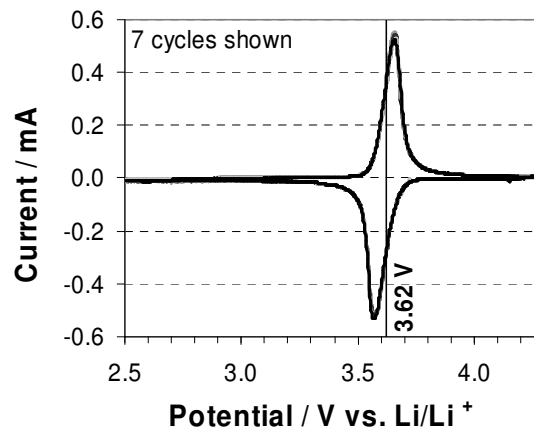


**Fig. 2:** CV of an X-GTP-PTMA composite electrode vs. metallic Li at 0.1 mV s<sup>-1</sup> in EC/DMC 1:1, 1M LiPF<sub>6</sub> electrolyte.

In galvanostatic cycling experiments on composite electrodes with the non-crosslinked GTP-PTMA, the initial specific charge was significantly lower than theoretically calculated from the nitroxide content. 45.1 Ah kg<sup>-1</sup> (76.7 Ah kg<sup>-1</sup>) and 58.7 Ah kg<sup>-1</sup> (86.9 Ah kg<sup>-1</sup>) were obtained during discharge (charge) at current rates of 0.1 and 0.5 C, respectively, the C-rate based on the theoretical

<sup>1</sup> Ciba Specialty Chemicals, Inc., Coatings Effects R&D, 4002 Basel

charge capacity of  $111.5 \text{ Ah kg}^{-1}$ . We attribute this low capacity, and the fact that higher capacities are obtained at higher currents, to the dissolution of the GTP-PTMA in the electrolyte. Dissolution may occur both in the discharged (= electroneutral) and/or charged (= positively charged) state. Upon cycling between 3.0 and 4.0 V, a rapid fading of the capacity is observed (figure 3).

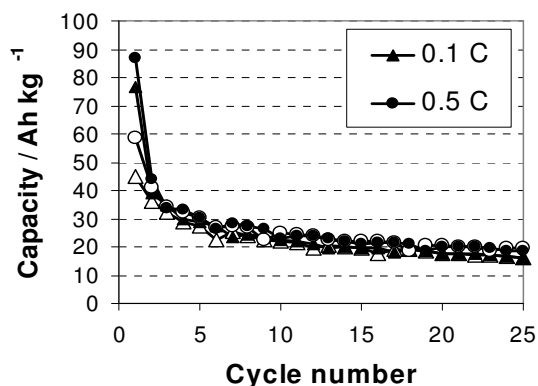


**Fig. 3:** Changes in charge (solid symbols) and discharge (empty symbols) capacities of GTP-PTMA with cycling in half-cells vs. metallic Li at 0.1 and 0.5 C rate. Electrolyte: EC/DMC 1:1, 1M LiPF<sub>6</sub>.

With the crosslinked X-GTP-PTMA, a reversible specific charge of ca.  $103 \text{ Ah kg}^{-1}$  at current rates up to 1 C could be obtained in galvanostatic cycling experiments between 3.0 and 4.0 V. This value is very close to the value of  $105.2 \text{ Ah kg}^{-1}$  theoretically calculated for a radical content of 93.4%, indicating a very good utilization of the nitroxide. The comparison of the cycling behavior of the two polymers demonstrates the severe impact of solubility on the performance of the ORB (Fig. 4). While most of the charge capacity is lost after only a few cycles with the non-crosslinked material, the fading is very low with X-GTP-PTMA, and after 25 cycles the initial reversible specific charge is preserved.

At 2 C rate, a slightly lower reversible specific charge of  $96.6 \text{ Ah kg}^{-1}$  was observed (most probably due to non-optimized electrode engineering). Capacity retention with cycling was excellent, though. After 200 cycles 95% of the initial reversible charge capacity was achieved (figure 5).

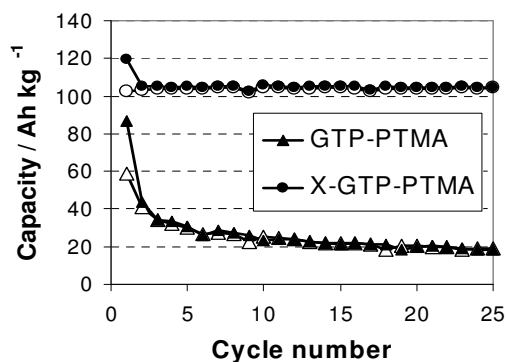


**Fig. 4:** Changes in charge (solid symbols) and discharge (empty symbols) capacities of non-crosslinked and cross-

linked PTMA with cycling in half-cells vs. metallic Li. Electrolyte: EC/DMC 1:1, 1M LiPF<sub>6</sub>.

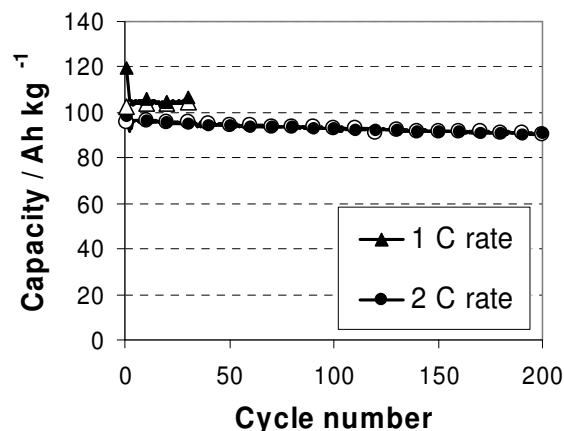


**Fig. 5:** Changes in charge (solid symbols) and discharge (empty symbols) capacities of X-GTP-PTMA with cycling in half-cells vs. metallic Li. Electrolyte: EC/DMC 1:1, 1M LiPF<sub>6</sub>.

## Conclusions

The new GTP-PTMA's can be utilized as active materials in positive electrodes of ORB's. The solubility of the polymer in the electrolyte plays a crucial role. Soluble materials result in rapid capacity fading of the battery. With the insoluble, crosslinked X-GTP-PTMA, a utilization of the NO\* groups close to 100% and high cycling stability can be achieved.

## References

- [1] L.B. Volodarsky, V.A. Reznikov, V.I. Ovcharenko, Synthetic Chemistry of Stable Nitroxides, CRC Press, Boca Raton (1994).
- [2] K. Nakahara, S. Iwasa, M. Satoh, Y. Morioka, J. Iriyama, M. Suguro, E. Hasegawa, Chem. Phys. Lett. **359**, 351 (2002).
- [3] L.F. Deng, H.X. Li, L.X. Xiao, Y.H. Zhang, J. Cent. South Univ. Technol. **10**, 190 (2003).
- [4] H. Nishide, S. Iwasa, Y.J. Pu, T. Suga, K. Nakahara, M. Satoh, Electrochim. Acta **50**, 827 (2004).
- [5] H. Nishide, T. Suga, ECS Interface **14(4)** 32 (2005).
- [6] T. Katsumata, M. Satoh, J. Wada, M. Shiotsuki, F. Sanda, T. Masuda, Macromol. Rapid Commun. **27**, 1206 (2006).
- [7] M. Winter, R.J. Brodd, Chem. Rev. **104**, 4245 (2004).
- [8] L. Bugnon, C. Morton, P. Novák, J. Vetter, P. Neszvadba, Chemistry of Materials submitted (2007).
- [9] P. Novák, W. Scheifele, F. Joho, O. Haas, J. Electrochem. Soc. **142**, 2544 (1995).

## CORRELATION BETWEEN THE ACTIVE SURFACE AREA OF GRAPHITE MATERIALS AND FIRST LITHIUM INTERCALATION

J. Ufheil, H. Buqa, F. Krumeich<sup>1</sup>, D. Goers<sup>2</sup>,  
H. Wilhelm<sup>2</sup>, M. E. Spahr<sup>2</sup>, J. Dentzer<sup>3</sup>  
C. Vix-Guterl<sup>3</sup>, P. Novák  
+41(0)56 310 2103  
[joachim.ufheil@psi.ch](mailto:joachim.ufheil@psi.ch)

It is well known that, when lithium is intercalated into graphite in ethylene carbonate (EC) containing electrolytes solvent co-intercalation could occur, leading to the destruction of the graphite structure (e.g., exfoliation). This exfoliation process can be suppressed if an efficient solid electrolyte interphase (SEI), i.e., a passivation layer, is formed. The objective of this work is to study the role played by the active surface area (ASA) of graphite materials during the first electrochemical lithium ion insertion. ASA which is related to the presence of defects at the carbon surface appears as a critical graphite surface parameter which influences the surface passivation mechanism and the graphite exfoliation. A representative synthetic graphite was selected and its ASA was modified by thermal treatment in argon and air. The first electrochemical lithium insertion of the as-received and heat-treated graphite materials was characterized in electrochemical lithium half-cells containing 1M LiPF<sub>6</sub> in EC:DMC (dimethyl carbonate) as electrolyte system.

### Experimental

Variation of the graphite surface characteristics was obtained through thermal modifications under several gas compositions without significantly changing the bulk properties, especially the total surface area and the particle size distribution of the product. For this, the TIMREX<sup>®</sup> SLX50 graphite (TIMCAL SA, Bodio, Switzerland) was heated at 1300 °C under an argon flow and maintained for 1 min or 1 hour at this temperature. After the heat treatment, the graphite sample was either cooled in an argon atmosphere until room temperature or quenched in air which causes a slight oxidation of the carbon surface. After cooling down to room temperature, the samples were exposed to air atmosphere. The ASA was determined by outgassing the sample at 950 °C under vacuum. An initial oxygen pressure of 66.5 Pa was introduced into the reactor at 300 °C causing chemisorptions of O<sub>2</sub> on the graphite surface. The O<sub>2</sub> chemisorption process over a period of 15 h at 300 °C led to the formation of surface oxide complexes at the graphite ASA. The amount of oxygen complexes formed was determined by mass spectrometry by measuring the amount of CO and CO<sub>2</sub> resulting from the decomposition of the oxygen complexes at

temperatures higher than their formation by performing a temperature-programmed desorption (TPD) step between 300 and 950 °C. Knowing the number of each moles of each gas desorbed and taking the area of an edge carbon site that chemisorbed an oxygen atom as 0.0083 nm<sup>2</sup>, the surface area occupied by chemisorbed oxygen can be determined. Detailed information can be found elsewhere [1].

The electrochemical experiments were performed in two-electrode arrangement in standard laboratory cells as described elsewhere [2]. The lithium foil (Aldrich) and 1 M LiPF<sub>6</sub> in EC:DMC [1:1] (Ferro, Germany) were used without any further treatment. Working electrodes were prepared by doctor blading the SLX50 graphite with polyvinylidene fluoride (SOLEF 1015, Solvay SA) binder onto a copper current collector. The electrodes were vacuum dried at 120 °C and contained ca. 10 mg of graphite (90 wt.% + 10 wt.% PVDF). Galvanostatic measurements were performed at specific currents of 10 mA/g of carbon to complete the SEI formation in the first Li<sup>+</sup> insertion cycle. After a potential of 5 mV vs. Li/Li<sup>+</sup> was reached, the discharging was continued until the current dropped below 5 mA/g. The charging was performed at a constant specific current of 10 mA/g until a cut-off potential of 1.5 V vs. Li/Li<sup>+</sup> was reached. All measurements were carried out at room temperature.

### Results and Discussion

The TPD curves of the different SLX50 graphite samples after chemisorption of O<sub>2</sub> at 300 °C showed that the formation of CO and CO<sub>2</sub> is completed below 900 °C as shown in figure 1 for the sample SLX50 treated in argon during 1 hour.

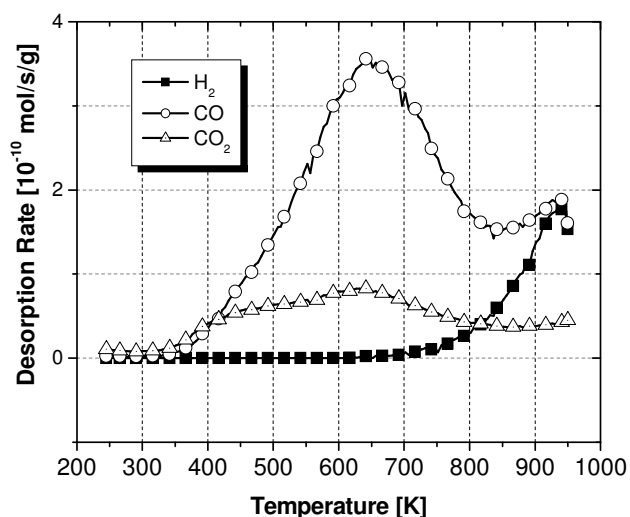


**Fig. 1:** Desorption rate of CO and CO<sub>2</sub> as a function of the desorption temperature after oxygen chemisorption for the "SLX50 1hr Ar" sample.

This indicates that the total amount of oxygen complexes formed on the active sites during the

<sup>1</sup> ETH Zürich

<sup>2</sup> TIMCAL SA, Bodio

<sup>3</sup> Institut de Chimie des Surfaces et Interfaces,  
Mulhouse, France

This indicates that the total amount of oxygen complexes formed on the active sites during the oxygen chemisorption was totally removed during the TPD. Above 800 °C, the main gas desorbed is H<sub>2</sub> resulting from structural rearrangements of the graphite surface, which were not completed by the heat treatment at 1300 °C in an argon atmosphere.

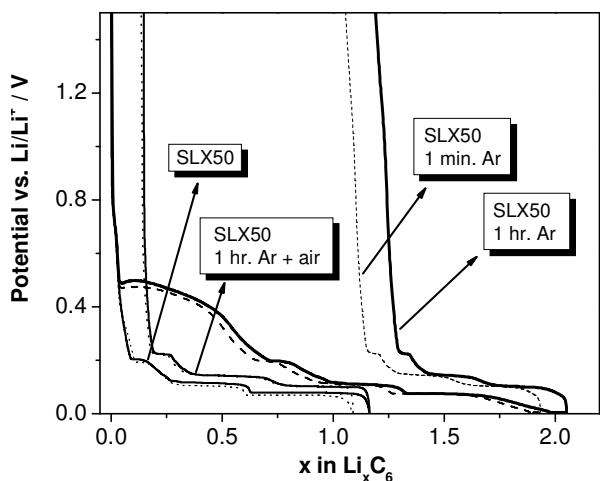


**Fig. 2:** First electrochemical lithium insertion into TIMREX® SLX50 (i) as received and (ii) heat treated at 1300 °C in argon for 1 min and 1 h, respectively, and subsequently cooled down in argon and air atmosphere, respectively, in EC:DMC, 1M LiPF<sub>6</sub> electrolyte

From the total amount of CO and CO<sub>2</sub> released after chemisorption, the ASA was calculated; the values obtained for the different SLX50 samples are reported in table 1.

**Table 1:** Active surface area (ASA) and irreversible capacity in the first cycle of graphite materials (“SLX50”: as-received sample; “SLX50 1hr. Ar”: as-received SLX50 sample treated 1 hour in an argon flow; “SLX50 1min. Ar”: as-received SLX50 sample treated 1 min in an argon flow; “SLX50 1hr. Ar + air”: as-received SLX50 sample treated 1 hour in an argon flow following by an air quenching for the cooling).

Graphite Sample	ASA m <sup>2</sup> /g	Irrev. Cap. %; 1 <sup>st</sup> cycle
SLX50	0.30	8
SLX50 1hr. Ar	0.065	57
SLX50 1min. Ar	0.092	54
SLX50 1hr. Ar+ air	0.44	10

As expected, the heat treatment in argon has increased the structural ordering of the graphite and therefore removed the surface defects as indicated by the decrease of the ASA values. Therefore, it is not surprising that the ASA is lower after 1 hour heat treatment compared to 1 minute. A subsequent air treatment leads to a mild oxidation of the graphite surface as pointed out by the increase of the ASA value after the argon treatment. It must be noted that the ASA value after air quenching is higher than the

value of the pristine sample indicating the presence of a higher amount of defects.

For a detailed investigation of the film formation in the first cycle, we analyzed the irreversible capacity (called also charge loss) and the galvanostatic charge curves of the first lithium insertion into the graphite. The charge losses (%) of the graphite samples during the first cycle are indicated in table 1. The curves of the first galvanostatic lithium intercalation into the graphite TIMREX® SLX50 and the three heat-treated SLX50 graphites are reported in figure 2.

The pristine sample as well as the sample cooled down in air show the typical insertion properties expected for a highly crystalline graphite material. A reversible capacity of about 365 mAh/g with a coulombic efficiency of 94 % could be observed at a specific current of 10 mA/g. No additional plateau is observed with these both samples suggesting that a protective passivation film was formed on the graphite surface. No exfoliation of the graphite can be observed. In contrast, the heat-treated SLX50 graphite samples cooled under Ar atmosphere show an additional irreversible potential plateau during the first electrochemical lithium insertion in EC:DMC (see figure 2). The process starts at about 450 mV vs. Li/Li<sup>+</sup> and was identified as graphite exfoliation. The potential plateau corresponds to the irreversible charge consuming process of film formation on the graphite surface freshly created by the exfoliation. This relatively low potential plateau is typical for exfoliation in an EC electrolyte [3]. As a consequence, this irreversible process significantly increases the loss of the specific charge during the first electrochemical lithium insertion as shown in table 1.

The comparison of the electrochemical data with the graphite surface characteristics reveals that the electrochemical behavior of the graphite can be correlated to the structural modifications occurring during the treatments [4].

## References

- [1] N.R. Laine, F.J. Vastola, P.L. Walker, J. Phys. Chem. **67**, 2030 (1963).
- [2] M.E. Spahr, H. Wilhelm, T. Palladino, N. Dupont-Pavlovsky, D. Goers, F. Joho, P. Novák, J. Power Sources **119-121**, 543 (2003).
- [3] M.E. Spahr, H. Buqa, A. Würsig, D. Goers, L. Hardwick, P. Novák, F. Krumeich, J. Dentzer, C. Vix-Guterl, J. Power Sources **153**, 300 (2006).
- [4] P. Novák, J. Ufheil, H. Buqa, F. Krumeich, M.E. Spahr, D. Goers, H. Wilhelm, J. Dentzer, R. Gadiou, C. Vix-Guterl, J. Power Sources, in press (2007).

FUEL CELLS

DIAGNOSTICS



## A COMPLETE SYSTEM FOR *IN SITU* X-RAY DIFFRACTION MEASUREMENTS ON ELECTROCHEMICAL SYSTEMS AT A SYNCHROTRON SOURCE

F. Rosciano, M. Holzapfel, H. Kaiser,  
W. Scheifele, P. Ruch, M. Hahn, R. Kötz,  
P. Novák  
+41(0)56 310 5426  
[fabio.rosciano@psi.ch](mailto:fabio.rosciano@psi.ch)

Portable power sources have undergone a quick evolution in the last decade, leading to smaller and more efficient devices for various applications ranging from personal electronic gadgets to hybrid vehicles. Among these, lithium-ion batteries are prominent for their ability to deliver both high power and high energy density. Lithium-ion batteries work on the following principle: both the anode and the cathode are based on host materials (normally layered) allowing reversible intercalation and deintercalation of lithium ions. Other electrochemical systems, such as supercapacitors, work with the same intercalation principle. The understanding of structural changes in these intercalation materials is an important prerequisite for the further improvement of the electrodes. An excellent method for studying the materials' structural changes during electrochemical cycling is X-ray diffraction. Most of the relevant materials are sensitive to humidity and/or air when partly charged. Thus, *in situ* experiments in hermetically sealed electrochemical cells are advantageous. Implementing the *in situ* cells at a synchrotron will allow for the required fast measurements with high resolution, qualities that cannot be achieved on conventional X-ray diffractometers.

Only few *in situ* electrochemical cells for XRD measurements have been described over the years. Our particular implementation is derived from the setup known as "coffee bag" cells [1] which has important advantages over other approaches, namely the use of cheap single-use components, easy fabrication of the cells, and good reproducibility of the electrochemical measurements. The main innovation in our new system presented here is the automatic sample changer: the collection of diffraction patterns at the MS beamline at the Swiss Light Source (SLS) is very fast (~10 sec), thus, for an efficient use of the costly beamtime many samples are automatically measured in parallel. The time-consuming manual manipulations in the hatch are no more necessary. (Note that the electrochemical processes have a time scale of hours.) The electrochemical cells are sequentially and repeatedly moved into the X-ray beam in a very precise manner and the X-ray patterns are recorded as a function of either time or according to any other electrochemical parameters like cell voltage or the amount of charge given to the battery.

## "Coffee Bag" Cells

The "coffee bag" electrochemical cells consist of several flat parts designed to keep the thickness of the assembled cell in the order of 500  $\mu\text{m}$  while minimizing the presence of materials, other than the active material, giving rise to X-ray reflexes. In figure 1 the schematic drawing of the cell is shown.

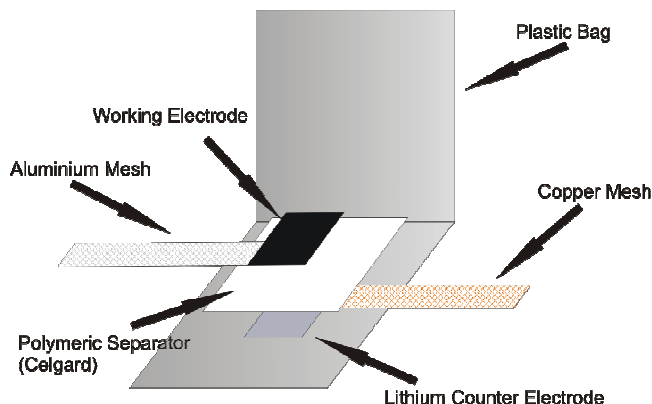


**Fig. 1:** Sketch of the coffee bag cell in its configuration for Li-ion batteries.

Most components of a lithium-ion battery are very sensitive to oxygen and moisture, thus, the strictest requirement on the *in situ* cell is the need of air and moisture tightness. For this reason the cells are sealed with a 117  $\mu\text{m}$  thick composite foil constituted by four layers, from the inside to the outside (i) polyethylene, (ii) aluminum, (iii) polyethylene, and (iv) oriented polyamide. The 12  $\mu\text{m}$  thick aluminum inner layer is a good barrier to  $\text{O}_2$  and  $\text{H}_2\text{O}$ . Of course, the use of such a composite foil introduces additional features in the XRD patterns but it is still a much better solution compared to standard *in situ* XRD cells using beryllium windows practically transparent to X-rays - apart from the health hazard of beryllium, corrosion of beryllium occurs at potentials positive to 4 V vs.  $\text{Li}/\text{Li}^+$ .

The electroactive mass is supported by a current collector made from expanded metal (Al or Cu, respectively, depending on the potential window of the particular material). The electrodes are prepared by the common "doctor blade" technique which consists of spreading a slurry in (an) organic solvent(s) of the electroactive material, a conductivity enhancer (graphite and/or carbon black), and a binder (e.g., PVdF). The slurry is first spread onto a non-adhesive sheet from which it is easily removed once dried. The free-standing electrodes (2cm x 2cm) are cut with a scalpel and then pressed on the respective current collectors. All cell components are then dried in vacuum at 120  $^\circ\text{C}$  overnight to remove all traces of solvents and humidity and subsequently transferred into an Ar-filled glove box. In the glove box the cells are assembled, filled with electrolyte, and sealed using a home-made machine that evacuates the cell and thermally seals the foil. For

experiments where the electrolyte amount is an important variable (such as in supercapacitor applications) and/or when the electrolyte cannot be evacuated because of high volatility, the alternative is to seal dry cells with a straw which is later used to fill in the electrolyte and then sealed manually [2]. To demonstrate the diffraction patterns resulting from the use of said coffee bag cells, the example of  $\text{LiCoO}_2$  is shown.  $\text{LiCoO}_2$  is the cathodic material of choice in many commercial Li-Ion batteries and has a layered structure of the space group  $R\bar{3}m$ . At high voltage, lithium ions are deintercalated from the structure and a second phase appears, mixed with the first one [3]. This second phase has a monoclinic space group and could be observed in our measurements, as shown in figure 2.

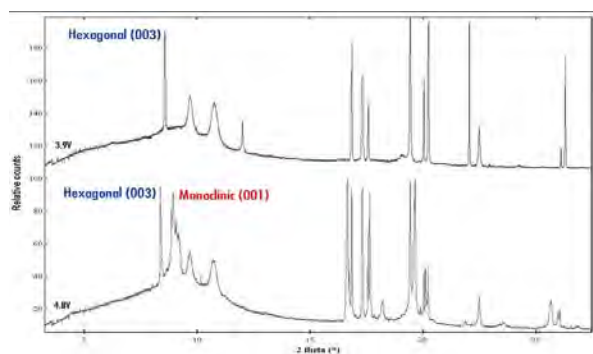


**Fig. 2:** Sample In-situ XRD measurements obtained in the coffee bag cell. At low voltage only the peaks relative to the hexagonal phase are visible, while at higher voltage the peaks relative to the monoclinic phase appear. The measurements were carried out against a metallic lithium counter electrode in standard LP30 electrolyte. Every measurement lasted 10 seconds.

The feature at low  $2\theta$  angles is due to the amorphous polymer fraction on the coffee bag.

### Automatic Sample Changer

The sample changer has been developed completely in house. It allows moving up to 32 cells into and out of the beam. It works using a “slideshow motion”; the cells are placed on a sliding carriage that moves in discrete steps. When the cell that is to be measured is in the correct position, a compressed air-operated slider pushes the cell holder in the beam. When the collection of diffraction pattern is finished, the cell holder is retracted into the carriage and the procedure is repeated for the next cell. Apart from the standard “coffee bag” cells, the sample changer can accommodate other types of experimental cells; the only condition is the cell thickness. In figure 3 the sample changer is shown.

Prior of being introduced in the machine, the cells are enclosed in special enclosures. These casings ensure that the cell is measured reproducibly in the same spot and that the correct amount of pressure is applied to the cell internals.

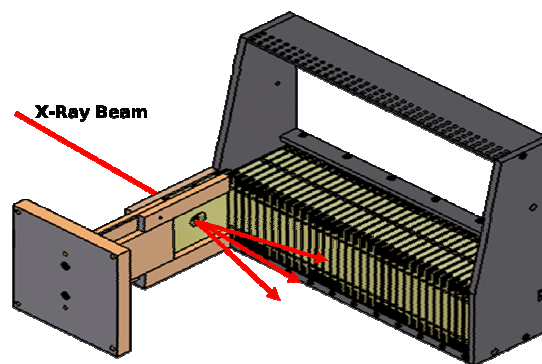


**Fig. 3:** Sketch of the automatic sample changer.

### Material Science Beamline @ SLS

We tested our setup at the MS Beamline at the Swiss Light Source. The main feature of this beamline is the MYTHEN microstrip detector [4]: this device allows for quick measurements, a key requirement to study systems whose state changes rapidly such as supercapacitors. When using MYTHEN, X-Rays are detected over a range of  $60^\circ$  all at the same time, thus eliminating the need for moving the detector in discrete steps. It is also a very sensitive detector, as it allows for an intrinsic resolution of  $0.004^\circ$ . With this system, a complete XRD pattern can be acquired in a few seconds, as opposed to the typical duration of a conventional measurement in the range of some hours.

### Summary

A complete system for XRD measurements at a synchrotron source has been presented. The system is primarily composed by specially engineered cells and an automatic sample changer, and relies on the good specifications of the MS Beamline at the Swiss Light Source.

### Acknowledgements

We are thankful to the MS Beamline team at the SLS, namely Dr. B. Schmitt and Dr. D. Maden, for their help in setting up the system, and Gruber Folie GmbH for providing the layered foil.

### References

- [1] J.M. Tarascon, A.S. Godzd, C. Schmutz, F. Shokoohi, P.C. Warren, *Solid State Ionics*, **86-88**, 49 (1996).
- [2] P.W. Ruch, M. Hahn, F. Rosciano, M. Holzapfel, B. Schmitt, W. Scheifele, H. Kaiser, P. Novák, R. Kötz, A. Wokaun, this report.
- [3] T. Ohzuku, A. Ueda, *J. Electrochem. Soc.* **141**, 2972 (1994).
- [4] B. Schmitt, C. Brönnimann, E.F. Eikenberry, F. Gozzo, C. Hörmann, R. Horisberger, B. Patterson, *Nucl. Instrum. Methods Phys. Res., Sect. A*, **501**, 267 (2003).

## IN SITU X-RAY DIFFRACTION OF CARBONS FOR SUPERCAPACITORS

P.W. Ruch, M. Hahn, F. Rosciano,  
M. Holzapfel, B. Schmitt, W. Scheifele,  
H. Kaiser, P. Novák, R. Kötz, A. Wokaun  
+41(0)56 310 4131  
[patrick.ruch@psi.ch](mailto:patrick.ruch@psi.ch)

The insertion of ions into carbonaceous host structures provides an attractive means for charge storage (e.g. in Li-ion batteries), but at the same time induces stresses due to considerable volume changes accompanying the insertion/deinsertion process. The above aspects become relevant in supercapacitors when attempting to increase the energy density by using larger potential windows. In order to examine the effects of ion insertion into graphitic carbons from typical supercapacitor electrolytes, graphite electrodes were studied during electrochemical cycling by *in situ* X-ray diffraction (XRD) at the Swiss Light Source (SLS).

### Experimental

*In situ* electrochemical pouch cells were assembled according to figure 1 [1]. Working electrodes were fabricated from powder graphite (SFG44, from Timcal, Switzerland) using 10 wt% polyvinylidene fluoride (PVDF, from Solay, Belgium) as a binder. An activated carbon cloth (ACC-568-15, American Kynol Inc., USA) was used as the counter electrode. After assembly, electrolyte solutions consisting of 1 M  $(C_2H_5)_4NBF_4$  in acetonitrile (AN) and in propylene carbonate (PC) were added through a tube prior to sealing of the cell.

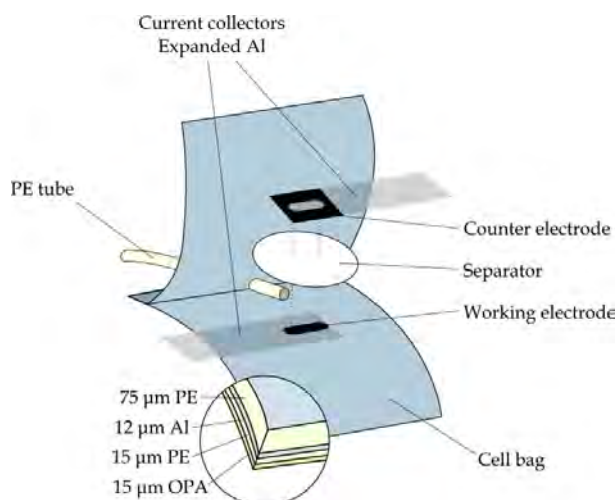


**Fig. 1:** Assembly of the pouch cell for *in situ* XRD measurements. The cell lining consisted of polyethylene (PE), aluminum (Al) and an oriented polyamide (OPA).

XRD measurements were performed at the Materials Science beam line of the SLS using an automatic sample changer [2] and a beam energy of 17.5 keV, ( $\lambda = 0.709 \text{ \AA}$ ). During acquisition of the patterns, the working electrode was cycled in the anodic and

cathodic potentials, respectively, using cyclic voltammetry at a scan rate of 0.3 mV/s.

### Results and Discussion

The cyclic voltammograms collected during the XRD measurements are summarized in figure 2. Current waves in the cathodic and anodic potential ranges correspond to the intercalation of cations,  $(C_2H_5)_4N^+$ , and anions,  $BF_4^-$ , respectively, into the graphite host structure.

During cation intercalation, disappearance of the 002 Bragg reflex was observed by *in situ* XRD, suggesting that the intercalation of  $(C_2H_5)_4N^+$  into the intralayer spacing of graphite occurs upon charging, but without the formation of well-defined stages in the bulk electrode.

For the intercalation of anions, a clear splitting of the 002 peak was seen along with the appearance of several new peaks indicating the formation of well-defined stages (figure 3).

The reappearance of the 002 Bragg reflex after deintercalation indicates that the original graphite structure is reestablished. However, an increase in the full width at half maximum (FWHM) of the peak indicates degradation of the structure. The two electrolyte systems are compared in both potential ranges in figure 4.

Clearly, the graphite electrodes are degraded after the first two cycles in both electrolyte systems. Under the present experimental conditions, however, the cycling of graphite in the anodic potential range in the PC-based electrolyte appears to have the least destructive effect on the electrode.

At the same time, the charge/discharge efficiencies in this range display the highest values of the four systems investigated (table 1). These high efficiencies are therefore most likely linked to a highly reversible intercalation and deintercalation into and out of the graphite host lattice with only little deterioration of the electrode.

**Table 1:** Discharge efficiencies and intercalation onsets of SFG44 in the different electrolyte systems investigated. In all cases, the electrolyte used was 1 M  $(C_2H_5)_4NBF_4$ .

Solvent	Potential range	Cycle	Discharge efficiency	Intercalation onset vs. Li/Li <sup>+</sup>
AN	cathodic	1	35 %	1.1 V
		2	48 %	1.1 V
AN	anodic	1	39 %	5.0 V
		2	-	5.0 V
PC	cathodic	1	59 %	0.9 V
		2	58 %	0.9 V
PC	anodic	1	65 %	4.9 V
		2	67 %	4.9 V

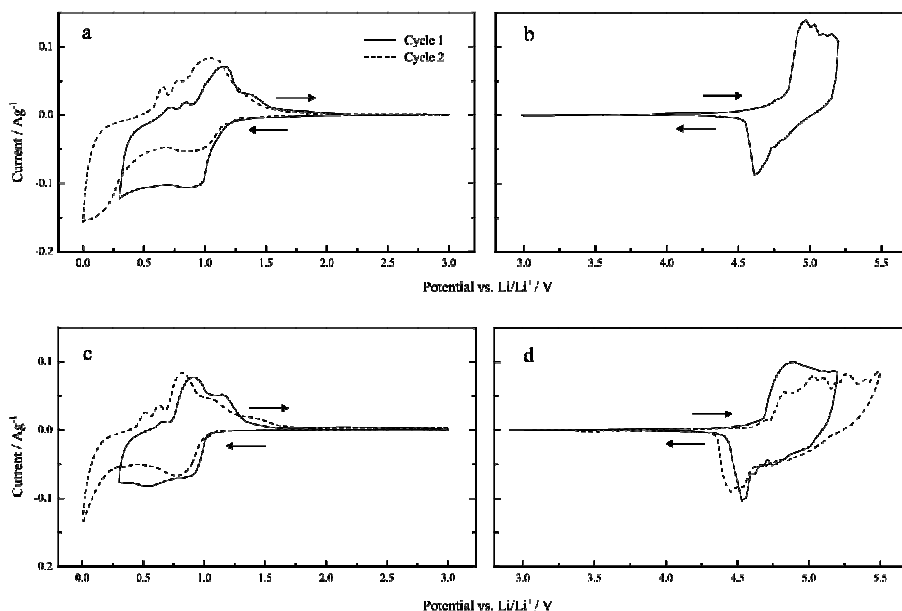


**Fig. 2:** Cyclic voltammograms for SFG44 in 1 M  $(C_2H_5)_4NBF_4$  in the cathodic and anodic potential ranges in AN (a, b) and PC (c, d).

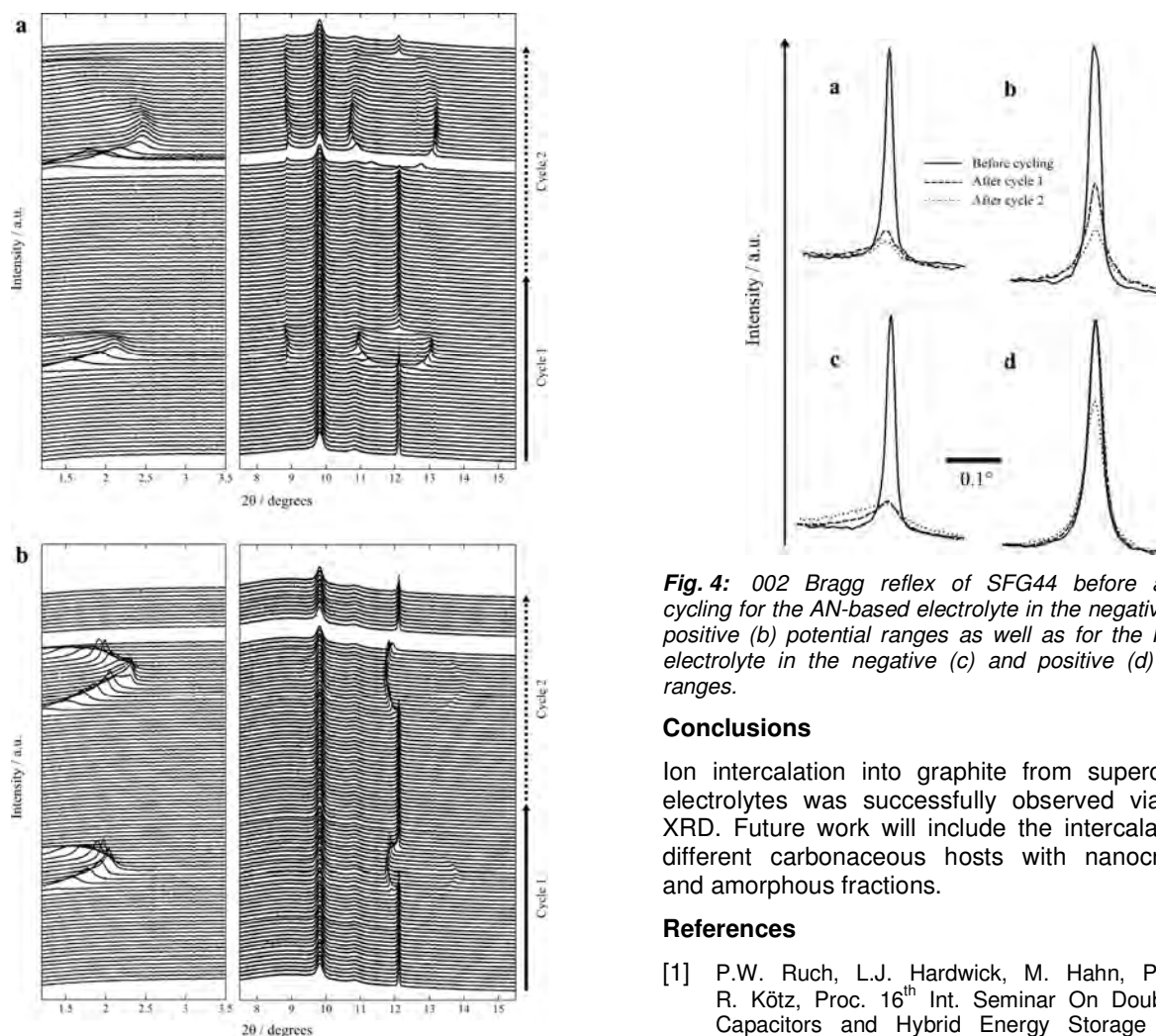


**Fig. 3:** In situ XRD patterns of SFG44 in the anodic potential range for the AN- (a) and PC-based (b) electrolytes.

**Fig. 4:** 002 Bragg reflex of SFG44 before and after cycling for the AN-based electrolyte in the negative (a) and positive (b) potential ranges as well as for the PC-based electrolyte in the negative (c) and positive (d) potential ranges.

## Conclusions

Ion intercalation into graphite from supercapacitor electrolytes was successfully observed via *in situ* XRD. Future work will include the intercalation into different carbonaceous hosts with nanocrystalline and amorphous fractions.

## References

- [1] P.W. Ruch, L.J. Hardwick, M. Hahn, P. Novák, R. Kötz, Proc. 16<sup>th</sup> Int. Seminar On Double Layer Capacitors and Hybrid Energy Storage Devices, Florida (2006).
- [2] F. Rosciano, M. Holzapfel, H. Kaiser, W. Scheifele, P. Ruch, M. Hahn, R. Kötz, P. Novák, this report.

## INVESTIGATION OF MESOPHASE PITCH DERIVED CARBONS FOR HIGH-ENERGY SUPERCAPACITORS

M. Hahn, P.W. Ruch, R. Kötzt  
+41(0)56 310 2128  
[matthias.hahn@psi.ch](mailto:matthias.hahn@psi.ch)

A major direction of today's research in supercapacitors (SC) is devoted to the increase of their energy density. This goal can either be achieved by increasing the voltage of the SC device, or by increasing the capacitance of the electrode material. A combination of both measures was recently suggested by Japanese researchers [1] who introduced a novel kind of electrode material, which they derived via a two-step pyrolysis / activation process from a mesophase pitch (MP), a class of material that is well known as a liquid crystalline precursor for the production of high modulus carbon fibres. The thus synthesized MP electrode material (Mesophase Pitch Activated Carbon, MPAC) was advertised to have both a superior volumetric capacitance, and also higher voltage stability than conventionally used activated carbons. In recent work we have investigated these claims.

### Experimental

The MPAC electrode material was synthesized according to the procedure given in the patent literature [2]. Briefly, 1 g of the mesophase pitch was first calcined for 2 hours at 800 °C, and in a subsequent step activated in a KOH melt (KOH to carbon ratio = 4:1). Both heat treatments were carried out in a horizontal tube furnace under a continuous stream of argon. After activation, the carbon was washed with hot hydrochloric acid and hot water, and finally dried at 130 °C in vacuum. Around 5 mg of the binder-free MPAC sample was then placed in a home-built electrochemical dilatometer with activated carbon serving both as the counter and as the pseudo reference electrode material. Details of the set-up are given in [2]. The height change of the MPAC working electrode was monitored during cycling to negative and positive potentials relative to the immersion potential (ip), respectively, using cyclic voltammetry at a scan rate of 2 mV/s. A solution of 1 M  $(C_2H_5)_4NBF_4$  in propylene carbonate was used as the electrolyte. The current is related to the mass of the sample and the scan rate, thus yielding the gravimetric capacitance.

### Results and Discussion

The cyclic voltammograms and the simultaneous dilatation record of the MPAC electrode are summarized in figure 1. During the first sweep to negative potentials a steep rise of the current and the simultaneous expansion of the material up to 60 % is seen at potentials below 1.5 V. Only after this initial electrochemical activation, that can probably be attributed to the insertion of the large  $(C_2H_5)_4N^+$  cations, the electrode attains its pronounced capacitive behaviour. During subsequent cycling in

the negative potential range the appearance of the voltammogram remains almost unchanged, while the periodic expansion is reduced to about 40%. Likewise, a capacitive steady state behaviour is observed in the positive potential range. However, the accompanying periodic swelling / shrinking is less pronounced, presumably due to the smaller size of the  $BF_4^-$  anions compensating the positive excess charge on the carbonaceous solid. In a separate experiment, the height change of a full capacitor cell was found to be insensitive to the pressure applied in the range of 1 to 50 bars. Higher loads can hardly be applied in a reasonable way on the SC housing.

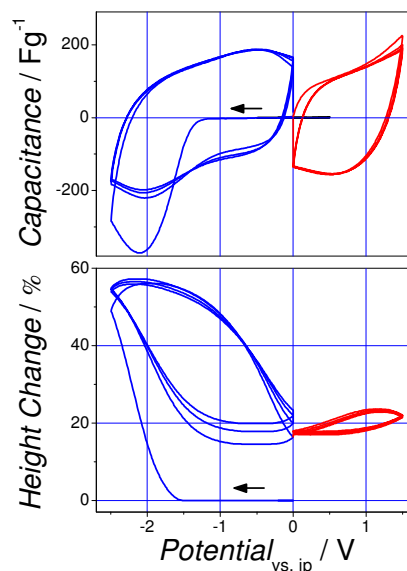


**Fig. 1:** Voltammograms and simultaneous dilatation records of the novel MPAC electrode.

### Conclusions

We could show that the novel MPAC electrode material displays the promised high gravimetric capacitance of up to 200  $Fg^{-1}$ . However, the material is shown to experience huge dimensional changes during charging / discharging that have to be attributed to the insertion of ions into the layered micro structure. It appears to be impossible to prevent the charging induced swelling by simple technical means, e.g. by stiffening the capacitor housing, in contrast to statements given in the patent literature [3]. The anticipated superior voltage stability of the MPAC electrode material will be addressed in future work.

### Acknowledgement

Financial support by Conception Development Michelin SA (CDM), Givisiez, is gratefully acknowledged.

### References

- [1] M. Takeuchi, K. Koike, T. Maruyama, A. Mogami, M. Okamura, *Electrochemistry* **66**, 1311 (1998).
- [2] M. Hahn, O. Barbieri, R. Gallay, R. Kötzt, *Carbon* **44**, 2523 (2006).
- [3] M. Takeuchi, K. Koike, A. Mogami, T. Maruyama, patent US 6721168 B2.

## XPS STUDY OF NITROGEN CONTAINING TEMPLATED CARBONS FOR SUPERCAPACITORS

R. Kötz, I. Czekaj, C. Vix-Guterl<sup>1</sup>, R. Gadiou<sup>1</sup>  
 +41(0)56 310 2057  
 ruediger.koetz@psi.ch

Templated carbons play an important role for investigating the effect of carbon pore structure on electrochemical double layer capacitor behaviour, because these carbons can be produced with well-defined pore size distribution. In addition, by the choice of precursor, the surface properties of the usable surface can be altered. By this approach it is expected to be able to separate between geometric and chemical effects and eventually improve the performance of high surface area carbon electrodes by surface modification.

The templated carbons were prepared using a silica template with a defined porosity (MCM-48 or SBA-15) and several carbon precursors (sucrose, glucose and aminoglucose). The synthesis requires four steps: (1) infiltration of the carbon precursor with a solution of sugar and sulfuric acid, drying at 100 °C followed by a pre-calcination at 150 °C during 6 h; (2) a second infiltration; (3) calcination at 900 °C in vacuum during 5 h; (4) etching with hydrofluoric acid for silica removal, washing and drying. The different materials used for this study are presented in table 1.

Sample	Silica Matrix	Precursor 1 <sup>st</sup> impregnation	Precursor 2 <sup>nd</sup> impregnation	SBET (m <sup>2</sup> /g)	N <sub>XPS</sub> (at%)
V15G	SBA15	Glucose	Glucose	1356	0
V15GNS	SBA15	Amino-Glucose	Sucrose	1194	2.7
V15GN	SBA15	Amino-Glucose	Amino-Glucose	989	4.1
V48G	MCM48	Glucose	Glucose	1447	0
V48S	MCM48	Sucrose	Sucrose	1680	0
V48GNS	MCM48	Amino-Glucose	Sucrose	1024	2.0
V48GN	MCM48	Amino-Glucose	Amino-Glucose	624	4.7

**Table 1:** Synthesis parameters, BET surface area and Nitrogen content of nanostructured carbon materials.

By using a nitrogen-containing precursor, it was possible to obtain carbon containing up to 5 at.% of nitrogen. The nitrogen composition determined by XPS and elemental analysis is close indicated that the nitrogen is present in the bulk and surface of the carbon. The data show that the use of aminosugars leads to a decrease of surface area of the resulting carbon.

All samples exhibit a significant microporous volume. It must be noted that this development of porosity from sugar precursors is related to the confined geometry in which the carbonization is done, the

carbonization of sugar in a free environment leads to materials with a very low porosity [1,2].

The nitrogen containing sites were studied by XPS. It is very important to decide whether the observed nitrogen originates from residual precursor material or from Nitrogen bonded directly to the carbon matrix of the porous material.

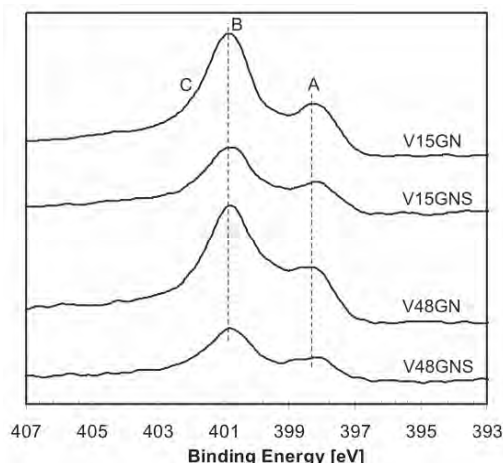


**Fig 1:** XPS spectra of the N1s peaks for nanostructured carbon materials.

The resulting XPS spectra for the N1s level are shown in figure 1. We observe two main peaks at a binding energy of 398.2 eV (A) and at 400.9 eV (B). In addition a broad shoulder can be identified at 402 eV (C). As expected (see table 1), the amount of nitrogen present in the final carbon increases after the second infiltration.

From XPS investigations on nitrogen-containing carbons [3,4] the two peaks with binding energies of 398.2 eV and 400.9 eV may be assigned to an environment of sp<sup>3</sup> and sp<sup>2</sup> hybridized carbons. Especially, they correspond to the presence of highly coordinated (quaternary) N atoms (401 eV) and pyridine-like N (398 eV), respectively. The quaternary nitrogen represents a N-atom that is included in a graphitic layer, substituting a C-atom. [4].

In addition, we observed a small shift of the C1s main peak (not shown) to higher binding energies together with an increased FWHM for the nitrogen-containing samples.

From the XPS results it is concluded, that the nitrogen of the investigated nanostructured carbons is part of the graphene network.

### References

- [1] R. Gadiou, C. Vix-Guterl, Ann. Chi. Phys. **30**, 425 (2005).
- [2] R. Gadiou, A. Didion, S. Saadallah, M. Couzi, J.N. Rouzeaud, P. Delhaes, C. Vix-Guterl, Carbon **44**, 3348 (2006).
- [3] J. Lahaye, G. Nansé, A. Bagreev, V. Strelko, Carbon **37**, 585 (1999).
- [4] E. Raymundo-Pineroa, D. Cazorla-Amorosa, A. Linares-Solanoa, J. Find, U. Wild, R. Schlögl, Carbon **40**, 597 (2002).

<sup>1</sup> Institut de Chimie des Surfaces et Interfaces, Mulhouse, France

## DILATOMETRIC STUDY OF LITHIUM INTERCALATION INTO GRAPHITE

M. Hahn, J. Ufheil, P.W. Ruch, D. Goers<sup>1</sup>,  
M. Spahr<sup>1</sup>, P. Novák, R. Kötz  
+41(0)56 310 2128  
[matthias.hahn@psi.ch](mailto:matthias.hahn@psi.ch)

During the last years, we have developed an electrochemical dilatometer, which is capable of monitoring the height change of electrodes during charging with a sub-micrometre resolution [1]. Recently, the long term drift stability of this instrument has been improved considerably, so that dimensional changes in the range of a few micrometres can now be followed over time periods of several days, under the rigorous exclusion of ambient air. The drift stability has opened the opportunity to measure experimentally demanding systems such as the lithium intercalation into graphite. Thus, in the context of lithium ion batteries, electrochemical dilatometry may now be considered as a complementary tool to other well established *in situ* techniques like AFM, X-ray diffraction, and Raman spectroscopy. Here we present exemplarily the height change observed for a powder-type graphite electrode upon first cycle Li intercalation.

### Experimental

Details of the set-up have been presented elsewhere [1]. In short, the dilatometer contains, hermetically sealed against ambient atmosphere, the graphite working electrode under investigation (10 mm dia., 100 µm thick), a lithium metal counter electrode, and a glass frit (3.5 mm thick) in between. A piece of Li positioned on the edge of the working electrode serves as the reference electrode. During the experiment, any charging induced height changes of the graphite electrode are transmitted through a thin titanium foil to a displacement transducer that is placed on top of the foil. A PVDF bound electrode, containing 90 % of graphite flakes (SFG44, Timcal) served as the working electrode. After filling the cell with LiPF<sub>6</sub> based electrolyte (LP30, Merck), the graphite electrode was cycled following the standard constant current (C/20 rate)/ constant voltage protocol.

### Results and Discussion

The potential profile and the simultaneous dilatation track recorded during first charging are shown in figure 1. Generally, the observed potential slopes may be attributed to the stoichiometry domains of pure intercalation phases (stages), while the potential plateaus are related to the coexistence of two phases (i.e., the transformation of one phase into another) [2]. Consequently, electrode swelling should primarily occur during the potential plateaus, and the associated height change can be calculated from the stoichiometry and the lattice parameters of the pure stages. For the case of Li intercalation, X-ray studies

indicate that Li intercalation commences with the formation of a diluted stage 1 [2]. This first potential slope (labeled 1d in figure 1) is followed by a plateau which is attributed to the transformation of this diluted stage 1 into a stage 4 compound (1d+4). During further lithiation, the pure stages 3 (with  $x = 0.22$ ), 2 ( $x = 0.5$ ) and 1 ( $x = 1.0$ ) are subsequently formed. Under the present conditions, and in variance with the behaviour of pyrolytic graphite [2], no formation of a diluted stage 2 compound (with  $x = 0.33$ ) can be seen.

Notably, the observed maximum expansion of 4.2 % is significantly lower than the 10.4 % widening of the interlayer spacing in the stage 1 compound LiC<sub>6</sub> [2]. This difference may be due to the almost random orientation of the graphite flakes in the powder electrode. In detail, the dilatation record shows three subsequent regions of constant slope which may be attributed to the initial formation of stage 1d, the transformation from stage 4 to 3, and that from stage 2 to 1, respectively. Interestingly, the transformation from stage 3 to 2 does not result in any expansion, a finding that is yet not understood.

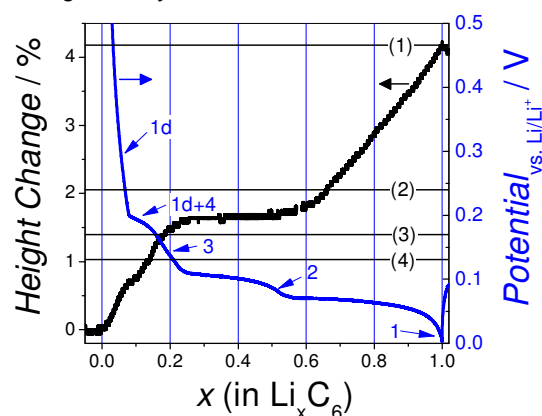


**Fig. 1:** Potential profile and simultaneous dilatation record of the graphite electrode during electrochemical lithiation. Arrows indicate stage formation along the potential curve [2]. Horizontal lines show the height change predicted for the pure phases (stage numbers in parentheses). These values are derived from X-ray results [2] and normalized to the actually measured expansion for the stage 1 compound LiC<sub>6</sub>.

### Conclusions

Electrochemical dilatometry is shown to be a valuable tool for the characterization of the lithium intercalation into technically relevant graphite electrodes. In future work, we will extend the investigations to other types of graphite and compare the macroscopic dilatation behaviour with the results obtained by complementary methods.

### Acknowledgement

Financial support by TIMCAL, Bodio, is gratefully mentioned.

### References

- [1] M. Hahn, O. Barbieri, R. Gallay, R. Kötz, Carbon **44**, 2523 (2006).
- [2] D. Billaud, F.X. Henry, M. Lelaurain, P. Willmann, J. Phys. Chem. Solids **57**, 775 (1996).

<sup>1</sup> TIMCAL, Bodio

# IMPEDANCE SPECTROSCOPY ON POROUS MATERIALS: A REVIEW AND APPLICATION TO THE STUDY OF GRAPHITE ELECTRODES FOR LITHIUM-ION BATTERIES

F. La Mantia, J. Vetter, P. Novák  
+41(0)56 310 2161  
[fabio.lamantia@psi.ch](mailto:fabio.lamantia@psi.ch)

The lithium-ion battery possesses the greatest energy density of all known rechargeable battery systems and has a power density close to the nickel-cadmium battery. The major challenge of lithium-ion battery research is to develop systems with even higher power and energy densities. Progress in the basic knowledge about this system is therefore of major importance. Impedance spectroscopy is a very powerful instrument in determining the rate of electrochemical processes and separating them, once a model for the behavior of the system is formulated. Shape of the impedance spectra can help to understand the electrochemical processes occurring at the surface. The present work starts from a general picture of porous systems. Impedance spectra of different types of graphite were acquired. All the data showed clearly the effect of porosity. Model for analyzing the data was obtained by simplifications of the basic equations; the results are similar to the equations obtained by De Levie [1]. The fitting data were compared to obtain information on the nature of the pores involved in the transport phenomena. A relationship between the adsorbing sites, evidenced by EIS, and the irreversible charge in the first cycle was found.

## Experimental

A separator-free three-electrode cell was used for the impedance measurements. The cell includes two electrodes with titanium current collectors of 1.33 cm<sup>2</sup> area. A gap of 1 mm remains between the two electrodes. The reference electrode is a piece of metallic lithium. Working electrodes were prepared starting from commercial powder graphites (TIMREX KS44, SFG44, and GN44, all from TIMCAL SA), mixing them with a solution of PVdF 6020 binder (Solvay). The solvent used was NMP. The final composition of the electrode was 90% (wt.) graphite and 10% binder. Cells were assembled and hermetically sealed under a high purity argon atmosphere (O<sub>2</sub> and H<sub>2</sub>O < 2 ppm). The counter electrode was made from metallic lithium. A mixture of EC:DMC (1:1 by weight) with 1M LiPF<sub>6</sub> was used as the electrolyte. Potentiostat/Galvanostat Model 273A (EG&G Princeton Applied Research) coupled with the Frequency Response Analyzer SI 1255 (Solartron) was used for performing both electrochemical impedance spectroscopy and cyclic voltammetry in a temperature chamber fixed at 25(±0.1) °C. For cycling the electrodes, cyclic voltammetry was performed between 1.5 and 0.09 V vs. Li/Li<sup>+</sup> at scan rate 0.2 mVs<sup>-1</sup>.

## Theoretical Background

In this section a simplified generalized model of porous electrodes is presented. It is based on the transmission line model (TLM) of De Levie [1]. The system under investigation is considered to be composed of a porous electrode immersed in a solution containing a single monovalent binary salt, which cations participate in an electrochemical reaction. The zero of the x axis is put in the boundary between the porous electrode and the current collector. The porous electrode has a thickness l and the current collector is considered inert in the solution. The pores can have different size, also changing along x. It is supposed that the centers of mass of each section of the pore can be aligned along the x axis. Focusing attention to a single electronic current line passing through the electrode, each time the line is near the solid phase/electrolyte interface, a part of the electronic current is converted into ionic current through the electrochemical process. There is a free path a<sub>k</sub> between (k-1)-th and k-th reaction site. It is a statistical parameter and represents the free path that the electron can move before reacting. It depends on the size and the shape of the pores. The surface process generates concentration gradients which are compensated by ion transport in the electrolyte. The analytical solution of the transport equations in the pores is very complicated. For this reason a simplified theory was formulated. It can be assumed that a pore can be divided into two regions, one in which there is only a radial transport and the second one with only axial transport. Then it is possible to define two areas and two perimeters for each section. A<sub>p</sub>(x) is the total area of the section at the position x, A<sub>J</sub>(x) is the area in which there is only axial transport, P<sub>p</sub>(x) is the perimeter of the section, and P<sub>J</sub>(x) is the perimeter of A<sub>J</sub>(x). We assumed that (i) the radial diffusion is negligible with respect to the radial migration and (ii) that A<sub>p</sub>/P<sub>p</sub> ≈ a(x). This assumption follows the logic: the greater the area with respect to the perimeter, the lower the possibility for the ions to be near the reaction sites. These simplifications permit to write down the following equations for the electrochemical system:

$$\left( \frac{\partial}{\partial x} + \frac{d \ln A_p}{dx} \right) \frac{\partial}{\partial x} \left[ \Delta \varphi + DF \rho_s \frac{(1-2t_+)}{t_+} C_w \right] = \frac{(\rho_s + \rho_E)}{a} j \quad (1)$$

$$\frac{\partial C}{\partial t} \Big|_{x_0, x} = 2D(1-t_+) \left( \frac{\partial}{\partial x} + \frac{d \ln A_p}{dx} \right) \left[ \frac{\partial C}{\partial x} \Big|_{x_0, x} \right] \quad (2)$$

The impedance response of the electrode can be then modeled starting from equations (1) and (2) for the case of the equilibrium current equal to 0. The following equation (3) is obtained,

$$Z_p(\omega) = \frac{\rho l}{A_p} \left\{ \frac{\cosh(\kappa l) + \beta}{\kappa l \sinh(\kappa l)} + \frac{\beta}{2} \right\} \quad (3)$$

where

$$\rho = \frac{\rho_S^2 + \rho_E^2}{\rho_S + \rho_E}; \beta = \frac{2\rho_S\rho_E}{\rho_S^2 + \rho_E^2}; \left( \kappa^2 = \frac{\rho_S + \rho_E}{aZ} \right) \quad (4)$$

The impedance of the single reaction site ( $Z$ ) affects the impedance of the entire porous electrode.

## Results and Discussion

Impedance spectra were recorded at different cycles for studying the effect of aging of the graphite during the very first cycles. The different types of graphite had different orientation and order of the crystallites. In figure 1 the first cyclic voltammograms for the investigated systems are reported. It can be stressed that, during the first cathodic cycle, all three types of graphite show a peak around 600 mV (vs. Li/Li<sup>+</sup>). Electrodes made from KS44 show two peaks, the first one is at the same potential as the others, and

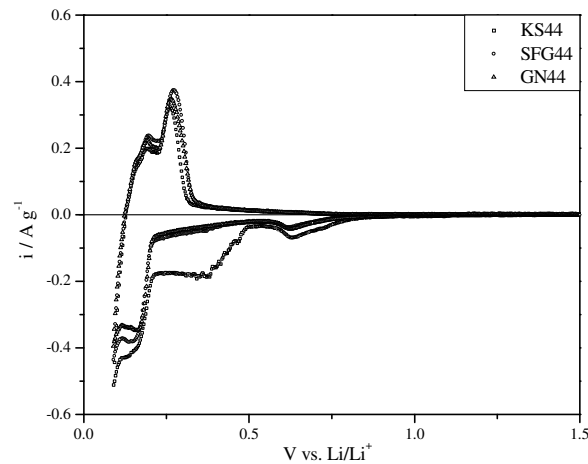


**Fig. 1:** First cyclic voltammetry for different types of graphite

the second one at around 350 mV, resembling a plateau. Both peaks can be attributed to the solid electrolyte interphase (SEI) formation. Competitive with the SEI formation process there is also another process, the exfoliation of the graphite. The exfoliation generates new fresh surface, on which the SEI has to be formed. When the whole active area is covered by the SEI, the exfoliation stops. In table I the irreversible and reversible charge and  $Q_p$ , the charge under the peak of the SEI formation (~600 mV vs. Li/Li<sup>+</sup>), is reported for the investigated systems at different cycles.

	Irrev. Charge / mAhg <sup>-1</sup>				Rev. Charge / mAhg <sup>-1</sup>				$Q_p$ / mAhg <sup>-1</sup>
	1st	2nd	5th	10th	1st	2nd	5th	10th	
KS44	93.6	13.0	3.72	2.14	59.6	65.5	62.2	59.7	12.2
SFG44	21.7	4.22	1.71	1.04	69.9	69.2	64.3	53.1	6.68
GN44	19.8	3.18	1.34	0.929	65.6	58.1	52.3	51.1	8.32

**Table 1:** Irreversible charge, reversible charge and  $Q_p$  for different types of graphite

We can observe that KS44 has the highest irreversible charge at each cycle and also the highest  $Q_p$ . As shown in eq. (3), the impedance response of the porous electrode depends on the electrochemical process. In all the acquired spectra, it is possible to

observe a depressed capacitive semicircle at high frequencies, due to the influence of the porosity on the electrode response. Nyquist plots for fresh graphite electrodes (all types) have suggested that, the electrochemical process before the SEI formation is an adsorption-like process. An adsorption reaction through surface states was chosen as the most plausible process. The choice was made by comparison of the parameters obtained from the classic absorption model and via surface state absorption. In table II the parameters obtained by fitting the impedance spectra measured before the SEI formation are reported. We want to stress that the value of  $C_{ad}$  is proportional to the number of adsorbing (or “active”) sites. The  $C_{ad}$  for KS44 is circa two times higher compared to SFG44 and GN44. Comparison with the values of the irreversible charge and  $Q_p$  shows a good correlation between the charge consumed for the SEI formation and the value of capacitance of adsorption. It is possible to suggest an interpretation of the adsorption sites, as the electrochemically active sites that react with the electrolyte and form either the nucleation sites for the SEI and/or the SEI itself. The irreversible charge follows the trend but has a much higher value, because of the exfoliation process.

	KS44	SFG44	GN44
$R_p$ / Wg <sup>-1</sup>	$1.34 \cdot 10^3$	$1.13 \cdot 10^3$	$1.42 \cdot 10^3$
$C_{dl}$ / Fg <sup>-1</sup>	$1.26 \cdot 10^{-2}$	$4.60 \cdot 10^{-3}$	$2.13 \cdot 10^{-3}$
$R_{ad}$ / Wg	$4.97 \cdot 10^{-10}$	$3.95 \cdot 10^{-3}$	$1.33 \cdot 10^{-2}$
$C_{ad}$ / Fg <sup>-1</sup>	$8.46 \cdot 10^{-1}$	$3.33 \cdot 10^{-1}$	$2.97 \cdot 10^{-1}$
$W / Ss^{-0.5}g^{-1}$	2.87	2.99	2.79
$R_{ss}$ / Wg	$9.54 \cdot 10^{-4}$	$3.46 \cdot 10^{-3}$	$5.00 \cdot 10^{-3}$
$C_{ss}$ / Fg <sup>-1</sup>	$3.26 \cdot 10^{-1}$	$1.77 \cdot 10^{-2}$	$1.63 \cdot 10^{-3}$

**Table 2:** Parameters obtained by impedance spectra fitting before SEI formation for different types of graphite

## Conclusions

Graphite electrodes were studied with impedance spectroscopy in a three-electrode, separator-free cell. Results have shown the important influence of electrode porosity on the impedance spectra. A general model was developed for describing the behavior of such electrodes. It was found that at high current densities and high resistance of the pores, the electrode can not be used homogeneously. Impedance spectra have further helped to understand better the processes involving SEI formation. The electrochemical process at the SEI free surface has showed an adsorption-like behavior of ions. Moreover, impedance spectra showed that a simple adsorption model can not explain completely the results unless the involvement of surface states is considered. Finally, a qualitative correlation was found between the adsorption sites and the charge consumed for the SEI formation.

## References

- [1] R. De Levie, *Electrochim. Acta* **8**, 751-780 (1963).



# THE ELECTROCHEMISTRY LABORATORY





The artistic pink elephant – created by the local artist Bruno Weber for PSI in 2003 - in front of the PSI auditorium loves to be the attraction for group pictures.

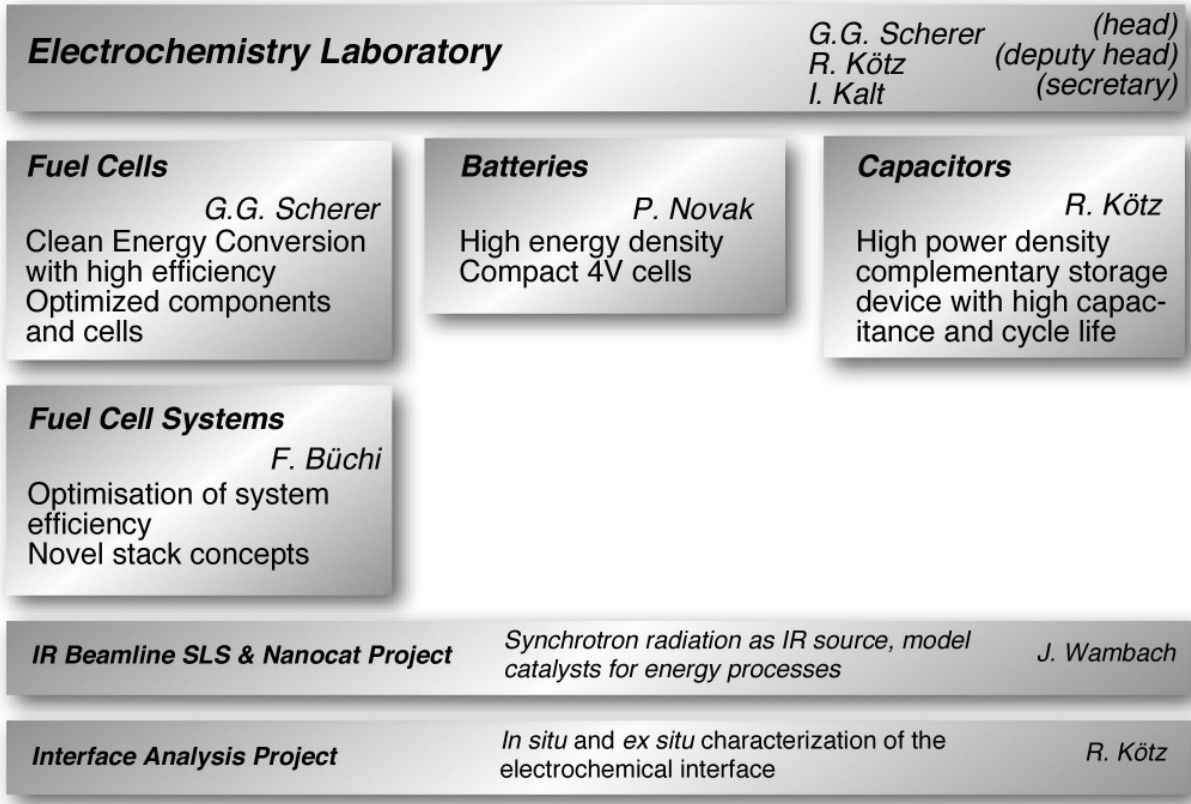
Above: The speakers of our 22<sup>nd</sup> One-Day-Symposium on "Electrochemistry in Biology and Medicine" in May 2006.

Below: The colleagues from Korea, Japan and PSI presenting their recent research at the 3<sup>rd</sup> Joint PSI-RCECS Meeting in August 2006.





# STRUCTURE





# ECL-PERSONNEL

## Staff

Alkan Gürsel Selmiye, Dr. ♦ Arcaro Manuel ♦  
Barbieri Olivier, Dr. (until May) ♦ Berchtold Bernd, Dr. (July to October) ♦ Büchi Felix, Dr. ♦  
Buqa Hilmi, Dr. (until April) ♦  
Czekaj Izabela, Dr. ♦  
Foelske Annette, Dr. ♦  
Geiger Friederike ♦ Gloor Thomas ♦ Gubler Lorenz, Dr. ♦  
Hahn Matthias, Dr. ♦ Holzapfel Michael, Dr. (until September) ♦  
Kaiser Hermann ♦ Kalt Isabella ♦ Kötz Rüdiger, Dr. ♦  
Maire Pascal (since October) ♦ Marmy Christian ♦  
Novak Petr, Dr. ♦  
Sauter Jean-Claude ♦ Scheifele Werner ♦ Scherer Günther G., Dr. ♦  
Schneider Ingo, Dr. ♦ Schulenburg Hendrik, Dr. (since June) ♦  
Tran Nicolas, Dr. (since March) ♦ Tsukada Akinori ♦  
Ufheil Joachim, Dr. ♦  
Vetter Jens, Dr. (until December) ♦ von Roth Fritz ♦  
Wambach Jörg, Dr. ♦ Wei Xun, Dr. ♦

## PhD Students

Ben Youcef Hicham ♦  
Boillat Pierre ♦ Borrmann Franziska (since July) ♦  
Dockheer Sindy (since December) ♦  
Ernst Frank ♦  
Farquet Patrick ♦ Flückiger Reto (since January) ♦ Freunberger Stefan (until December) ♦  
Hardwick Laurence (until November) ♦  
Kramer Denis ♦ Kuhn Holger (until June) ♦  
La Mantia Fabio ♦ Loviat François ♦  
Patey Timothy (since April) ♦  
Reiner Andreas (until December) ♦ Reum Mathias ♦ Rosciano Fabio ♦ Ruch Patrick ♦  
Santis Marco (until May) ♦ Schuler Gabriel (since March) ♦ Seyfang Bernhard (since March)  
♦ Slaski Michal (until October) ♦  
Wallasch Frank (since June) ♦

# AWARDS

**A. Reiner,  
G.G. Scherer,  
A. Wokaun**

Second-best poster  
*Platinum/Carbon co-sputtered fuel cell electrodes*  
10<sup>th</sup> Ulm ElectroChemicalTalks, Electrochemical Energy Storage and  
Conversion, Ulm, June 27-28, 2006

**P. Ruch**

*Alu-Award 2006*  
Aluminium-Verband Schweiz

# THESE PHD STUDENTS FROM ECL GRADUATED IN 2006

**Dr. Nina K. Beck**



*Methanol tolerant oxygen reduction catalysts derived from transition metal oxides*

Ph.D. Thesis, No. 16647, ETH Zürich, May 2006.

Advisors: Prof. Dr. A. Wokaun (PSI/ETH)  
Dr. G.G. Scherer (PSI)

**Dr. Marco V. Santis**



*Investigation of current density inhomogeneities in polymer electrolyte fuel cells*

PhD Thesis No. 16905, ETH Zürich, Oktober 2006.

Advisors: Prof. Dr. A. Wokaun (PSI/ETH)  
Dr. G.G. Scherer (PSI); Dr. F. Büchi (PSI)

**Dr. Holger Kuhn**

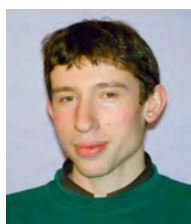


*In situ Charakterisierung von Polymer-Elektrolyt Brennstoffzellen mittels elektrochemischer Impedanzspektroskopie*

PhD Thesis No. 16929, ETH Zürich, November 2006.

Advisors: Prof. Dr. A. Wokaun (PSI/ETH)  
Dr. G.G. Scherer (PSI)

**Dr. Stefan A. Freunberger**



*Mass and charge transfer on various relevant scales in polymer electrolyte fuel cells*

PhD Thesis No. 16991, ETH Zürich, December 2006.

Advisors: Prof. Dr. A. Wokaun (PSI/ETH)  
Dr. F. Büchi (PSI)

**Dr. Michal Slaski**



*Radiation grafted fuel cell membranes with improved oxidative stability*

PhD Thesis No. 16995, ETH Zürich, December 2006.

Advisors: Prof. Dr. A. Wokaun (PSI/ETH)  
Dr. G.G. Scherer (PSI); Dr. S. Alkan-Gürsel (PSI)

**Dr. Laurence J. Hardwick**



*In situ Raman microscopy of insertion electrodes for lithium-ion batteries and supercapacitors*

PhD Thesis No. 16992, ETH Zürich, December 2006.

Advisors: Prof. Dr. A. Wokaun (PSI/ETH)  
PD Dr. P. Novák (PSI)

# EXCHANGE STUDENTS, DIPLOMA THESES, SUMMER STUDENTS

<b>N. Siegmund</b>	<i>Effect of crosslinker for poly (ethylene-alt-tetrafluoroethylene) based grafted films and membranes</i> TU Munich, Germany, August 2005 – January 2006.
<b>M. Lanfranconi</b>	<i>Untersuchungen zur Präparation von Polymerelektrolyt-Brennstoffzellenkatalysatoren mittels Co-sputtern von Pt/C</i> Fachhochschule beider Basel, October 2005 – January 2006.
<b>H. Fuchs</b>	<i>Entwicklung einer Software zur Durchführung orts aufgelöster zyklischer Voltammetrie an Polymer Elektrolyt Brennstoffzellen</i> TU Wien, Austria, ETH Zürich, November 2005 – February 2006.
<b>S. Schumann</b>	<i>In situ IR-Spektroskopie an Lithiumionen-Zellen</i> ETH Zürich, February – March 2006.
<b>R. Krischek</b>	<i>Darstellung und Charakterisierung von dotierten Olivinphasen <math>Li_{1-x}M_xM'PO_4</math> (<math>M = Ti, Mg; M' = Fe, Co</math>) als positive Elektrodenmaterialien für Lithiumionen-Batterien</i> ETH Zürich, February – March 2006.
<b>U. Frischknecht</b>	<i>Experimentelle Untersuchung von Zell-Interaktionen in PEFC Stapeln</i> Universität Basel, February – March 2006.
<b>R. Müller</b>	<i>Qualitative analysis of rapid ageing protocols for fuel cell membranes</i> Hochschule für Forstwirtschaft, Rottenburg, Germany, May – August 2006.
<b>A.S. Degris</b>	<i>Charakterisierung von Aktivmaterialien in Lithiumionen-Batterien</i> Ecole Nationale Supérieure d'Electrochimie et d'Electrometallurgie , Grenoble, France May – August 2006.
<b>J.D. Fernandez</b>	<i>Diffusivity characterization of gas diffusion layer materials with an EIS-based method</i> Universidad de Murcia, Spain, July – October 2006.
<b>C. Heid</b>	<i>Characterization of radiation grafted membranes by differential scanning calorimetry, thermogravimetric analysis and contact angle measurements</i> Universität Bern, July – October 2006.
<b>C. Suter</b>	<i>Untersuchung des Einflusses von Kanalprozessen auf die Impedanzantwort von Polymer Elektrolyt Brennstoffzellen</i> ETH Zürich, July – October 2006.
<b>M. Hofer</b>	<i>Lokale Stromdichten in PE-Brennstoffzellen</i> Berner Fachhochschule für Technik und Informatik, Biel, October-December 2006.

# SEMINAR, INVITED SPEAKERS

<b>Dr. M. Wohlfahrt-Mehrens</b> ZSW Ulm, DE	<i>Synthese und Charakterisierung von Lithiumübergangsmetallphosphaten als Kathodenmaterialien für Lithium-Ionenbatterien</i> February 06, 2006.
<b>Dr. F. Krumeich</b> ETH Zürich	<i>Electron microscopical methods for the characterization of nano materials</i> February 27, 2006.
<b>Dr. H. Hoster</b> Universität Ulm, DE	<i>Quantitative Korrelation von Struktur und elektrochemischen Eigenschaften wohldefinierter Bimetalloberflächen</i> March 13, 2006.
<b>Dr. M. Ruge</b> Berner Fachhochschule, Biel	<i>Von der Idee über die Probleme zur Lösung, die Entwicklung eines luftgekühlten 500W PEM-Brennstoffzellenstapel</i> March 20, 2006.
<b>Dr. J. Kunze</b> Institut für Werkstoffwissenschaften, Erlangen, DE	<i>Electrochemical formation of TiO<sub>2</sub> nanotubes - self-organized growth and applications</i> April 03, 2006.
<b>Dr. Ch. Stone</b> Ballard Power Systems, Burnaby, CA	<i>PEM Fuel Cells: Technology and challenges for commercialization</i> April 05, 2006.
<b>Prof. W.H. Koppenol</b> ETH Zürich	<i>Fenton and his reaction</i> April 06, 2006.
<b>Dr. M. Oszcipok</b> Fraunhofer Institut, Freiburg, DE	<i>Start- und Abschaltvorgänge in PEM-Brennstoffzellen unter 0 °C</i> April 10, 2006.
<b>Dr. B. Andreaus</b> Simon Fraser University Burnaby, CA	<i>Activity of fuel cell catalysts for CO-Electrooxidation – insight from kinetic modeling</i> May 08, 2006.
<b>Prof. Fritz Stöckli</b> Universität Neuenburg	<i>Structural and chemical characterization of carbons used in supercapacitors</i> May 15, 2006.
<b>Dr. L. Rubatat</b> Universität Freiburg	<i>Structural studies of nafion and fluorous di-block copolymer membranes</i> May 12, 2006.
<b>Dr. C. Vix-Guterl</b> Institut de Chimie des Surfaces et Interfaces (ICSI), Mulhouse Cedex, FR	<i>Carbon materials synthesized in a confined medium - study of their performance in energy-related applications</i> May 22, 2006.
<b>Dr. E. K. Erdle,</b> DaimlerChrysler, Ulm, DE	<i>Brennstoffzellen-Fahrzeuge bei DaimlerChrysler - Entwicklung und Perspektiven</i> May 29, 2006.

<b>Dr. R. Gallay</b> Maxwell Technologies, Rossens	<i>Double layer capacitor application requirements</i> June 12, 2006.
<b>Prof. K. Ota</b> Yokohama National University, JP	<i>Hydrogen and fuel cells activities in Japan</i> June 16, 2006.
<b>Prof. J. Vörös</b> ETH Zürich	<i>Electronically controlled surfaces for biological applications</i> Juni 19, 2006.
<b>Dr. S. Duval</b> Empa, Dübendorf	<i>Ceramic proton conducting electrolytes for application in fuel cells at intermediate temperatures</i> July 03, 2006.
<b>Prof. G. Jerkiewicz</b> Queen's University, Kingston, Ontario, CA	<i>Recent advances in the comprehension of the under-potential deposition of H on Pt-group metals: Thermodynamics, surface science, and electrochemical nanogravimetry</i> July 17, 2006.
<b>Dr. M. Spahr</b> Timcal SA, Bodio	<i>Graphit- und Russsmaterialien in elektrochemischen Systemen</i> August 21, 2006.
<b>Dr. A. Schuler</b> Hexis AG, Winterthur	<i>Das Hexis Brennstoffzellensystem - der lange Weg zum Produkt</i> September 11, 2006.
<b>Prof. A. McEvoy</b> EPF Lausanne	<i>Solid oxide fuel cell anodes and their reaction to sulfur</i> September 18, 2006.
<b>Dr. O. Smirnova</b> Universität Genf	<i>New approaches to electronic conductivity measurements of alkali</i> September 25, 2006.
<b>L. Matejcek</b> General Motors Europe, Glattbrugg	<i>Alternative Antriebe aus der Sicht von GM</i> Oktober 02, 2006.
<b>Dr. T. Centeno</b> INCAR, Spain, ES	<i>Activated carbons for supercapacitors</i> October 30, 2006.
<b>Prof. A.G. Stefanopoulou</b> University of Michigan, US	<i>Modeling and parameterization of fuel cell stack system dynamics</i> November 06, 2006.
<b>Dr. H. Dietsch</b> Universität Freiburg	<i>Nanoparticles hybrid systems: Synthesis of a tailored composite model</i> November 13, 2006.
<b>Dr. G. Foti</b> EPF Lausanne	<i>Electrochemical promotion of catalysis. The NEMCA effect.</i> November 20, 2006.
<b>Dr. T. Bürgi</b> Uni Neuchâtel	<i>In situ infrared spectroscopy of catalytic interfaces, chiral surfaces and nanoparticles</i> November 27, 2006.
<b>Dr. P. Hasler</b> SAM Private Equity, Zürich	<i>Why and how we invest in battery and fuel cell companies?</i> December 04, 2006.
<b>Dr. T. Zambelli</b> ETH Zürich	<i>Imaging molecular orbitals by UHV STM at 4K</i> December 11, 2006.

# CONFERENCES – WORKSHOPS

## Electrochemistry in Biology and Medicine

22<sup>nd</sup> One-Day-Symposium  
May 11, 2006  
Organizers: G.G. Scherer and R. Kötz

Contributions from:

Prof. Raimund Dutzler, Universität Zürich  
Dr. Patrick L.T.M. Frederix, Universität Basel  
Dr. Philippe Kern, EMPA, Thun  
Dr. Christoph Ritter, Roche Diagnostic GmbH, Graz, Austria  
Dr. Samuel Terrettaz, EPF Lausanne  
Prof. Roger Thull, Universität Würzburg, Germany

## Third PSI-RCECS Joint Seminar

Fuel Cells, Li-Batteries, Capacitors  
August 23 – 24, 2006  
Organizers: G.G. Scherer and R. Kötz

Contributions from RCECS delegation:

Prof. Jae Jeong Kim, Seoul National University, Korea  
Prof. Junbom Kim, University of Ulsan, Korea  
Prof. Kwang Bum Kim, Yonsai University, Korea  
Prof. Young Gyu Kim, Seoul National University, Korea  
Prof. Isao Mochida, Kyushu University, Japan  
Prof. Seung Mo Oh, Seoul National University, Korea  
Prof. Byungwoo Park, Seoul National University, Korea  
Prof. Soo Gil Park, Chungbuk National University, Korea  
Prof. Yung-Eun Sung, Seoul National University, Korea  
Prof. Yongsug Tak, Inha University, Korea  
Prof. Jun-ichi Yamaki, Kyushu University, Japan

Contributions from PSI:

Dr. Felix Büchi  
Dr. Lorenz Gubler  
Dr. Matthias Hahn  
Patrick Ruch  
Andreas Reiner  
Dr. Ingo Schneider  
Bernhard Seyfang  
Dr. Joachim Ufheil  
Dr. Jens Vetter

# REVIEW ACTIVITIES OF THE LABORATORY

## Journals

Applied Spectroscopy ♦

Carbon ♦ Chemistry of Materials ♦

Electrochimica Acta ♦ Electrochemistry Communications ♦ Electrochemical and Solid-State Letters ♦

Journal of Electroanalytical Chemistry ♦ Journal of the Electrochemical Society ♦ Journal of Fuel Cell Science and Technology (ASME) ♦ Journal of Physical Chemistry ♦ Journal of Power Sources ♦

Langmuir ♦

Materials Science and Engineering B ♦

Nature Materials ♦

Science ♦ Solid State Ionics ♦

## Organisations

Alexander von Humboldt-Stiftung, Germany ♦

John Simon Guggenheim Memorial Foundation, New York, USA ♦

Mistra, The Swedish Foundation for Strategic Environmental Research ♦

PSI FOKO, Switzerland ♦

Technische Universität München, Germany ♦ Technische Universität Bergakademie Freiberg, Germany ♦

Universität Ulm, Germany ♦

## Co-Referee's Report for Dissertations

N.K. Beck, PSI/ETH ♦

S.A. Freunberger, PSI/ETH ♦

H. Kuhn, PSI/ETH ♦

C. Perrot, Université Joseph Fourier, Grenoble, France ♦

M.V. Santis, PSI/ETH ♦ M. Slaski, PSI/ETH ♦

# INDUSTRIAL PARTNERS

**The Laboratory had the pleasure to collaborate with the following industrial partners during the year 2005:**

**Axpo Holding AG, Switzerland ♦**

**BASF AG, Ludwigshafen, Germany ♦**

**Ciba SC, Basel, Switzerland ♦**

**Construction Développement Michelin SA (CDM), Givisiez, Switzerland ♦**

**CEKA Elektrowerkzeuge AG, Wattwil, Switzerland ♦**

**Degussa, Creavis Technology & Innovation, Marl, Germany ♦**

**Ferro GmbH, Frankfurt/Main, Germany ♦**

**Honeywell Chemical Specialties, Seelze, Germany ♦**

**Maxwell Technologies SA, Rossens, Switzerland ♦**

**Nissan Motors Co., Ltd. Yokosuka, Japan ♦**

**Straumann Institut AG, Waldenburg, Switzerland ♦**

**TIMCAL AG, Bodio, Switzerland ♦**

**Volvo, Sweden ♦**



## PROJECT COLLABORATIONS WITH EXTERNAL PARTNERS

### SBF

F.N. Büchi Project Leader	<i>HYTRAN (Hydrogen and Fuel Cell Technologies for Road Transport)</i> EU-Project
P. Novák Project Leader	<i>ALiSTORE (Advanced lithium energy storage systems based on the use of nano-powders and nano-composite electrodes/electrolytes)</i> EU-Project (Network of Excellence)
P. Novák Project Leader	<i>LiBERAL (Lithium battery evaluation and research – accelerated life test direction)</i> EU-Project

### BFE

F.N. Büchi Project Leader	<i>Numerische Modellierung von PE Brennstoffzellen, Weiterentwicklung und erste Validierung des 2D+1 Modellansatzes</i> mit ZHW, Winterthur
R. Kötz Project Leader	<i>Integrated micro-supercapacitor</i> with NTB, Buchs
G.G. Scherer Project Leader	<i>Polymer Elektrolyt Brennstoffzellen mit H<sub>2</sub> und Methanol als Brennstoff</i> bis 30.6.06
G.G. Scherer, L. Gubler Project Leader	<i>Protonen-leitende Polymermembranen für Brennstoff- und Elektrolysezellen</i> ab 1.9.2006

### Gebert Ruef Stiftung

F.N. Büchi Project Leader	<i>SIMPEM (Simulation von Polymer Elektrolyt Brennstoffzellen und Stapeln)</i> mit ZHW, Winterthur
------------------------------	---

### Industry

P. Dietrich Project Leader	<i>Research collaboration</i> Construction Développement Michelin SA (CDM), Givisiez
L. Gubler Project Leader	<i>Eignung von Polyisobutylen basierten Filmen als Grundpolymer für die Strahlenpfpfung</i> BASF AG, Ludwigshafen, Germany
L. Gubler Project Leader	<i>Charakterisierung von Celtec®-V Membranen für die Direkt Methanol Brennstoffzelle</i> Pemeas Fuel Cell Technologies, Frankfurt (Main), Germany
M. Holzapfel Project Leader	<i>Nano-Silizium und ionische Flüssigkeiten für Lithiumionen-Batterien</i> Degussa AG, CREAVIS Technologies & Innovation, Marl, Germany
P. Novák Project Leader	<i>Elektrochemische Charakterisierung von Oxiden für Lithiumionen-Batterien</i> Ferro GmbH, Frankfurt (Main), Germany

G.G. Scherer Project Leader	<i>Diagnostics of polymer electrolyte fuel cells</i> Nissan Motor Co. Ltd. Yokohama, Japan
G.G. Scherer Project Leader	<i>Diagnostics of polymer electrolyte fuel cells</i> Automotive Industries
J. Ufheil Project Leader	<i>Rechargeable magnesium batteries</i> Nissan Motor Co. Ltd., Yokohama, Japan
J. Ufheil Project Leader	<i>Graphite für die negative Elektrode der Lithiumionen-Batterie</i> TIMCAL SA, Bodio
J. Vetter Project Leader	<i>Electrochemical characterization of polymeric organic active materials</i> CIBA SC, Basel

## KTI

F.N. Büchi Project Leader PSI	<i>Brennstoffzellenstapel mit erweiterter Funktionalität</i> CEKA AG, Wattwil und FH Bern
----------------------------------	--

## SNF

P. Novák Project Leader	<i>Synthesis and characterization of advanced electroactive materials for electrodes of rechargeable lithium-ion batteries</i>
----------------------------	--

## TEACHING ACTIVITIES

### University Level Teaching

PD Dr. P. Novák, Prof. Dr. A. Wokaun	<i>Technische Elektrochemie</i> ETH Zürich, WS 2006/2007
PD Dr. P. Novák	<i>Electrochemistry of lithium-ion batteries</i> Fudan University, Shanghai, China, block lectures in July 2006
Prof. Dr. A. Wokaun, Dr. G.G. Scherer, Prof. Dr. K. Boulouchos	<i>Technik erneuerbarer Energien, Teil 2</i> ETH Zürich, SS 2006

## PUBLICATIONS

### Books and Reviewed Book Chapters

R. Kötz, K.S. Nahm <sup>1</sup> , J.K. Park <sup>2</sup> , G.Q. Sun <sup>3</sup> , Q. Xin <sup>3</sup> Guest Editors, Special Issue	<i>Electrochemical energy conversion and storage</i> 56 <sup>th</sup> Annual ISE Meeting, Busan, Korea, 25-30 September 2005 Electrochim. Acta <b>52</b> , 4, 1439-1824 (2006). <sup>1</sup> Chonbuk National University, Chonju, Korea <sup>2</sup> Korea Advanced Institute of Science and Technology, Daejeon, Korea <sup>3</sup> Dalian Institute of Chemical Physics, Dalian, China
--	---

### Peer Reviewed Papers

S. Alkan Gürsel, Z. Yang <sup>1</sup> , B. Choudhury <sup>1</sup> , M.G. Roelofs <sup>1</sup> , G.G. Scherer	<i>Radiation-grafted membranes using a trifluorostyrene derivative</i> J. Electrochem. Soc. <b>153</b> (10), A1964-A1970 (2006). <sup>1</sup> DuPont Central Research and Development, Wilmington, USA
A.R. Armstrong <sup>1</sup> , M. Holzapfel, P. Novák, C.S. Johnson <sup>2</sup> , S.-H. Kang <sup>2</sup> , M.M. Thackeray <sup>2</sup> , P.G. Bruce <sup>1</sup>	<i>Demonstrating oxygen loss and associated structural reorganization in the lithium battery cathode Li[Ni<sub>0.2</sub>Li<sub>0.2</sub>Mn<sub>0.6</sub>]O<sub>2</sub></i> J. Am. Chem. Soc. <b>128</b> , 8694-8698 (2006). <sup>1</sup> University of St. Andrews, Scotland <sup>2</sup> Argonne National Laboratory, Argonne, Illinois, USA

- F. Atchison, B. Blau,  
M. Daum, P. Fierlinger,  
A. Foelske, P. Geltenbort<sup>1</sup>,  
M. Gupta, R. Henneck,  
S. Heule, M. Kasprzak,  
M. Kuzniak, K. Kirch,  
M. Meier, A. Pichlmaier,  
Ch. Plonka<sup>1</sup>, R. Reiser,  
B. Theiler, O. Zimmer<sup>2</sup>,  
G. Zsigmond
- Diamondlike carbon can replace beryllium in physics with ultracold neutrons*  
Physics Letters **B 642**, 24–27 (2006).  
<sup>1</sup> ILL, Grenoble, France  
<sup>2</sup> TU München, Germany
- O. Barbieri, M. Hahn,  
A. Foelske, R. Kötz
- Effect of electronic resistance and water content on the performance of RuO<sub>2</sub> for supercapacitors*  
J. Electrochem. Soc. **153** (11), A2049-A2054 (2006).
- N.K. Beck, B. Steiger,  
G.G. Scherer, A. Wokaun
- Methanol tolerant oxygen reduction catalysts from electrochemically pre-treated Bi<sub>2</sub>Pt<sub>2-y</sub>Ir<sub>y</sub>O<sub>7</sub> pyrochlores*  
Fuel Cells **06**, 26-30 (2006).
- M. Bosco, F. Hajbolouri,  
T.-B. Truong, E. De Boni,  
F. Vogel, G.G. Scherer
- Link-up of a bench-scale "shift-less" gasoline fuel processor to a polymer electrolyte fuel cell*  
J. Power Sources **159**, 1034–1041 (2006).
- T. Brys, M. Daum,  
P. Fierlinger, A. Foelske,  
M. Gupta, R. Henneck,  
S. Heule, M. Kasprzak,  
K. Kirch, M. Kuzniak,  
T. Lippert, M. Meier,  
A. Pichlmaier,  
U. Straumann<sup>1</sup>
- Diamond-like carbon coatings for ultracold neutron applications*  
Diamond Relat. Mater. **15**, 928-931 (2006).  
<sup>1</sup> University of Zurich
- H. Buqa, A. Würsig,  
J. Vetter, M.E. Spahr<sup>1</sup>,  
F. Krumeich<sup>2</sup>, P. Novák
- SEI film formation on highly crystalline graphitic materials in lithium-ion batteries*  
J. Power Sources **153**, 385-390 (2006).  
<sup>1</sup> TIMCAL SA, Bodio  
<sup>2</sup> ETH Zürich
- H. Buqa, M. Holzapfel,  
F. Krumeich<sup>1</sup>, C. Veit<sup>2</sup>,  
P. Novák
- Study of styrene butadiene rubber and sodium methyl cellulose as binder for negative electrodes in lithium-ion batteries*  
J. Power Sources **161**, 617-622 (2006).  
<sup>1</sup> ETH Zürich  
<sup>2</sup> Degussa AG, CREAVIS Technologies & Innovation, Marl, Germany
- F.P. Campana, M. Hahn,  
A. Foelske, P. Ruch, R. Kötz,  
H. Siegenthaler<sup>1</sup>
- Intercalation into and film formation on pyrolytic graphite in a supercapacitor-type electrolyte (C<sub>2</sub>H<sub>5</sub>)<sub>4</sub>NBF<sub>4</sub> / propylene carbonate*  
Electrochem. Comm. **8**, 1363-1368 (2006).  
<sup>1</sup> University of Bern
- Th. Dumont, T. Lippert,  
M. Döbeli, H. Grimmer,  
J. Ufheil, P. Novák,  
A. Würsig, U. Vogt<sup>1</sup>,  
A. Wokaun
- Influence of experimental parameter on the Li-content of LiMn<sub>2</sub>O<sub>4</sub> electrodes produced by pulsed laser deposition*  
Appl. Surf. Sci. **252**, 4902-4906 (2006).  
<sup>1</sup> Empa Dübendorf
- A. Foelske, O. Barbieri,  
M. Hahn, R. Kötz
- An X-ray photoelectron spectroscopy study of hydrous ruthenium oxide powders with various water contents for supercapacitors*  
Electrochem. Solid State Let. **9**, A268-A272 (2006).
- A. Foelske, B. Steiger,  
N.K. Beck, R. Kötz,  
G.G. Scherer, A. Wokaun
- Electrochemically pretreated Bi<sub>2</sub>Pt<sub>2-y</sub>Ir<sub>y</sub>O<sub>7</sub> pyrochlores – an X-ray photoelectron spectroscopy study*  
Surf. Interface Anal. **38**, 210-214 (2006).

- S.A. Freunberger, M. Santis, I.A. Schneider, A. Wokaun, F.N. Büchi *In-plane effects in large scale PEFC, I. Model formulation and validation*  
J. Electrochem. Soc. **153**, A396-A405 (2006).
- S.A. Freunberger, A. Wokaun, F.N. Büchi *In-plane effects in large scale PEFC, I. The influence of cooling strategy on cell performance*  
J. Electrochem. Soc. **153**, A909-A913 (2006).
- S.A. Freunberger, M. Reum, A. Wokaun, F.N. Büchi *Expanding current distribution measurement in PEFCs to sub-millimeter resolution*  
Electrochem. Comm. **8**, 1438-1438 (2006).
- S.A. Freunberger, M. Reum, J. Evertz<sup>1</sup>, A. Wokaun, F.N. Büchi *Measuring the current distribution in PEFCs with sub-millimeter resolution, I. Methodology*  
J. Electrochem. Soc. **153**, A2158-A2165 (2006).  
<sup>1</sup> tribecraft AG, Zürich
- L. Gubler, M. Slaski, A. Wokaun, G.G. Scherer *Advanced monomer combinations for radiation grafted fuel cell membranes*  
Electrochem. Comm. **8**, 1215-1219 (2006).
- M. Hahn, R. Kötz, R. Gallay<sup>1</sup>, A. Siggel<sup>2</sup> *Pressure evolution in propylene carbonate based electrochemical double layer capacitors*  
Electrochim. Acta **52**, 1709–1712 (2006).  
<sup>1</sup> Maxwell Technologies SA, Rossens  
<sup>2</sup> Honeywell Specialty Chemicals, Seelze, Germany
- M. Hahn, O. Barbieri, F. Campana, R. Kötz, R. Gallay<sup>1</sup> *Carbon based double layer capacitors with aprotic electrolyte solutions: The possible role of intercalation / insertion processes*  
Applied Physics **A 82**, 633-638 (2006).  
<sup>1</sup> Maxwell Technologies SA, Rossens
- M. Hahn, O. Barbieri, R. Gallay<sup>1</sup>, R. Kötz *A dilatometric study of the voltage limitation of carbonaceous electrodes in aprotic EDLC type electrolytes by charge-induced strain*  
Carbon **44**, 2523-2533 (2006).  
<sup>1</sup> Maxwell Technologies SA, Rossens
- L.J. Hardwick, M. Hahn, P. Ruch, M. Holzapfel, W. Scheifele, H. Buqa, F. Krumeich<sup>1</sup>, P. Novák, R. Kötz *An in situ Raman study of the intercalation of supercapacitor-type electrolyte into microcrystalline graphite*  
Electrochim. Acta **52**, 675-680 (2006).  
<sup>1</sup> ETH Zürich
- L.J. Hardwick, H. Buqa, P. Novák *Graphite surface disorder detection using in situ Raman microscopy*  
Solid State Ionics **177**, 2801-2806 (2006).
- M. Holzapfel, H. Buqa, L.J. Hardwick, M. Hahn, A. Würsig, W. Scheifele, P. Novák, R. Kötz, C. Veit<sup>1</sup>, F.-M. Petrat<sup>1</sup> *Nano silicon for lithium-ion batteries*  
Electrochim. Acta **52**, 973-978 (2006).  
<sup>1</sup> Degussa AG, CREAVIS Technologies & Innovation, Marl, Germany
- R. Kötz, M. Hahn, R. Gallay<sup>1</sup> *Temperature behavior and impedance fundamentals of supercapacitors*  
J. Power Sources **154**, 550-555 (2006).  
<sup>1</sup> Maxwell Technologies SA, Rossens
- H. Kuhn, B. Andreaus, A. Wokaun, G.G. Scherer *Electrochemical impedance spectroscopy applied to polymer electrolyte fuel cells with a pseudo reference electrode arrangement*  
Electrochim. Acta **51**, 1622–1628 (2006).
- M. Kuhnke, G.L. Dumitru<sup>1</sup>, T. Lippert, E. Ortelli<sup>2</sup>, G.G. Scherer, A. Wokaun *Micromachining of carbon materials and laser micropatterning of metal films used as masks for reactive ion etching*  
J. Laser Micro/Nanoengineering **1**, 67-73 (2006).  
<sup>1</sup> University of Applied Science Aargau, Windisch  
<sup>2</sup> Dyconex AG, Bassersdorf

- S. Mitov<sup>1</sup>, G. Hübner<sup>1</sup>,  
H.P. Brack, G.G. Scherer,  
E. Roduner<sup>1</sup> *In situ electron spin resonance study of styrene grafting of electron irradiated fluoropolymer films for fuel cell membranes*  
J. Polym. Sci.: Part B: Polym. Phys. **44**, 3323–3336 (2006).  
<sup>1</sup> University of Stuttgart, Germany
- P. Morf, F. Raimondi,  
H-G. Nothofer<sup>1</sup>, B. Schnyder,  
A. Yasuda<sup>1</sup>, J.M. Wessels<sup>1</sup>,  
T.A. Jung *Dithiocarbamates: functional and versatile linkers for the formation of self-assembled monolayers*  
Langmuir **22**, 658-663 (2006).  
<sup>1</sup> Sony Deutschland GmbH, Stuttgart, Germany
- T. Ogasawara<sup>1</sup>, A. Débart<sup>1</sup>,  
M. Holzapfel, P. Novák,  
P.G. Bruce<sup>1</sup> *Rechargeable Li<sub>2</sub>O<sub>2</sub> electrode for lithium batteries*  
J. Am. Chem. Soc. **128**, 1390-1393 (2006).  
<sup>1</sup> University of St. Andrews, Scotland
- T. Rager *Structured radiation-grafted polymer films and membranes*  
J. Appl. Polym. Sci. **100**, 292-294 (2006).
- A. Reiner, B. Steiger,  
G.G. Scherer, A. Wokaun *Influence of the morphology on the platinum electrode surface activity*  
J. Power Sources **156**, 28-32 (2006).
- M. Santis, S.A. Freunberger,  
A. Reiner, F.N. Büchi *Homogenization of the current density in polymer electrolyte fuel cells by in-plane cathode catalyst gradients*  
Electrochim. Acta **51**, 5383-5393 (2006).
- M. Santis, S.A. Freunberger,  
M. Papra, A. Wokaun,  
F.N. Büchi *Experimental investigation of coupling phenomena in polymer electrolyte fuel cell stacks*  
J. Power Sources **161**, 1076-1083 (2006).
- M.E. Spahr<sup>1</sup>, H. Buqa,  
A. Würsig, D. Goers<sup>1</sup>,  
L. Hardwick, P. Novák,  
F. Krumeich<sup>2</sup>, J. Dentzer<sup>3</sup>,  
C. Vix-Guterl<sup>3</sup> *Surface reactivity of graphite materials and their surface passivation during the first electrochemical lithium insertion*  
J. Power Sources **153**, 300-311 (2006).  
<sup>1</sup> TIMCAL SA, Bodio  
<sup>2</sup> ETH Zürich  
<sup>3</sup> Institut de Chimie des Surfaces et Interfaces, Mulhouse, France
- J. Vetter, M. Holzapfel,  
A. Wuersig, W. Scheifele,  
J. Ufheil, P. Novák *In situ study on CO<sub>2</sub> evolution at lithium-ion battery cathodes*  
J. Power Sources **159**, 277-281 (2006).
- J. Zhang<sup>1</sup>, D. Kramer,  
R. Shimo<sup>1</sup>, Y. Ono<sup>1</sup>,  
E. Lehmann, A. Wokaun,  
K. Shinohara<sup>1</sup>, A. Wokaun,  
G.G. Scherer *In situ diagnostic of two-phase flow phenomena in polymer electrolyte fuel cells by neutron imaging – Part B. Material variations*  
Electrochim. Acta **51**, 2715-2727 (2006).  
<sup>1</sup> Nissan Motors Co. Ltd., Yokosuka, Japan

## Other Papers

- J. Bernard, S. Delprat,  
F.N. Büchi, T.M. Guerra *Fuel cell hybrid vehicles: Global optimization based on optimal control theory*  
Int. Rev. Elect. Eng. (I.R.E.E.) **1**, n. 3 (2006).
- F.N. Büchi, S.A.  
Freunberger, M. Santis *What is learned beyond the scale of single cells?*  
ECS Transactions **1**, 963-968 (2006).
- F.N. Büchi, A. Delfino<sup>1</sup>,  
P. Dietrich,  
S.A. Freunberger, R. Kötz,  
D. Laurent<sup>1</sup>, P.-A. Magne<sup>1</sup>,  
D. Olsommer<sup>1</sup>, G. Paganelli<sup>1</sup>,  
A. Tsukada, P. Varenne<sup>1</sup>,  
D. Walser<sup>1</sup> *Electrical drivetrain concept with fuel cell system and supercapacitor – Results of the „Hy-LIGHT<sup>®</sup>“-vehicle*  
5. VDI Tagung Innovative Fahrzeugantriebe, Dresden, Deutschland, November 9-10, VDI-Band **1972**, 415-429 (2006).  
<sup>1</sup> Conception et Développement Michelin, Givisiez

- H. Buqa, P. Novák,  
F. Krumeich<sup>1</sup>, M.E. Spahr<sup>2</sup>,  
D. Goers<sup>2</sup>, H. Wilhelm<sup>2</sup>,  
J. Dentzer<sup>3</sup>, C. Vix-Guterl<sup>3</sup>
- Réactivité de surface du graphite lors de la première insertion électrochimique du lithium*  
Proc. MATERIAUX 2006, Dijon, France, November 13-17, AF-15-0875, Symposium 15 (2006).  
<sup>1</sup> ETH Zürich  
<sup>2</sup> TIMCAL SA, Bodio  
<sup>3</sup> Institut de Chimie des Surfaces et Interfaces (ICSI), Mulhouse, France
- A. Didion<sup>1</sup>, R. Gadiou<sup>1</sup>,  
R. Gearba<sup>1</sup>, D. Ivanov<sup>1</sup>,  
I. Czekaj, R. Kötz, C. Vix-Guterl<sup>1</sup>
- Synthèse de nouveaux matériaux carbonés nanostructurés par réplique négative à partir d'aminosucres*  
Proc. MATERIAUX 2006, Dijon, France, Novembre 13-17 (2006).  
<sup>1</sup> Institut de Chimie des Surfaces et Interfaces (ICSI), Mulhouse, France
- L. Gubler, M. Slaski,  
A. Wokaun, G.G. Scherer
- Aging Tests of Radiation Grafted Fuel Cell Membranes*  
Electrochem. Soc. Trans. **3**, 569-577 (2006).
- M. Hahn, P.W. Ruch,  
R. Gallay<sup>1</sup>, A. Siggel<sup>2</sup>,  
R. Kötz
- Voltage limitation of supercapacitors by charge-induced strain and gas evolution.*  
Proc. ESSCAP 2006, Lausanne, November 2-3 (2006).  
<sup>1</sup> Maxwell Technologies SA, Rossens,  
<sup>2</sup> Honeywell Specialty Chemicals, Seelze, Germany
- M. Hahn, P.W. Ruch,  
O. Barbieri, A. Foelske,  
R. Kötz, R. Gallay<sup>1</sup>
- Activated carbons for supercapacitors. The impact of charge-induced strain on life time and performance issues.*  
Proc. Carbon 2006, Aberdeen, Scotland, July 16-21 (2006).  
<sup>1</sup> Maxwell Technologies SA, Rossens
- D. Kramer, I.A. Schneider,  
A. Wokaun, G.G. Scherer
- Oscillations in the gas channels – The forgotten player in impedance spectroscopy in polymer electrolyte fuel cells B. Modeling the wave*  
ECS Transactions **3** (1), 1249 (2006).
- Y. Koudai, K. Izekoe,  
Y. Tasaki, D. Kramer,  
E. Lehmann, G.G. Scherer
- Analysis of gas diffusion layer and flow field design using neutron radiography*  
ECS Transactions **3** (1), 397 (2006).
- F. La Mantia, J. Vetter,  
P. Novák
- Characterization of materials for lithium-ion batteries with EIS, studied through a coupled partial ion-transfer model*  
Technische Mitteilungen **99**, 227-230 (2006).
- P. Nesvadba<sup>1</sup>, C. Morton<sup>1</sup>,  
T. Hintermann<sup>1</sup>, M. Ohwa<sup>2</sup>,  
T. Takeuchi<sup>2</sup>, J. Vetter,  
P. Novák, M. Satoh<sup>3</sup>
- Advanced nitroxides as electrode material for organic radical batteries*  
Ext. Abstracts, 47th Battery Symposium in Japan, Tokyo, Japan, March 28-31 (2006).  
<sup>1</sup> CIBA SC, Basel  
<sup>2</sup> CIBA SC, Amagasaki & Tokyo, Japan  
<sup>3</sup> NEC Corporation, Ibaraki, Japan
- P. W. Ruch, L.J. Hardwick,  
M. Hahn, P. Novák, R. Kötz
- In situ Raman and XRD studies of ion insertion from supercapacitor-type electrolyte into graphitic materials*  
Proc. 16<sup>th</sup> International Seminar on Double Layer Capacitors and Hybrid Energy Storage Devices, Deerfield Beach, Florida, December 4-6, 285-294 (2006).
- G.G. Scherer, A. Reiner,  
X. Wei, N.K. Beck,  
A. Foelske, R. Kötz,  
S. Alkan-Gürsel, M. Slaski,  
H. Ben youcef, L. Gubler,  
A. Wokaun
- Materials research for polymer electrolyte fuel cells – Activities at Paul Scherrer Institut*  
Libro de Comunicaciones, CONAPICCE 2006, Madrid, Spain, October 18-20 (2006).
- I.A. Schneider, D. Kramer,  
A. Wokaun, G.G. Scherer
- Oscillations in the gas channels – The forgotten player in impedance spectroscopy in PEFCs*  
ECS Transactions, **3** (1), 1001-1010 (2006).

J. Vetter, H. Buqa,  
M. Holzapfel, M. Pascaly<sup>1</sup>,  
P. Novák

*Lithium-ion battery electrolytes - insights and recent progress*  
Ext. Abstracts, 47th Battery Symposium in Japan, Tokyo, Japan,  
November 26-28, 1F13-IL (2006).  
<sup>1</sup> Degussa AG, CREAVIS Technologies & Innovation, Marl, Germany.

## TALKS

### Invited Talks

- S. Alkan Gürsel *Polymer electrolyte membranes for fuel cells by radiation induced grafting: State of the art at PSI*  
IRaP 2006, Antalya, Turkey, September 23-28, 2006.
- F.N. Büchi *Measuring the current density distribution in PEFC with sub-mm resolution*  
DaimlerChrysler Forschungszentrum, Ulm, Germany, April 12, 2006.
- F.N. Büchi *Fuel cell – supercap hybrid electric drivetrain*  
F&E Kolloquium, HOPPECKE Batterien GmbH & Co. KG, Brilon, Germany, April 26, 2006.
- F.N. Büchi *What is learned beyond the scale of single cells?*  
210<sup>th</sup> Joint ECS Meeting, Cancun, Mexico, November 2, 2006.
- L. Gubler *PSI Electrochemistry Laboratory: Contributions to efficient energy storage and conversion*  
EMPA Thun, November 16, 2006.
- D. Kramer *Mass transport aspects of PEFCs under two-phase flow conditions*  
Workshop on Neutron Imaging for Fuel Cells, Daejeon, Korea, May 12, 2006.
- P. Novák *Oxygen, hydrogen and CO<sub>2</sub> development in lithium-ion batteries*  
13<sup>th</sup> Int. Meeting on Lithium Batteries, Biarritz, France, June 18-23, 2006.
- P. Novák *Interfaces in lithium-ion batteries*  
Shanghai Jiao Tong University, Shanghai, China, July 18, 2006.
- P. Novák *Relationship between surface chemistry and lithium intercalation properties of graphite*  
Annual Meeting GFECI-2006, Autrans, France, March 29, 2006.
- P. Novák *Grundlagen und technischer Entwicklungsstand von wiederaufladbaren Hochleistungs-Lithiumionen-Batterien*  
Workshop Lithiumionen-Batterien in der Automobilindustrie, Hanau, Germany, January 26, 2006.
- P.W. Ruch *Time-resolved in situ X-ray diffraction of carbons for supercapacitors*  
7<sup>th</sup> SLS Users Meeting, Paul Scherrer Institut, Villigen, September 29, 2006.
- G.G. Scherer *Recent developments and new trends in radiation grafted fuel cell membranes at Paul Scherrer Institut*  
Japan Atomic Energy Agency, Quantum Beam Science Directorate, Takasaki, Japan, February, 28, 2006.
- G.G. Scherer *Polymer membran degradation - A literature survey*  
NISSAN Research Center, Kanagawa, Japan, March 2, 2006.
- G.G. Scherer *Recent progress in the development of in situ characterization methods at Paul Scherrer Institut*  
Nissan Research Center, Kanagawa, Japan, March 2, 2006.

- G.G. Scherer *Recent advances in the development of in situ diagnostic methods for polymer electrolyte fuel cells at Paul Scherrer Institut*  
Yokohama National University, Yokohama, Japan, March 3, 2006.
- G.G. Scherer *Combined in situ characterization methods for polymer electrolyte fuel cells*  
39<sup>th</sup> Heyrovský Discussion & 7<sup>th</sup> International Symposium on EIS, Castle Trest, Czech Republic, June 4-8, 2006.
- G.G. Scherer *In situ diagnostic methods for polymer electrolyte fuel cells: Recent progress achieved at Paul Scherrer Institut*  
10<sup>th</sup> Ulm Electrochemical Talks, Neu Ulm, Germany, June 27-28, 2006.
- G.G. Scherer *Aspects of materials research for polymer electrolyte fuel cells*  
Keynote Lecture, 57<sup>th</sup> Annual ISE Meeting Edinburgh, UK, August 27 – September 1, 2006.
- G.G. Scherer *The potential of in situ diagnostic methods to elucidate the performance of polymer electrolyte fuel cells*  
Nordic PEMFC 06, Stockholm, Sweden, September 25-27, 2006.
- G.G. Scherer *Aspects of materials research for polymer electrolyte fuel cells*  
CONAPPICE, Madrid, Spain, September 18-20, 2006.
- G.G. Scherer *Recent advances in the development of in situ diagnostic methods for polymer electrolyte fuel cells*  
CEA, Grenoble, France, November 24, 2006.
- G.G. Scherer *Materials research for polymer electrolyte fuel cells*  
Achema 2006, Frankfurt am Main, Germany, Mai 15-19, 2006.
- J. Vetter *Lithium-ion battery electrolytes - insights and recent progress*  
47<sup>th</sup> Battery Symposium in Japan, Tokyo, Japan, November 19-22, 2006.
- J. Vetter *Application of in situ techniques for investigations in lithium-ion battery materials*  
210<sup>th</sup> Electrochem. Soc. Meeting, Cancun, Mexico, October 30 – November 3, 2006.

## Other Talks

- O. Barbieri, M. Hahn,  
A. Foelske, R. Kötz *Relation between electronic resistance and capacitance for highly aqueous RuO<sub>2</sub>*  
57<sup>th</sup> Annual ISE Meeting, Edinburgh, UK, August 27 – September 01, 2006.
- F.N. Büchi *Fuel cell systems research at PSI*  
3<sup>rd</sup> PSI-RCECS Joint Seminar, Paul Scherrer Institut, August 22-23, 2006.
- F.N. Büchi, A. Delfino<sup>1</sup>,  
P. Dietrich,  
S.A. Freunberger, R. Kötz,  
D. Laurent<sup>1</sup>, P. Magne<sup>1</sup>,  
D. Olsommer<sup>1</sup>, G. Paganelli<sup>1</sup>,  
A. Tsukada, P. Varenne<sup>1</sup>,  
D. Walsler<sup>1</sup> *Electrical drivetrain concept with fuel cell system and supercapacitor - Results of the « HY-LIGHT @» - vehicle*  
5. VDI-Tagung mit Fachausstellung, Dresden, Germany, November 9–10, 2006.  
<sup>1</sup> Conception et Développement Michelin SA, Givisiez
- R. Flückiger, A. Tiefenauer<sup>1</sup>,  
M. Ruge<sup>2</sup>, C. Aebi<sup>3</sup>,  
F.N. Büchi *Thermal management of an edge-air-cooled PEFC stack*  
3<sup>rd</sup> Fuel Cell Research Symposium Modelling and Experimental Validation, Dübendorf, March 16-17, 2006.  
<sup>1</sup> Zurich University of Applied Science, Winterthur  
<sup>2</sup> Berne University of Applied Science, Biel  
<sup>3</sup> CEKA Elektrowerkzeuge AG, Wattwil

- S.A. Freunberger, F.N. Büchi *Cell interaction phenomena in PEFC stacks*  
57<sup>th</sup> Annual ISE Meeting, Edinburgh, UK, August 27 – September 1, 2006.
- S.A. Freunberger,  
U. Frischknecht,  
I.A. Schneider, F.N. Büchi *Influence of the cooling strategy on the local cell performance*  
3<sup>rd</sup> Fuel Cell Research Symposium, EMPA Dübendorf, March 15-16, 2006.
- L. Gubler, M. Slaski,  
A. Wokaun, G.G. Scherer *Aging tests of radiation grafted fuel cell membranes*  
210<sup>th</sup> Joint ECS Meeting, Cancun, Mexico, October 29 - November 3, 2006.
- L. Gubler, S. Alkan Gürsel,  
M. Slaski, G.G. Scherer *Characterization of fuel cell performance and durability using MEAs with radiation grafted membranes*  
3<sup>rd</sup> PSI-RCECS Joint Seminar, Paul Scherrer Institut, Villigen, August 23-24, 2006.
- M. Hahn, H. Buqa,  
P.W. Ruch, O. Barbieri,  
A. Foelske, P. Novák,  
R. Kötz *A dilatometric study of ion intercalation from aprotic solutions into carbonaceous materials*  
57<sup>th</sup> Annual Meeting ISE, Edinburgh, UK, August 27 - September 1, 2006.
- M. Hahn, P.W. Ruch,  
O. Barbieri, A. Foelske,  
R. Kötz, R. Gallay<sup>1</sup> *Activated carbons for supercapacitors. The impact of charge-induced strain on life time and performance issues.*  
Carbon 2006, Aberdeen, Scotland, July 16–21, 2006.  
<sup>1</sup> Maxwell Technologies SA, Rossens
- M. Hahn, H. Buqa, P. Ruch,  
P. Novák, R. Kötz *A dilatometric study of ion intercalation from aprotic solutions into carbonaceous materials*  
3<sup>rd</sup> PSI-RCECS Joint Seminar, Paul Scherrer Institut, Villigen, August 23-24, 2006.
- M. Hahn, P.W. Ruch,  
R. Gallay<sup>1</sup>, A. Siggel<sup>2</sup>,  
R. Kötz *Voltage limitation of supercapacitors by charge-induced strain and gas evolution.*  
ESSCAP 2006, Lausanne, November 2-3, 2006.  
<sup>1</sup> Maxwell Technologies SA, Rossens  
<sup>2</sup> Honeywell Specialty Chemicals, Seelze, Germany
- L.J. Hardwick, M. Holzapfel,  
A. Wokaun, P. Novák *An in situ Raman microscopic study of electrochemical lithium insertion into anatase TiO<sub>2</sub>*  
209<sup>th</sup> Electrochem. Soc. Meeting, Denver, Colorado, USA, May 8-12, 2006.
- D. Kramer, I.A. Schneider,  
A. Wokaun, G.G. Scherer *Oscillations in the gas channels – The forgotten player in impedance spectroscopy in polymer electrolyte fuel cells B. Modelling the wave*  
210<sup>th</sup> Joint ECS Meeting, Cancun, Mexico, October 29 - November 3, 2006.
- R. Kötz, P.W. Ruch,  
L.J. Hardwick, M. Hahn,  
P. Novák, *In situ Raman and XRD studies of ion insertion from supercapacitor-type electrolyte into graphitic materials*  
16<sup>th</sup> International Seminar on Double Layer Capacitors and Hybrid Energy Storage Devices, Deerfield Beach, Florida, USA, December 4-6, 2006.
- Y. Koudai, K. Izekoe,  
Y. Tasaki, D. Kramer,  
E. Lehmann, G.G. Scherer *Analysis of gas diffusion layer and flow field design in a fuel cell*  
210<sup>th</sup> Joint ECS Meeting, Cancun, Mexico, October 29 - November 3, 2006.
- P. Novák, H. Buqa,  
L.J. Hardwick, M. Holzapfel,  
W. Scheifele, J. Ufheil,  
J. Vetter *In situ analysis of interfaces in nonaqueous electrochemical systems*  
57<sup>th</sup> Annual ISE Meeting, Edinburgh, UK, August 27 – September 1, 2006.
- A. Reiner, F. Hajbolouri,  
M. Doebeli, S. Abolhassani-  
Dadras, A. Wokaun,  
G.G. Scherer *Co-sputtering: A novel approach for low Pt loading fuel cell electrodes*  
57<sup>th</sup> Annual ISE Meeting, Edinburgh, UK, August 27 - September 1, 2006.

- A. Reiner, G.G. Scherer, A. Wokaun  
*Novel electrocatalytic layers prepared by co-sputtering*  
3<sup>rd</sup> PSI-RCECS Joint Seminar, Paul Scherrer Institut, Villigen, August 23-24, 2006.
- M. Reum, S.A. Freunberger, F.N. Büchi  
*Measuring the current density in PEFCs with sub-millimeter resolution – fundamental insights*  
57<sup>th</sup> Annual ISE Meeting, Edinburgh, UK, August 27 – September 1, 2006.
- M. Reum, S.A. Freunberger, F.N. Büchi  
*Measuring the local current density distribution on a sub-millimeter scale*  
3<sup>rd</sup> Fuel Cell Research Symposium Modelling and Experimental Validation, Empa, Dübendorf, March 16-17, 2006.
- P.W. Ruch, L. Hardwick, F. Rosciano, M. Hahn, M. Holzapfel, B. Schmitt, H. Kaiser, W. Scheifele, P. Novák, R. Kötz, A. Wokaun  
*In situ Raman and X-ray diffraction studies of carbons for supercapacitors*  
3<sup>rd</sup> PSI-RCECS Joint Seminar, Paul Scherrer Institut, Villigen, August 23-24, 2006.
- P.W. Ruch, L.J. Hardwick, M. Hahn, O. Barbieri, A. Foelske, P. Novák, R. Kötz, A. Wokaun  
*In situ Raman and XRD studies of carbons for supercapacitors*  
57<sup>th</sup> Annual ISE Meeting, Edinburgh, UK, August 27 - September 1, 2006.
- I.A. Schneider, D. Kramer, A. Wokaun, G.G. Scherer  
*Oscillations in the gas channels – The forgotten player in impedance spectroscopy in PEFCs*  
210<sup>th</sup> Joint ECS Meeting, Cancun, Mexico, November 2, 2006.
- I.A. Schneider, D. Kramer, A. Wokaun, G.G. Scherer, E. Lehmann  
*Spatially resolved in situ characterization of PEFCs*  
3<sup>rd</sup> PSI-RCECS Joint Seminar, Paul Scherrer Institut, Villigen, August 23-24, 2006.
- M. Schnippering<sup>1</sup>, A. Foelske, R. Kötz, M. Carrara<sup>1</sup>, H. Siegenthaler<sup>1</sup>, D.J. Fermín<sup>1</sup>  
*Electrochemical and spectroscopic characterisation of 2D assemblies of silver nanoparticles*  
22<sup>nd</sup> Annual SAOG Meeting, Fribourg, January 20, 2006.  
<sup>1</sup> Department für Chemie und Biochemie, Universität Bern
- B.C. Seyfang, M. Kuhnke, T. Lippert, G.G. Scherer, A. Wokaun  
*Microstructures for H<sub>2</sub>O<sub>2</sub>-investigations and micro fuel cells*  
3<sup>rd</sup> PSI-RCECS Joint Seminar, Paul Scherrer Institut, Villigen, August 23-24, 2006.
- J. Ufheil, M. Holzapfel, H. Buqa, L.J. Hardwick, W. Scheifele, F.O. Ernst<sup>1</sup>, S.E. Pratsinis<sup>1</sup>, F.-M. Petrat<sup>2</sup>, P. Novák  
*Nano particles for Li-ion batteries*  
3<sup>rd</sup> PSI-RCECS Joint Seminar, Paul Scherrer Institut, Villigen, August 23-24, 2006.  
<sup>1</sup> ETH Zürich  
<sup>2</sup> Degussa AG, Creavis, Marl, Germany
- J. Vetter, M. Holzapfel, P. Novák, C. Jost<sup>1</sup>, A. Prodi-Schwab<sup>1</sup>  
*Stable cycling of lithium-ion batteries with ionic liquid based electrolytes*  
3<sup>rd</sup> PSI-RCECS Joint Seminar, Paul Scherrer Institut, Villigen, August 23-24, 2006.  
<sup>1</sup> Degussa AG, Creavis, Marl, Germany

## POSTERS

- S. Alkan Gürsel, H. Ben youcef, J. Schneider<sup>1</sup>, L. Gubler, G.G. Scherer, A. Wokaun  
*Synthesis and characterization of radiation-grafted membranes for polymer electrolyte fuel cells*  
SCS 2006 (Swiss Chemical Society) Fall Meeting, Zürich, October 13, 2006.  
<sup>1</sup> ETH Zürich
- H. Ben youcef, S. Alkan Gürsel, A. Wokaun, G.G. Scherer  
*Influence of crosslinking on irradiated ETFE based grafted membranes*  
PGS 2006 Fall Meeting, Polymer Group Switzerland, Zürich, October 13, 2006.

- H. Ben youcef, S. Alkan Gürsel, A. Wokaun, G.G. Scherer  
*Radiation induced grafting of styrene onto ETFE: Influence of crosslinker*  
IRaP 2006, Antalya, Turkey, September 23-28, 2006.
- P. Boillat, I.A. Schneider, D. Kramer, H. Kuhn, G.G. Scherer, A. Wokaun  
*Advanced characterization methods for polymer electrolyte fuel cells*  
4<sup>th</sup> European Summer School on Electrochemical Engineering, Palic, Serbia and Montenegro, September 17-22, 2006.
- F.N. Büchi, S.A. Freunberger, M. Reum  
*Local current measurements in PEFC on the sub-millimeter scale*  
Gordon Research Conference on Fuel Cells, Smithfield, RI, USA, July 23-28, 2006.
- L. Bugnon<sup>1</sup>, C. Morton<sup>1</sup>, P. Nesvadba<sup>1</sup>, J. Vetter, P. Novák  
*Poly(4-methacryloyloxy-TEMPO) via group transfer polymerization and its evaluation in organic radical battery*  
Swiss Chemical Society – Fall Meeting, University of Zurich, October 13, 2006.  
<sup>1</sup> CIBA SC, Basel
- H. Buqa, P. Novák, F. Krumeich<sup>1</sup>, M.E. Spahr<sup>2</sup>, D. Goers<sup>2</sup>, H. Wilhelm<sup>2</sup>, J. Dentzer<sup>3</sup>, C. Vix-Guterl<sup>3</sup>  
*The importance of the active surface area of graphite materials in the first lithium intercalation*  
13<sup>th</sup> Int. Meeting on Lithium Batteries, Biarritz, France, June 18-23, 2006.  
<sup>1</sup> ETH Zürich  
<sup>2</sup> TIMCAL SA, Bodio  
<sup>3</sup> Institut de Chimie des Surfaces et Interfaces, Mulhouse, France
- I. Czekaj, F. Raimondi, J. Wambach, S. Biollaz, A. Wokaun  
*Nanoanalysis of surface processes at Ni/Al<sub>2</sub>O<sub>3</sub> catalyst during methanation*  
CEAC Summer Workshop, ETH Zürich, July 10-11, 2006.
- I. Czekaj, F. Raimondi, J. Wambach, A. Wokaun  
*Surface processes at Ni-based catalyst during methanation at the atomic level*  
4<sup>th</sup> International TRI/Princeton Workshop "Characterization of Porous Materials: From Angstroms to Millimeters", Princeton, NJ, USA, June 21-23, 2006.
- I. Czekaj, F. Raimondi, J. Wambach, A. Wokaun  
*Deactivation mechanism of Ni-based catalyst during methanation processes*  
10<sup>th</sup> International Symposium on Catalyst Deactivation, Berlin, Germany, February 5-8, 2006.
- I. Czekaj, F. Raimondi, J. Wambach, S. Biollaz, A. Wokaun  
*Surface processes at Ni-based catalyst during methanation: X-ray photoelectron spectroscopy and theoretical studies*  
22<sup>nd</sup> Annual SAOG Meeting, Fribourg, January 20, 2006.
- P. Farquet, C. Padeste, H.H. Solak, S. Alkan Gürsel, G.G. Scherer, A. Wokaun  
*Micro-structured proton-conducting membranes by radiation grafting*  
Junior Euromat 2006, Lausanne, September 4-8, 2006.
- P. Farquet, G.G. Scherer, C. Padeste, H.H. Solak, S. Alkan Gürsel, A. Wokaun  
*Micro-structured proton-conducting membranes by radiation grafting*  
CONAPPICE 2006, Madrid, Spain, October 18-20, 2006.
- P. Farquet, C. Padeste, H.H. Solak, S. Alkan Gürsel, G.G. Scherer, A. Wokaun  
*EUV radiation grafting of nanostructured polymer brushes by RAFT-mediated polymerization*  
IRaP, Antalya, Turkey, September 23-28, 2006.
- R. Flückiger, A. Tiefenauer<sup>1</sup>, M. Ruge<sup>2</sup>, C. Aebi<sup>3</sup>, F.N. Büchi  
*Thermal analysis and optimization of a portable, edge-air-cooled PEFC stack*  
4<sup>th</sup> European Summer School on Electrochemical Engineering, Palić, Serbia and Montenegro, September 17-22, 2006.  
<sup>1</sup> Zurich University of Applied Science, Winterthur  
<sup>2</sup> Berne University of Applied Science, Biel  
<sup>3</sup> CEKA Elektrowerkzeuge AG, Wattwil

- A. Foelske, B. Steiger,  
N.K. Beck, R. Kötzt,  
G.G. Scherer, A. Wokaun  
*A methanol tolerant oxygen reduction catalyst - An X-ray photoelectron spectroscopy study of  $Bi_2Pt_{2-x}Ir_xO_7$  pyrochlores*  
22<sup>nd</sup> Annual SAOG Meeting, Fribourg, January 20, 2006.
- S.A. Freunberger,  
U. Frischknecht, F.N. Büchi  
*Influence of the cooling strategy on the local performance of PEFC*  
57<sup>th</sup> Annual ISE Meeting, Edinburgh, UK, August 27-September 1, 2006.
- P. Novák, L.J. Hardwick,  
M. Holzapfel, A. Wokaun  
*Relationship between surface heterogeneity and performance of electrodes for lithium-ion batteries*  
13<sup>th</sup> Int. Meeting on Lithium Batteries, Biarritz, France, June 18-2, 2006.
- M. Papra<sup>1</sup>, D. Ohms<sup>1</sup>,  
F.N. Büchi, E. Cattaneo<sup>1</sup>,  
R. Markolf<sup>1</sup>, B. Riegel<sup>1</sup>,  
G. Schädlich<sup>1</sup>  
*Hybrid power concepts - Direct parallel operation of polymer electrolyte fuel cells and alkaline batteries*  
10<sup>th</sup> Ulmer ElektroChemical Talks (UECT), Ulm, Germany, June 27-28, 2006.  
<sup>1</sup> Hoppecke Batterien GmbH, Brilon, Germany
- J. Reim<sup>1</sup>, H. Rentsch<sup>1</sup>,  
P. Novák, W. Scheifele  
*Synthesis and characterization of doped  $Li[Mn_{0.5-x/2}Ni_{0.5-x/2}Co_x]O_2$  cathode materials*  
13<sup>th</sup> Int. Meeting on Lithium Batteries, Biarritz, France, June 18-23, 2006.  
<sup>1</sup> Ferro GmbH, Frankfurt/Main, Germany
- A. Reiner, F. Hajbolouri,  
M. Döbeli<sup>1</sup>, A. Wokaun,  
G.G. Scherer  
*Novel fuel cell catalyst layers prepared by co-sputtering platinum and carbon*  
22<sup>nd</sup> SAOG Meeting 06, Fribourg, January 20, 2006.  
<sup>1</sup> Paul Scherrer Institut, c/o Institute for Particle Physics, ETH Zürich
- A. Reiner, G.G. Scherer,  
A. Wokaun  
*Fuel cell electrodes prepared by co-sputtering platinum and carbon*  
2<sup>nd</sup> Workshop of the network, Efficient Oxygen Reduction for the Electrochemical Energy Conversion, Ulm, Germany, April 6-7, 2006.
- M. Reum, S.A. Freunberger,  
F.N. Büchi  
*Impact of flow field geometry on local current distribution on the sub-millimeter scale in PEFC*  
57<sup>th</sup> Annual ISE Meeting, Edinburgh, UK, August 27 - September 1, 2006.
- F. Rosciano, M. Holzapfel,  
P. Novák  
*A multi-sample automatic system for in situ X-ray diffraction synchrotron measurements, applied to insertion compounds*  
10<sup>th</sup> EPDIC-10, Geneva, August 31 – September 9, 2006.
- M. Schnippering<sup>1</sup>,  
M. Carrara<sup>1</sup>, A. Foelske,  
R. Kötzt, D.J. Fermín<sup>1</sup>  
*Modulation of the electrode work function by self-assembled metal nanoparticles*  
57<sup>th</sup> Annual ISE Meeting, Edinburgh, UK, August 27 - September 1, 2006.  
<sup>1</sup> University of Bern
- B.C. Seyfang, M. Kuhnke,  
T. Lippert, G.G. Scherer,  
A. Wokaun  
*A novel concept for micro fuel cells using micro-structured glassy carbon*  
European Summer School on Electrochemical, Palic, Serbia and Montenegro, September 17-22, 2006.
- B.C. Seyfang, M. Kuhnke,  
T. Lippert, G.G. Scherer,  
A. Wokaun  
*Micro polymer electrolyte fuel cells – a novel, simplified concept*  
CONNAPICE, Madrid, Spain, October 18-20, 2006.
- M. Slaski, L. Gubler,  
A. Wokaun, G.G. Scherer  
*A comparison of styrene and alpha-methylstyrene based radiation grafted fuel cell membranes*  
210<sup>th</sup> Joint ECS Meeting, Cancun, Mexico, October 29 - November 3, 2006.
- J. Ufheil, F.O. Ernst<sup>1</sup>,  
S.E. Pratsinis<sup>1</sup>, P. Novák  
*Tailored nano particles for batteries made by flame spray pyrolysis*  
57<sup>th</sup> ISE Meeting, Edinburgh, UK, August 27 – September 1, 2006.  
<sup>1</sup> ETH Zürich

## PATENT APPLICATIONS

Z. Yang, M.G. Roelofs<sup>1</sup>,  
S. Alkan Gürsel,  
G.G. Scherer

*Process to prepare stable trifluorostyrene containing compounds grafted to base polymers using an alcohol/water mixture*  
WO Patent. 2006102672A1(2006).

<sup>1</sup> DuPont Central Research and Development, Wilmington, USA

## CONFERENCES, WORKSHOPS & EXHIBITIONS

R. Kötz *57<sup>th</sup> Annual ISE Meeting*  
Edinburgh, UK, August 27 - September 1, 2006.  
Symposium Organizer

R. Kötz *ESSCAP 2006, 2<sup>nd</sup> European Symposium on Super Capacitors and Applications*  
Lausanne, November 2-3, 2006.  
Member of International Scientific Committee

P. Novák *1<sup>st</sup> Symposium on Impedance Spectroscopy*  
Essen, Germany, May 16-17, 2006.  
Scientific Program Committee

P. Novák *57<sup>th</sup> Annual ISE Meeting*  
Edinburg, UK, August 27 - September 1, 2006.  
Symposium Organizer

## MEMBERSHIPS IN EXTERNAL COMMITTEES

F.N. Büchi *International Society of Electrochemistry*  
Regional Representative Switzerland

R. Kötz *International Society of Electrochemistry*  
Past-Chair Divison 3; Electrochemical Energy Conversion and Storage

P. Novák *International Society of Electrochemistry*  
Member of Executive Committee (Treasurer) and Council

P. Novák *International Society of Electrochemistry*  
Member of Scientific Meeting Committee

P. Novák *The Electrochemical Society, Inc.*  
Member of the Technology Award Committee of the Battery Division

G.G. Scherer *International Society of Electrochemistry*  
Vice-Chair Divison 3; Electrochemical Energy Storage and Conversion

G.G. Scherer *Beirat Forschungsallianz Brennstoffzelle Baden-Württemberg, Germany*  
Deputy Speaker

G.G. Scherer *Maturitätsprüfungskommission der Kantonsschulen Baden, Wettingen und Wohlen*  
Mitglied

G.G. Scherer *MISTRA, The Swedish Foundation for Strategic Environmental Research*  
Member International Advisory Board

PAUL SCHERRER INSTITUT



Paul Scherrer Institut, 5232 Villigen PSI, Switzerland  
Tel. +41 (0)56 310 21 11, Fax +41 (0)56 310 21 99  
[www.psi.ch](http://www.psi.ch)